ABSTRACT

Title of Dissertation: PREPARATION OF POLYELECTROLYTE MEMBRANES EMBEDDED WITH ZEOLITE NANOPARTICLES FOR ENHANCED PERFORMANCE IN FORWARD OSMOSIS

Yan Kang, Doctor of Philosophy, 2016

Dissertation directed by: Assistant Professor Baoxia Mi
Department of Civil and Environmental Engineering

Water scarcity is a global issue that has already affected every continent. Membrane technology is considered as one of the most promising candidates for resolving this worsening issue. Among all the membrane processes, the emerging forward osmosis (FO) membrane process is osmotically-driven and has unique advantages compared with other traditional pressure-driven membrane processes. One of the major challenges to advancing the FO membrane process is the lack of a suitable membrane. Polyelectrolyte thin film prepared via layer-by-layer (LbL) technique has demonstrated its excellent performance in many applications including electronics, optics, sensors, etc. Recent studies have revealed the potential of polyelectrolyte thin films in acting as the active separation layer of FO membranes, but significant efforts are still needed to improve the membrane performance and understand the transport mechanisms. This dissertation introduces a novel approach to prepare a zeolite-

embedded polyelectrolyte composite membrane for enhanced FO performance. This membrane takes advantages of the versatile LbL process to unprecedentedly incorporate high loading of zeolite nanoparticles, which are anticipated to facilitate water transport due to the uniquely interconnected structure of zeolites. Major topics discussed in this dissertation include: (1) the synthesis and evaluation of the polyelectrolyte-zeolite composite FO membrane, (2) the examination of the fouling resistance to identify its technical limitations, (3) the demonstration of the membrane regenerability as an effective strategy for membrane fouling control, and (4) the investigation of crosslinking effects on the membrane performance to elucidate the transport mechanisms involved in the zeolite-embedded polyelectrolyte membranes. Comparative studies have been made between polyelectrolyte membranes with and without zeolite incorporation. The findings suggest that the zeolite-embedded membrane, although slightly more susceptible to silica scaling, has demonstrated enhanced water flux and separation capability, good resistance to organic fouling, and complete regenerability for fouling control. Additionally, the embedded zeolite nanoparticles are proved to be able to create fast pathways for water transport. Overall, this work provides a novel strategy to create zeolite-polymer composite membranes with enhanced separation performance and unique fouling mitigation properties.

PREPARATION OF POLYELECTROLYTE MEMBRANES EMBEDDED WITH ZEOLITE NANOPARTICLES FOR ENHANCED PERFORMANCE IN FORWARD OSMOSIS

by

Yan Kang

Dissertation submitted to the Faculty of the Graduate School of the
University of Maryland, College Park, in partial fulfillment
of the requirements for the degree of
Doctor of Philosophy
2016

Advisory Committee:
Professor Alba Torrents
Professor Allen P. Davis
Assistant Professor Baoxia Mi, Chair
Associate Professor Chunsheng Wang
Assistant Professor Dongxia Liu

To my family

Acknowledgements

I would like to express my deepest gratitude to my advisor Dr. Baoxia Mi. This dissertation would not be possible without her constant support and enlightening guidance. I would like to give my sincere appreciation to Dr. Alba Torrents, Dr. Allen Davis, Dr. Dongxia Liu and Dr. Chunsheng Wang for serving on my dissertation committee and for their kind help. Special thanks go to Dr. Dongxia Liu for providing necessary supplies and materials for my research.

I want to thank all the people who have been helpful in numerous ways: Michael Lee, Dr. Yaolin Liu, Dr. Meng Hu, Catherine Birney, Dr. Haiyin Yu, Dr. Yong Gao, Dr. Qian Yang, Yoontaek Oh, Sunxiang Zheng, Dr. Limei Jin. I also want to thank Dr. Sz-Chian Liou and the support from the Maryland NanoCenter and its AIMLab.

I am incredibly grateful for my parents. They have been with me through it all, from the beginning of my life to now. Without their love and encouragement, nothing would have been possible. I also appreciate the support and care from my other family members and friends who have endured this long journey with me.

This work was mainly supported by the National Science Foundation (NSF) under Grant Number CBET-1154572 and CBET-1351430. The American Membrane Technology Association (AMTA) also supported in the form of student fellowship. I was additionally supported by the Graduate Student Summer Research Fellowship and the Dean's Fellowship from University of Maryland. The financial support is gratefully acknowledged.

Table of Contents

Table of Contents iv
List of Figures vii
Chapter 1 : Introduction 1
1.1 Background 1
1.2 Objectives 4
1.3 Research Structure 5
1.4 Dissertation Organization 6
1.5 References 7
Chapter 2 : Literature Review 13
2.1 Forward Osmosis (FO) Process 13
2.2 Concentration Polarization 17
2.2.1 External Concentration Polarization 17
2.2.2 Internal Concentration Polarization 18
2.2.3 Modeling of Concentration Polarization 20
2.3 Membrane Fouling 23
2.3.1 Types of Fouling 23
2.3.2 Fouling Recovery and Membrane Regeneration 25
2.4 Current Development of FO Membranes 26
2.4.1 Membrane Materials 26
2.4.2 Membrane Structure 30
2.4.3 Strategies for Fouling Mitigation 31
2.4.4 Draw Solutes 33
2.5 References 34
Chapter 3 : Layer-by-layer Assembly of Zeolite/polyelectrolyte Nanocomposite Membranes 45
3.1 Introduction 45
3.2 Materials and Methods 47
3.2.1 Materials and Zeolite/Membrane Synthesis 47
3.2.1 Zeolite/Membrane Characterizations 49
3.2.2 Membrane Performance Tests 50
3.3 Results and Discussion 51
3.3.1 Membrane Characterizations and Validations of Zeolite Incorporation 51
3.3.2 Extremely High Zeolite Loading Enabled by Trilayer Assembly 55
3.3.3 Effects of Zeolite Incorporation on Membrane Performance 61
3.4 Conclusions 65
3.5 Acknowledgements 66
3.6 References 67
Chapter 4 : Fouling Study on Zeolite/polyelectrolyte Nanocomposite Membranes 72
4.1 Introduction 72
4.2 Materials and Methods 74
4.2.1 Membrane Synthesis 74
4.2.2 Fouling Experiments 75

4.3 Results and Discussion 77
4.3.1 Effects of One-sided and Double-sided Coating 77
4.3.2 Fouling on Bilayers and Trilayers 81
4.3.3 QCM-D Measurements of Fouling Process 82
4.4 Conclusions 84
4.5 Acknowledgements 84
4.6 References 85
Chapter 5 : Membrane Regeneration of Polyelectrolyte Membranes 88
5.1 Introduction 88
5.2 Materials and Methods 90
5.2.1 Membrane Synthesis 90
5.2.2 Membrane Performance and Regeneration Tests 91
5.2.3 Membrane Characterizations 92
5.3 Results and Discussion 93
5.3.1 Membrane Characterizations and Performance 93
5.3.2 Effects of Acid Treatment 99
5.3.3 Regeneration Process in FO 107
5.4 Conclusions 109
5.5 Acknowledgements 110
5.6 References 110
Chapter 6 : Crosslinking of Polyelectrolyte-Zeolite Composite Membranes 117
6.1 Introduction 117
6.2 Materials and Methods 119
6.2.1 Membrane Synthesis and Crosslinking 119
6.2.2 Membrane Performance Tests 120
6.2.3 Membrane Characterizations 121
6.3 Results and Discussion 122
6.3.1 Crosslinking Validation 122
6.3.2 Crosslinking Effects on PAN-supported Trilayer Membranes 126
6.3.3 Crosslinking Effects on Silica Trilayer Membranes 128
6.3.4 Crosslinking Effects on PSf-supported Trilayer Membranes 133
6.3.5 Unique Transport Behavior of Trilayer Membranes 135
6.4 Conclusions 141
6.5 Acknowledgements 142
6.6 References 142
Chapter 7 : Conclusions 146
Chapter 8 : Future Work 150

List of Tables

Table 3.1. Atomic percentage of silicon and aluminum in the trilayer membrane characterized by XPS analysis. 58

List of Figures

Figure 1.1. Overview of research tasks with solid arrows representing the focus of this dissertation. 5
Figure 2.1. Schematic diagram of the FO process. Water can spontaneously transport from the feed to the draw. 14
Figure 2.2. Schematic diagram of RO ($\Delta p > \Delta\pi$), FO ($\Delta p = 0$) and PRO ($\Delta p < \Delta\pi$) processes. Δp is the external (hydraulic) pressure applied and $\Delta\pi$ is the osmotic pressure across the membrane. 16
Figure 2.3. Concentration profiles of ICP and ECP. The effective osmotic pressure difference is noted as $\Delta\pi_{eff}$, and the theoretically predicted osmotic pressure difference is noted as $\Delta\pi_{theory}$. Water flux is expected higher in PRO mode than in FO mode for asymmetric FO membranes. 19
Figure 2.4. Molecular structure of (a) cellulose triacetate (CTA) and (b) polyamide (PA). 28
Figure 3.1. XRD pattern of the synthesized LTA zeolite particles. 51
Figure 3.2. (a) The morphology of the LTA nanoparticles characterized by SEM and (b) the size distribution measured by DLS. 52
Figure 3.3. SEM images of the pristine PAN support. The top surface has a pore size of ~10 nm and the bottom surface has pore size up to 50 nm. The thickness is around 60 μm. 52
Figure 3.4. Schematic of layer-by-layer assembly of trilayer and bilayer membranes using polydopamine-treated PAN as a support. Only one trilayer or bilayer on each side of the support is shown for the sake of clarity. 53
Figure 3.5. SEM images of the top and bottom surfaces of membranes with different numbers of trilayers or bilayers. 55
Figure 3.6. FTIR spectra of (a) trilayer or bilayer membranes after each deposition step and (b) bilayer and trilayer membranes with different numbers of layers. 56
Figure 3.7. Surface elemental composition obtained by XPS analysis for the bottom surface of trilayer membranes. 58
Figure 3.8. (a) Mass of deposited PEI, LTA zeolite nanoparticles, and PAA within each deposition cycle during the LbL assembly of trilayer membranes, obtained by QCM-D measurement. (b) Weight percentage for LTA zeolite nanoparticles in the trilayer membranes. 60
Figure 3.9. (a) Water flux data for trilayer and bilayer membranes in FO and PRO modes. (b) Reverse solute flux data for trilayer and bilayer membranes in FO and PRO modes. 61
Figure 3.10. Water flux and reverse solute flux for trilayer membranes (with different last layers) in FO mode. The negatively charged surface (PAA) shows better membrane performance for its strong repulsive force to citrates. 63
Figure 3.11. (a)Water flux and (b)reverse solute flux for trilayer membranes using TSC or sucrose as draw solutes in FO mode. The two draw solutions generate a similar osmotic pressure according to the Morse equation. The water flux using sucrose as draw solutes is lower than that using TSC but the reverse solute flux is comparable. 64

Figure 3.12. Comparison of the performance of the 1-trilayer zeolite membrane and a commercial citrate triacetate (CTA) FO membrane in terms of (a)water flux and (b)TSC rejection..... 65
Figure 4.1. Membrane performance and the flux recovery rates of double-sided trilayer membranes (FO and PRO modes) and one-sided trilayer membrane (PRO mode) under (a, b) BSA or (c, d) alginate fouling. The one-sided membranes showed much less resistance to the organic foulants in PRO mode. 78
Figure 4.2. SEM images for both top and bottom surfaces of the (a, d) control PAN support and membranes coated with (b, e) 2 bilayers (smooth) or (c, f) 2 trilayers (rough). The multilayers can fully cover the pores of the support..... 79
Figure 4.3. (a) Membrane performance and (b) the flux recovery rates of double-sided trilayer membranes (FO and PRO modes) and one-sided trilayer membrane (PRO mode) under silica scaling. The LTA-embedded layers showed lower resistance to the silica scaling..... 80
Figure 4.4. (a) Membrane performance and (b) the flux recovery rates of bilayer and trilayer membranes under silica scaling (FO mode). The bilayers without LTA incorporation was almost free of silica scaling..... 81
Figure 4.5. (a) BSA and alginate fouling profiles and (b) the recovery rates on 2-bilayer and 2-trilayer membranes. The trilayer membranes performed similarly to the bilayer membranes in organic fouling experiments..... 82
Figure 4.6. Weight deposition of different foulants (alginate, BSA, and silica scaling) on 2 trilayers measured via QCM-D..... 83
Figure 5.1. A schematic drawing of the regenerating process that involves removal of the fouled layer by acid treatment and deposition of new polyelectrolyte layers..... 92
Figure 5.2. SEM images of the PSf support before and after different number of bilayers deposition. 94
Figure 5.3. FTIR spectra of (a) the polyelectrolyte membranes with different number of bilayers and (b) 2-bilayer and 4-bilayer membranes before and after acid treatment. 95
Figure 5.4. (a) Water flux and (b) reverse solute flux for the polyelectrolyte membranes with different number of bilayers (2, 4 or 6)..... 96
Figure 5.5. A schematic model of the proposed transport mechanism to explain the unique water flux behavior of (a) PSf-supported and (b) PAN-supported membranes. The effectiveness of each active layer is noted for different settings..... 98
Figure 5.6. SEM images for top and bottom surfaces of PSf support before and after 2-bilayer polyelectrolyte deposition. 99
Figure 5.7. The effects of acid treatment ranging between pH 3 and pH 2 on a 2-bilayer film coated on a QCM-D sensor. The mass (frequency) change was not obvious within such pH range..... 100
Figure 5.8. Mass deposition measured via QCM-D: (a) mass removal effect of acid on 2-bilayer film and (b)the regenerating process with constructing the new bilayer for 4 cycles..... 102
Figure 5.9. Cross-sectional SEM for 6-bilayer and 2-bilayer membranes to illustrate the reduced thickness of polyelectrolyte layer after acid treatment..... 103

Figure 5.10. (a)TEM images for a 2-bilayer film before and after acid treatment (pH 1) and (b) EDX spectrum of the treated sample. The Cu and Si came from the TEM copper grid and the detector. 106
Figure 5.11. (a)The pure water flux of the clean polyelectrolyte membranes treated by acid and regenerated for 3 cycles without fouling presence. (b)Water flux of the fouled and regenerated membranes for 3 cycles (c)An example of data collection in fouling experiments. All data were collected in FO mode, draw: 0.5M TSC, feed: 20 mM NaCl, 0.5 M $CaCl_2$, and 200 mg/L alginate for fouling experiments). 108
Figure 6.1. FTIR spectra of GA treatment on 2-bilayer and 2-trilayer membranes using (a) PAN or (b) PSf support. GA effects are more obvious in PAN-supported membranes. 123
Figure 6.2. Cross-sectional SEM images of 2 bilayers on (a) PAN and (b) PSf support. The estimated thickness of the active layers was noted in red bar. 124
Figure 6.3. (a)Mass addition from GA treatment. (b) the mass loss of 2-bialyer or 2-trialyer films in NaCl solutions measured by QCM-D. The sensors were soaked in each solution for 24 hours and then stabilized in pure water. All mass numbers were measured in pure water environment. 126
Figure 6.4. (a, b) Water flux and reverse solute flux for PAN-supported 2-bilayer and (c, d) for 2-trilayer membrane before and after GA treatment. 128
Figure 6.5. SEM image of bare silica nanoparticles. The nanoparticles have a diameter in range of 40-60 nm. 130
Figure 6.6. (a) Water flux and (b) reverse solute flux of trilayer silica membranes (PEI-Silica-PAA) before and after GA treatment. The trilayer membranes showed less response to the GA treatment. 130
Figure 6.7. SEM images of silica-embedded 1-trilayer and 2-trilayer (at different magnifications) membranes on the PAN support. 132
Figure 6.8. The mass deposition of silica trilayer on the QCM-D sensors. The second trilayer consists of a large amount of polyelectrolytes. 133
Figure 6.9. (a, b) Water flux and reverse solute flux for PSN-supported 2-bilayer and (c, d) for 2-trilayer membrane before and after GA treatment. The trilayer membranes showed less response to the GA treatment. 135
Figure 6.10. SEM images of 2 trilayer membranes supported by PAN or PSf (top surface). The PAN shows a more uniform surface morphology with particle-like features. 137
Figure 6.11. A schematic drawing of the transport behavior of trilayer membranes. 137
Figure 6.12. SEM images of the regular 2 trilayers of PEI-LTA-PAA and the new 2 trilayers of (PEI-LTA)×2-PAA on the PSf support. A more scattered particle distribution is observed in the new trilayer membrane. 140
Figure 6.13. (a) Water flux and (b) reverse solute flux of PSf-supported membrane with the trilayer of (PEI-LTA)×2-PAA deposited. This type of trilayer membrane shows a higher flux than the membrane with regular trilayers of PEI-LTA-PAA. This trilayer membranes also affected insignificantly by the GA treatment. 141

Chapter 1: Introduction

1.1 Background

Water scarcity is one of the most challenging issues that the whole world faces. The need for adequate and safe water has become even more intense because of population growth, industrialization, and continuous pollution due to human activities. The development of efficient and environmentally sustainable approaches to provide ample water is in high priority. Membrane technology has been recognized as one of the most effective approaches to addressing the global water scarcity problem since decades ago. Various membrane-related processes, such as reverse osmosis (RO), nanofiltration (NF), ultrafiltration (UF) and forward osmosis (FO), are of great importance and have been widely used, because of their capability to effectively purify nontraditional water sources.[1-4]

In addition, the FO and its relative pressure-retarded osmosis (PRO) are particularly interesting. Unlike the other processes (RO/NF/UF) that require tremendous input of physical pressure and energy, the FO and PRO processes take advantages of osmotic pressure created by the concentration or chemical gradients between two solutions (namely draw and feed). Therefore, these processes could utilize alternative energy sources to purify water. Given the fact that sufficient energy supply is also a challenging issue, this energy-saving advantage of the FO and PRO processes may play an important role in the water treatment and purification industry in near future.[5-7]

A typical FO membrane is semi-permeable and consists of two parts: a dense, thin (< 200 nm) active layer that acts as the main separation barrier and one or more porous layers that are mechanically strong to support the active layer. Both of the active layer and the support of the FO membranes are required to have reasonable chemical stability, high permeability to water, and good fouling resistance. At the current stage, two types of membranes, the active layers of which are made of polyamide (PA) and cellulose triacetate (CTA), are the most commonly used.[8-14] In addition to these two types of membranes, membranes with an active layer that is composed of polyelectrolytes have also been proved effective in composing a FO membrane.[15-18] Nevertheless, studies with an emphasis on the polyelectrolyte membranes for FO processes are still limited. Many unique properties of polyelectrolyte have not been fully exploited yet for FO/PRO membranes. Generally, polyelectrolyte layers for FO membranes are fabricated via a layer-by-layer technique in aqueous solution. This approach is facile, versatile and environmental-friendly. Thus, the polyelectrolyte membrane may be possibly tuned to fit in many applications.[19-21]

The current FO membranes still have difficulties in achieving high water permeability and require further improvements. [6, 7] With the rapid advances in nanotechnology, membranes for water treatment have been benefited extensively in a diverse way.[22-29] Among all the nanomaterials, zeolite has shown many unprecedented properties that can largely enhance membrane performance for water purification.[11, 22, 23, 30-37] Improvements on membranes have been long performed in numerous ways. Zeolites are one type of the materials that have drawn significant interests. Zeolites are well-defined frameworks of aluminosilicates with interconnected pores in sub-nano

dimensions. A continuous zeolite film can effectively reject small molecules but allow fast transport of water molecules.[31, 38-40] Membranes made of pure zeolite crystals are typically very brittle and have little flexibility, which is detrimental to membrane separation performance in the real world operation. Embedding zeolites into polymeric FO membranes is a more practical approach, but only few studies have focused on zeolite-embedded FO membranes. Moreover, only a small loading of zeolite is incorporated in these studies. [23, 37] The benefits of zeolite embedding in this scenario may be limited. Hence, there is a need to achieve a high loading of zeolite to further examine its effectiveness and to maximize benefits.

Furthermore, fouling is a universal issue for membranes. There are four types of major fouling processes: organic, inorganic, biological and colloidal.[41] Numerous studies focus on improving fouling resistance of membranes, but the study on zeolite-embedded membranes is much less comprehensive. Research is needed, therefore, to understand the effects of different foulants on zeolite-embedded composite membranes. Additionally, some unique characteristics of polyelectrolytes can be further utilized in mitigating membrane fouling. One example is to regenerate the polyelectrolyte layers by taking the advantages of a simple and versatile layer-by-layer method. This application can be hardly achieved on the conventional PA and CTA membranes. The regeneration process of polyelectrolyte membranes has been already demonstrated for filtration membrane systems, but no reports have been given for FO membranes.[42-44] Therefore, there is a need to extend the scope of regenerable polyelectrolyte membranes in the FO applications.

1.2 Objectives

The main purpose of this work is to demonstrate that achieving a high loading of zeolite nanoparticles in layer-by-layer assembled polyelectrolytes can result in a high-performance composite membrane. Two module polyelectrolytes, poly(acrylic acid) (PAA) and polyethyleneimine (PEI), are used to demonstrate this work. The zeolite nanoparticles used for demonstration is Linde Type A (LTA), one of the most common and important zeolites. The main hypothesis is that these two weak polyelectrolytes can also provide electrostatic attractions to hold zeolite nanoparticles and can be further crosslinked or regenerated using their chemically reactive functional groups.

Specific objectives for this work:

Objective I: To synthesize a membrane using PEI and PAA via layer-by-layer assembly with and without LTA nanoparticles embedded between the polyelectrolyte layers to make a composite membrane.

Objective II: To evaluate the FO performance of LTA-embedded membranes by comparing with the LTA-free polyelectrolyte membranes.

Objective III: To investigate the fouling behaviors of the LTA-embedded composite and LTA-free polyelectrolyte membranes under different module foulants.

Objective IV: To study the regenerability of the active layer of the polyelectrolyte membrane by deconstructing and rebuilding polyelectrolyte layers for fouling control.

Objective V: To examine the effects of polyelectrolyte crosslinking on the performance of LTA-embedded composite membrane.

1.3 Research Structure

In general, the physiochemical properties of the proposed membranes have been evaluated using different characterization tools, including Fourier transform infrared spectroscopy (FTIR), scanning electron microscopy (SEM), X-ray photoelectron spectroscopy (XPS), quartz crystal microbalance with dissipation (QCM-D) and transmission electron microscopy (TEM). Membrane performance and fouling tests have been conducted using a lab-scale FO system. Figure 1.1 gives a schematic overview of the main tasks in this dissertation. Briefly, the tasks include synthesis of LTA-embedded and LTA-free polyelectrolyte membranes, validation of LTA incorporation, test of membrane performance and fouling behaviors in FO process, evaluation of membrane regenerability and investigation on effects of crosslinking. The regenerability was only tested on zeolite-free polyelectrolyte membranes by assuming a similarity between the two types of the membranes in regenerating process.

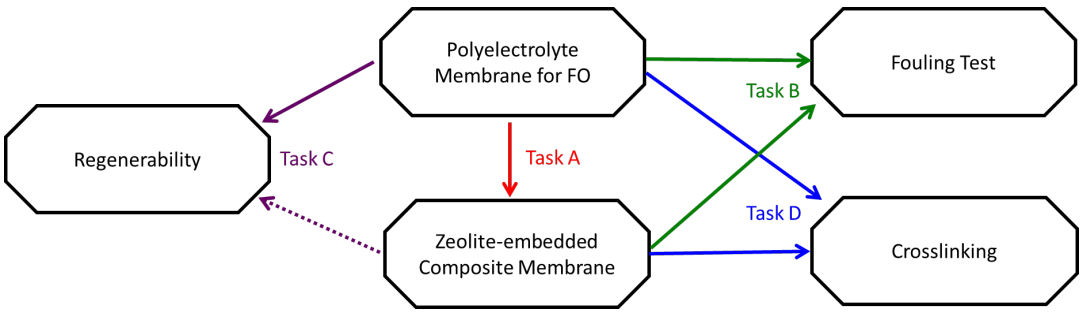

Figure 1.1. Overview of research tasks with solid arrows representing the focus of this dissertation.

1.4 Dissertation Organization

This dissertation is composed of eight chapters. In addition to this introduction, the remaining seven chapters are briefly described as follows (Chapter 3-6 are present in journal manuscript format):

Chapter 2: A literature review is summarized on the historic achievements and current developments regarding the FO membrane process.

Chapter 3: The synthesis of polyelectrolyte-zeolite composite membranes is described. Multiple characterization tools have been employed to validate the success of zeolite embedding. The membrane performance has also been evaluated in a lab-scale FO system and compared with zeolite-free polyelectrolyte membranes.

Chapter 4: The membrane behaviors in the presence of organic foulants and silica scaling are included in this chapter. Both the zeolite-free and zeolite-embedded polyelectrolyte membranes have been evaluated and compared under fouling conditions. The comparison of fouling behaviors between one-sided and double-sided coating of polyelectrolyte layers are also discussed.

Chapter 5: The membrane regenerability of the polyelectrolyte membrane without zeolite incorporation in FO process is explored. Strong acid has been used to trigger the delaminating of the active polyelectrolyte layer. The regenerating process has been understood by characterizing the membranes via various tools.

Chapter 6: The performance of the composite membrane after crosslinking is present in this chapter. The membrane performance has been found varied when using different support layers and the possible reasons have been discussed.

Chapter 7: Major findings in this study on the polyelectrolyte-zeolite composite membranes have been summarized in this chapter.

Chapter 8: This chapter concludes the implications from this work and identifies the possible topics for future research.

1.5 References

1. Montgomery, M. A.; Elimelech, M., Water and sanitation in developing countries: Including health in the equation. *Environ Sci Technol* **2007,** *41*, (1), 17-24.

2. Elimelech, M.; Phillip, W. A., The Future of Seawater Desalination: Energy, Technology, and the Environment. *Science* **2011,** *333*, (6043), 712-717.

3. Penate, B.; Garcia-Rodriguez, L., Current trends and future prospects in the design of seawater reverse osmosis desalination technology. *Desalination* **2012,** *284*, 1-8.

4. Shannon, M. A.; Bohn, P. W.; Elimelech, M.; Georgiadis, J. G.; Marinas, B. J.; Mayes, A. M., Science and technology for water purification in the coming decades. *Nature* **2008,** *452*, (7185), 301-310.

5. Cath, T. Y.; Childress, A. E.; Elimelech, M., Forward osmosis: Principles, applications, and recent developments. *J Membrane Sci* **2006,** *281*, (1-2), 70-87.

6. Zhao, S. F.; Zou, L.; Tang, C. Y. Y.; Mulcahy, D., Recent developments in forward osmosis: Opportunities and challenges. *J Membrane Sci* **2012,** *396*, 1-21.

7. Alsvik, I. L.; Hagg, M. B., Pressure Retarded Osmosis and Forward Osmosis Membranes: Materials and Methods. *Polymers-Basel* **2013,** *5*, (1), 303-327.

8. Su, J. C.; Yang, Q.; Teo, J. F.; Chung, T. S., Cellulose acetate nanofiltration hollow fiber membranes for forward osmosis processes. *J Membrane Sci* **2010,** *355*, (1-2), 36-44.

9. Tiraferri, A.; Yip, N. Y.; Phillip, W. A.; Schiffman, J. D.; Elimelech, M., Relating performance of thin-film composite forward osmosis membranes to support layer formation and structure. *J Membrane Sci* **2011,** *367*, (1-2), 340-352.

10. Yip, N. Y.; Tiraferri, A.; Phillip, W. A.; Schiffman, J. D.; Elimelech, M., High Performance Thin-Film Composite Forward Osmosis Membrane. *Environ Sci Technol* **2010,** *44*, (10), 3812-3818.

11. Wei, J.; Qiu, C. Q.; Tang, C. Y. Y.; Wang, R.; Fane, A. G., Synthesis and characterization of flat-sheet thin film composite forward osmosis membranes. *J Membrane Sci* **2011,** *372*, (1-2), 292-302.

12. Li, Z. Y.; Yangali-Quintanilla, V.; Valladares-Linares, R.; Li, Q. Y.; Zhan, T.; Amy, G., Flux patterns and membrane fouling propensity during desalination of seawater by forward osmosis. *Water Res* **2012,** *46*, (1), 195-204.

13. Gu, J. E.; Lee, S.; Stafford, C. M.; Lee, J. S.; Choi, W.; Kim, B. Y.; Baek, K. Y.; Chan, E. P.; Chung, J. Y.; Bang, J.; Lee, J. H., Molecular Layer-by-Layer Assembled Thin-Film Composite Membranes for Water Desalination. *Adv Mater* **2013,** *25*, (34), 4778-4782.

14. Sun, Y. N.; Xue, L. X.; Zhang, Y. J.; Zhao, X. L.; Huang, Y.; Du, X. D., High flux polyamide thin film composite forward osmosis membranes prepared from porous substrates made of polysulfone and polyethersulfone blends. *Desalination* **2014,** *336*, 72-79.

15. Qiu, C. Q.; Qi, S. R.; Tang, C. Y. Y., Synthesis of high flux forward osmosis membranes by chemically crosslinked layer-by-layer polyelectrolytes. *J Membrane Sci* **2011,** *381*, (1-2), 74-80.

16. Saren, Q.; Qiu, C. Q.; Tang, C. Y. Y., Synthesis and Characterization of Novel Forward Osmosis Membranes based on Layer-by-Layer Assembly. *Environ Sci Technol* **2011,** *45*, (12), 5201-5208.

17. Qi, S. R.; Qiu, C. Q.; Zhao, Y.; Tang, C. Y. Y., Double-skinned forward osmosis membranes based on layer-by-layer assembly-FO performance and fouling behavior. *J Membrane Sci* **2012,** *405*, 20-29.

18. Duong, P. H. H.; Zuo, J.; Chung, T. S., Highly crosslinked layer-by-layer polyelectrolyte FO membranes: Understanding effects of salt concentration and deposition time on FO performance. *J Membrane Sci* **2013,** *427*, 411-421.

19. Bertrand, P.; Jonas, A.; Laschewsky, A.; Legras, R., Ultrathin polymer coatings by complexation of polyelectrolytes at interfaces: suitable materials, structure and properties. *Macromol Rapid Comm* **2000,** *21*, (7), 319-348.

20. Tang, Z. Y.; Wang, Y.; Podsiadlo, P.; Kotov, N. A., Biomedical applications of layer-by-layer assembly: From biomimetics to tissue engineering. *Adv Mater* **2006,** *18*, (24), 3203-3224.

21. Ariga, K.; Hill, J. P.; Ji, Q. M., Layer-by-layer assembly as a versatile bottom-up nanofabrication technique for exploratory research and realistic application. *Phys Chem Chem Phys* **2007,** *9*, (19), 2319-2340.

22. Lind, M. L.; Jeong, B. H.; Subramani, A.; Huang, X. F.; Hoek, E. M. V., Effect of mobile cation on zeolite-polyamide thin film nanocomposite membranes. *J Mater Res* **2009,** *24*, (5), 1624-1631.

23. Jeong, B. H.; Hoek, E. M. V.; Yan, Y. S.; Subramani, A.; Huang, X. F.; Hurwitz, G.; Ghosh, A. K.; Jawor, A., Interfacial polymerization of thin film nanocomposites: A new concept for reverse osmosis membranes. *J Membrane Sci* **2007,** *294*, (1-2), 1-7.

24. Tiraferri, A.; Kang, Y.; Giannelis, E. P.; Elimelech, M., Superhydrophilic Thin-Film Composite Forward Osmosis Membranes for Organic Fouling Control: Fouling Behavior and Antifouling Mechanisms. *Environ Sci Technol* **2012,** *46*, (20), 11135-11144.

25. Bui, N. N.; McCutcheon, J. R., Hydrophilic Nanofibers as New Supports for Thin Film Composite Membranes for Engineered Osmosis. *Environ Sci Technol* **2013,** *47*, (3), 1761-1769.

26. Hu, M.; Mi, B., Enabling Graphene Oxide Nanosheets as Water Separation Membranes. *Environ Sci Technol* **2013,** *47*, (8), 3715-3723.

27. Liu, Y.; Rosenfield, E.; Hu, M.; Mi, B., Direct observation of bacterial deposition on and detachment from nanocomposite membranes embedded with silver nanoparticles. *Water Res* **2013,** *47*, (9), 2949-2958.

28. Perreault, F.; Tousley, M. E.; Elimelech, M., Thin-Film Composite Polyamide Membranes Functionalized with Biocidal Graphene Oxide Nanosheets. *Environmental Science & Technology Letters* **2013,** *1*, 71-76.

29. Gao, Y.; Hu, M.; Mi, B. X., Membrane surface modification with TiO2-graphene oxide for enhanced photocatalytic performance. *J Membrane Sci* **2014,** *455*, 349-356.

30. Fu, Y. J.; Hu, C. C.; Lee, K. R.; Lai, J. Y., Separation of ethanol/water mixtures by pervaporation through zeolite-filled polysulfone membrane containing 3-aminopropyltrimethoxysilane. *Desalination* **2006,** *193*, (1-3), 119-128.

31. Kazemimoghadam, M.; Mohammadi, T., Synthesis of MFI zeolite membranes for water desalination. *Desalination* **2007,** *206*, (1-3), 547-553.

32. Lind, M. L.; Ghosh, A. K.; Jawor, A.; Huang, X. F.; Hou, W.; Yang, Y.; Hoek, E. M. V., Influence of Zeolite Crystal Size on Zeolite-Polyamide Thin Film Nanocomposite Membranes. *Langmuir* **2009,** *25*, (17), 10139-10145.

33. Kong, C. L.; Shintani, T.; Tsuru, T., "Pre-seeding"-assisted synthesis of a high performance polyamide-zeolite nanocomposite membrane for water purification. *New J Chem* **2010,** *34*, (10), 2101-2104.

34. Dong, H.; Qu, X. Y.; Zhang, L.; Cheng, L. H.; Chen, H. L.; Gao, C. J., Preparation and characterization of surface-modified zeolite-polyamide thin film nanocomposite membranes for desalination. *Desalin Water Treat* **2011,** *34*, (1-3), 6-12.

35. Fathizadeh, M.; Aroujalian, A.; Raisi, A., Effect of added NaX nano-zeolite into polyamide as a top thin layer of membrane on water flux and salt rejection in a reverse osmosis process. *J Membrane Sci* **2011,** *375*, (1-2), 88-95.

36. Ivan, A.; Ghindeanu, D. L.; Danciulescu, V.; Raducu, A.; Nechifor, A. C., Composite polyaniline-zeolite membrane material for wastewater ultrafiltration. *Optoelectron Adv Mat* **2012,** *6*, (11-12), 1134-1138.

37. Ma, N.; Wei, J.; Liao, R. H.; Tang, C. Y. Y., Zeolite-polyamide thin film nanocomposite membranes: Towards enhanced performance for forward osmosis. *J Membrane Sci* **2012,** *405*, 149-157.

38. Davis, M. E.; Lobo, R. F., Zeolite and Molecular-Sieve Synthesis. *Chem Mater* **1992,** *4*, (4), 756-768.

39. Li, L. X.; Dong, J. H.; Nenoff, T. M.; Lee, R., Desalination by reverse osmosis using MFI zeolite membranes. *J Membrane Sci* **2004,** *243*, (1-2), 401-404.

40. Duke, M. C.; O'Brien-Abraham, J.; Milne, N.; Zhu, B.; Lin, J. Y. S.; da Costa, J. C. D., Seawater desalination performance of MFI type membranes made by secondary growth. *Sep Purif Technol* **2009,** *68*, (3), 343-350.

41. Guo, W. S.; Ngo, H. H.; Li, J. X., A mini-review on membrane fouling. *Bioresource Technol* **2012,** *122*, 27-34.

42. Pejman Ahmadiannamini, M. L. B., Volodymyr V. Tarabara, Sacrificial polyelectrolyte multilayer coatings as an approach to membrane fouling control: Disassembly and regeneration mechanisms. *J Membrane Sci* **2015,** *491*, 10.

43. Irigoyen, J.; Politakos, N.; Murray, R.; Moya, S. E., Design and Fabrication of Regenerable Polyelectrolyte Multilayers for Applications in Foulant Removal. *Macromol Chem Phys* **2014,** *215*, (16), 1543-1550.

44. Shazia Ilyas, J. d. G., Kitty Nijmeijer, Wiebe M. de Vos, Multifunctional polyelectrolyte multilayers as nanofiltration membranes and as sacrificial layers for easy membrane cleaning. *Journal of Colloid and Interface Science* **2015,** *446*, 8.

Chapter 2: Literature Review

2.1 Forward Osmosis (FO) Process

Osmosis is a physical process that describes the spontaneous net movement of solvent molecules (water in most cases) through a selectively permeable membrane when a concentration gradient is present across the membrane. The osmotic pressure generated on the two sides of the membrane is in positive relationship with the concentration gradient. The osmosis process exists everywhere. In biological systems, osmosis is a vital process: the cells of most organisms will be dehydrated when exposed in saline environments, given that biological membranes are semipermeable. The osmosis phenomenon has been discovered and utilized since the early days. People once used salt to desiccate food for long-term preservation. Up to now, the osmosis phenomenon has been extended to a wide range of applications such as water treatment, power generation, food processing, drug delivery and many other novel processes.[1-8] This dissertation will mainly focus on forward osmosis (FO) process through polymeric membranes for water treatment and desalination.

Nowadays, reverse osmosis (RO) is still a more common process in the field of water treatment and desalination. Similarly to conventional filtration processes, the RO uses hydraulic pressure to oppose the osmotic pressure between a retentate (or concentrate which refers to the aqueous solution that needs to be treated or purified) and a permeate (or filtrate which refers to the treated or purified water). The applied pressure in the RO process is required to be greater than the osmotic pressure caused

by the concentration gradient between the retentate and the permeate to generate net water flux. Comparatively, the FO process utilizes the osmotic pressure rather than counter it. The main advantages of the FO include a lower demand on energy and a less propensity of membrane fouling. A schematic diagram of the FO process is illustrated in (Figure 2.1). Water can transport spontaneously from a solution feed (low concentration side) to a draw solution (high concentration side).

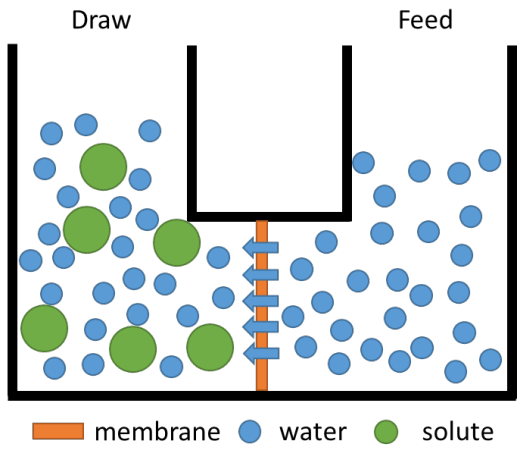

Figure 2.1. Schematic diagram of the FO process. Water can spontaneously transport from the feed to the draw.

The driving force in the FO process is the solute concentration difference across the membrane, which allows transport of water molecules but retain most solute molecules or ions on one side. The osmotic pressure in an aqueous solution with low solute concentration can be approximately estimated using Morse equation (Equation 1):

$$\pi = nCRT \quad \text{(Equation 1)}$$

where π is the osmotic pressure, n is the dimensionless van't Hoff factor, C is the molar concentration of the solutes, R is the gas constant, and T is the thermodynamic (absolute) temperature. The water flux can be generally described using the following equation (Equation 2):

$$J_w = A(\Delta\pi - \Delta p) \quad \text{(Equation 2)}$$

where J_w is the water flux across the membrane, A is the water permeability constant Δp is the external (hydraulic) pressure applied, and Δπ is the osmotic pressure difference across the membrane.

In the case of FO, Δp is zero. For RO, Δp is greater than Δπ. There is another type of processes called pressure-retarded osmosis (PRO), in which Δp is greater than zero but smaller than Δπ. In this scenario, hydraulic pressure is still applied in the opposite direction of the osmotic pressure gradient (similar to RO), but the applied pressure is smaller than the osmotic pressure so the net water flux is still from the feed solution to the concentrated draw solution. This applied pressure can be converted for power generation or other purposes. A schematic diagram of FO, PRO, and RO processes is illustrated in Figure 2.2.

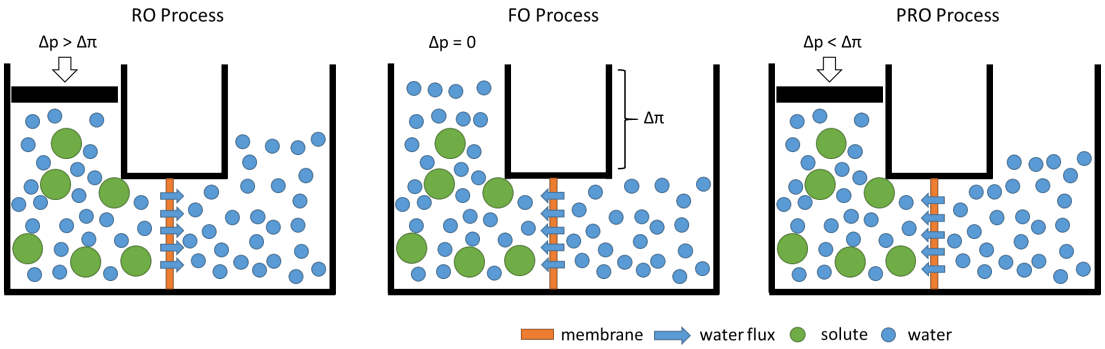

Figure 2.2. Schematic diagram of RO ($\Delta p > \Delta \pi$), FO ($\Delta p = 0$) and PRO ($\Delta p < \Delta \pi$) processes. Δp is the external (hydraulic) pressure applied and $\Delta \pi$ is the osmotic pressure across the membrane.

Ideally, the semi-permeable membranes can prevent any mass transport (unwanted solutes) except water molecules. However, in real operation the solutes in draw solution (or in the retentate for RO) will gradually diffuse through the membrane, dramatically lowering the quality of the treated water. Likewise, a solute permeability coefficient of the membrane is introduced to describe the reverse solute transport. The solute permeability coefficient is commonly determined using Equation 3 and from RO-type experiments:

$$B = \frac{(1-R)A(\Delta p - \Delta \pi)}{R} \qquad \text{(Equation 3)}$$

where B is the solute permeability coefficient and R is the salt rejection. The most frequently used FO membranes are made of polyamide or cellulose triacetate. Their rejection to sodium chloride can reach more than 99%.

2.2 Concentration Polarization

In real FO and PRO operations, the water flux observed is much less than expected using Equation 1, even for having draw solution at low concentrations.[4, 9-11] In other words, the real osmotic pressure difference across the membrane is much lower than the difference between the two bulk solutions. Also for RO, the water flux at a certain hydraulic pressure is much lower than theoretical prediction. This lower-than-expected water flux (or osmotic pressure) is mainly attributed to phenomena called concentration polarization (CP).

2.2.1 External Concentration Polarization

In RO or other pressure-driven membrane processes, solutes build up at the retentate side near the membrane, giving a higher solute concentration than that in bulk solution. The applied hydraulic pressure has to overcome the resulting osmotic pressure from the increased solute concentration which essentially leads to the tremendous cost of RO operation.[12, 13] In FO and PRO operations, the water comes from the feed side dilutes the draw side near the membrane, causing a lower osmotic pressure for driving water transport. These phenomena are usually called external concentration polarization (ECP). For RO, it may refer to concentrative ECP while for FO and PRO it may indicate dilutive ECP. The fouling induced by ECP in FO and PRO processes is found to be slightly less intensive in comparison with its effects in RO. The concentrative and dilutive ECP can be minimized by creating flow and turbulence at the membrane surface or by manipulating the water flux. According to

some recent modeling and simulations, the ECP has been found to play a minor role in leading to the lower-than-expected water flux in FO and PRO processes.[11]

2.2.2 Internal Concentration Polarization

Most FO membranes are asymmetric and behave in a more complex way. Internal concentration polarization (ICP) is generally accepted as the main reason for the lower-than-expected water flux in FO and PRO processes. An asymmetric FO membrane typically has two parts: a dense and thin active layer with solute selectivity and one or more porous support layers. The ICP phenomenon can happen in both active layer and support layer but is more predominant in the thick support layer. When the porous membrane support layer faces the draw solution (FO mode), the draw solution within the support layer becomes diluted and the net concentration gradient across the active layer is reduced. This is noted as dilutive ICP.[11] If the support layer faces the feed solution (PRO mode), the diffusing solutes stay within the support layer and result in the less concentration gradient across the active layer. This is noted as concentrative ICP, which is similar to the concentrative ECP except that it occurs inside the porous support layer.[11]

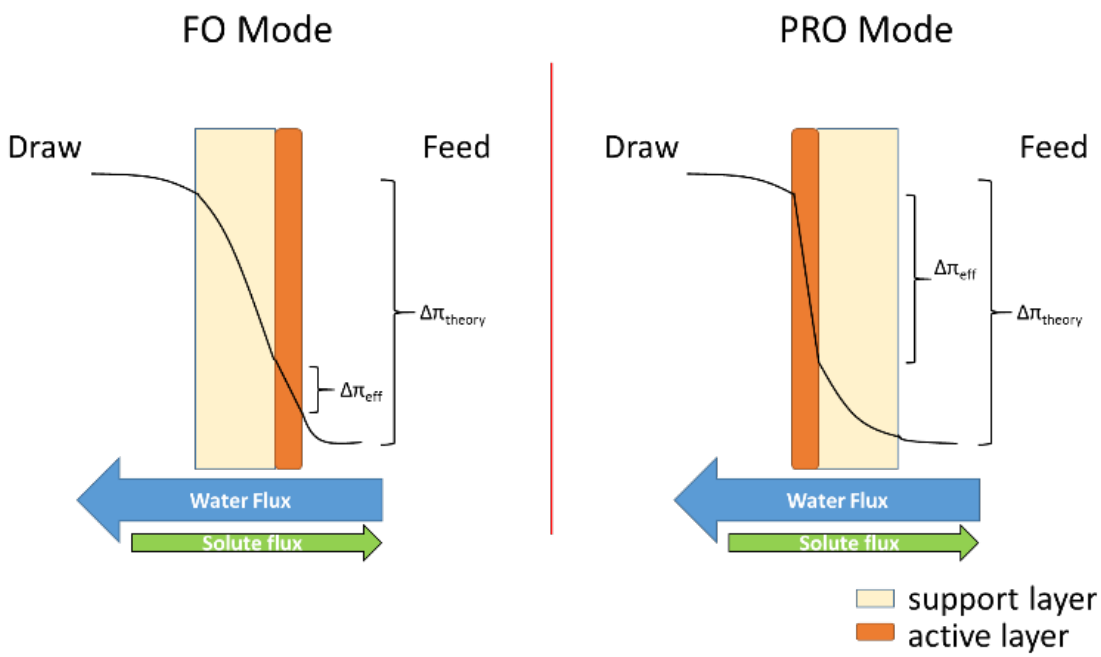

Figure 2.3. Concentration profiles of ICP and ECP. The effective osmotic pressure difference is noted as $\Delta\pi_{eff}$, and the theoretically predicted osmotic pressure difference is noted as $\Delta\pi_{theory}$. Water flux is expected higher in PRO mode than in FO mode for asymmetric FO membranes.

Figure 2.3 presents the concentration profiles affected by ICP and ECP in FO and PRO operations. ECP is usually negligible compared with ICP. For ICP, it can be obviously seen that the effective osmotic pressure difference ($\Delta\pi_{eff}$) is much less than the osmotic pressure difference based on theoretical prediction ($\Delta\pi_{theory}$), especially for FO mode. The ICP is difficult to be minimized by creating flow and turbulence as it takes place within the porous support layer.

2.2.3 Modeling of Concentration Polarization

A mode for ECP has been firstly brought using boundary layer thin film theory.[14, 15] The general equation for describing the CP in RO is expressed in Equation 4:

$$\frac{C_r}{C_p} = \exp\left(\frac{J_w}{k}\right) \qquad \text{(Equation 4)}$$

where J_w is the water flux, k is the mass transfer coefficient, C_r is the concentration of the retentate and C_p is the concentration of permeate. The mass transfer coefficient (k) can be calculated using Sherwood number (Sh), solute diffusion coefficient (D) and hydraulic diameter (D_h):

$$k = \frac{ShD}{D_h} \qquad \text{(Equation 5)}$$

In FO, the feed solution concentration is usually low, so Equation 4 can be replaced by the osmotic pressure of the feed solution at the membrane surface ($\pi_{f,m}$) and in the bulk ($\pi_{f,b}$), as expressed in Equation 6:

$$\frac{\pi_{f,m}}{\pi_{f,b}} = \exp\left(\frac{J_w}{k_{feed}}\right) \qquad \text{(Equation 6)}$$

where k_{feed} is the mass transfer coefficient on the feed side. Likewise, the ECP effect on the draw side can be estimated using (Equation 7):

$$\frac{\pi_{d,m}}{\pi_{d,b}} = \exp\left(-\frac{J_w}{k_{draw}}\right) \qquad \text{(Equation 7)}$$

where k_{draw} is the mass transfer coefficient on the draw side, $\pi_{d,m}$ and $\pi_{d,b}$ are the osmotic pressure of the draw solution at the membrane surface and in the bulk, respectively. In FO mode where there is no hydraulic pressure, Equation 8 can be obtained by substituting the effective osmotic pressure of the draw and feed solutions in Equation 6 and Equation 7 into Equation 2:

$$J_w = A\left[\pi_{d,b} exp\left(-\frac{J_w}{k_{draw}}\right) - \pi_{f,b} exp\left(\frac{J_w}{k_{feed}}\right)\right] \qquad \text{(Equation 8)}$$

In this equation, both concentrative and dilutive ECP has been considered. This model assumes that (1) the mass transfer coefficients on the feed and draw sides are different, (2) the feed and draw concentrations are relatively low and (3) the membrane is asymmetric. These assumptions limit the suitability of the model.
The ICP phenomena have been adapted and modeled for asymmetric membranes following a similar approach.[16] When the membrane support layer faces the draw solution (FO mode), the dilutive ICP can be described as:

$$J_w = \frac{1}{K} ln \frac{A\pi_{d,b}+B}{A\pi_{f,b}+B+J_w} \qquad \text{(Equation 9)}$$

where K is the resistance to solute diffusion within the membrane porous support layer defined as:

$$K = \frac{t\tau}{\varepsilon D_s} \qquad \text{(Equation 10)}$$

where t, τ and ε are the thickness, tortuosity, and porosity of the membrane, and D_s is the diffusion coefficient of the solute.[17] Note that t, τ and ε indicate the membrane structural information and are often used for evaluating membranes. When the membrane orientates in the other way (PRO mode), Equation 9 can be rewritten to the following form:

$$J_w = \frac{1}{K} ln \frac{A\pi_{d,b} + B - J_w}{A\pi_{f,b} + B} \qquad \text{(Equation 11)}$$

Because both ECP and ICP occur simultaneously, an overall equation has been developed, which is shown as:

$$J_w = A[\pi_{d,b} exp(-J_w K) - \pi_{f,b} exp\left(\frac{J_w}{k}\right)] \qquad \text{(Equation 12)}$$

$$J_w = A[\pi_{d,b} expexp\left(-\frac{J_w}{k}\right) - \pi_{f,b}(-J_w K)] \qquad \text{(Equation 13)}$$

where Equation 12 is for FO mode and Equation 13 is for PRO mode.[14, 15]

The model discussed above still have some limitations. For instance, it would over-estimate the water flux when the draw solution concentration is high. Some modified models with complexities have been developed.[18, 19] Also, a few modeling techniques such as the finite element method[20, 21], computational fluid dynamics[22] and numerical

simulation[23] have been used for investigating the CP phenomena. The modeling and simulation for FO processes are still ongoing and significantly benefit the society for evaluating FO membranes and adjusting operation conditions.

2.3 Membrane Fouling

Membrane fouling describes the accumulation of foreign substances on the membrane surfaces or in the membrane pores that lowers water production and quality. Membrane fouling is also an inevitable phenomenon in all membrane processes. As in pressure-driven membrane systems (RO, MF, UF etc.), a common operation protocol is to control the trans-membrane pressure to achieve a constant permeate flux. The pressure required to maintain such a constant flux dramatically increases when the membrane fouling occurs. This essentially shortens membrane life and causes additional maintenance costs.

2.3.1 Types of Fouling

The membrane fouling is caused by complex and combined physical and chemical interactions between the membrane surface and the various foulants in the feed solution in a FO process (or the retentate solution in RO). The fouling behavior has been demonstrated highly affected by the solution chemistry (pH, ionic strength, etc.), composition, membrane properties (material, surface morphology, surface charge, hydrophobicity, etc.) and even operation conditions.[24, 25] In general, the membrane fouling can be classified into four different groups according to the causing foulants: colloidal, organic, inorganic and micro-biological.

Colloidal fouling is mainly led by particulates and particles with a size range from a few nanometers to a few micrometers in waters and wastewaters. The examples of particulates and particles are clay minerals, colloidal silica and sulfur, precipitated crystals, iron and aluminum compounds and some undissolved large molecules (e.g. polysaccharide, peptidoglycans, and proteins). Generally, the colloidal fouling is considered attributed to pore blocking, which is typically followed by a cake layer formation.[26] A cake compression usually happens after the cake formation, which make the overall situation even worse.[27] The colloidal fouling can also contribute to a severer concentration polarization, because the accumulation of matters on top of the membrane surface increases the concentration gradient that opposes the direction of water flow.

Organic fouling refers to the adsorption of organic matters which are naturally present in surface water or are synthetic and added from human activities.[28] Because most of the membranes are made of polymers, they usually show good affinity to organic foulants.[29] A hydrophilic charged surface is believed to have the least fouling potential.[30, 31] Similar to the colloidal foulants, the organic foulants can adsorb in the membrane pores, block the water transport and then form a gel layer. Organic matters that have chemical functionalities and deformability may bind particles and other foulants together, resulting in a firm and stable layer.

Inorganic fouling usually indicates the precipitation of inorganic matters due to some hydrolysis and oxidation reactions. Inorganic fouling sometimes refers to mineral scaling, which has different mechanisms compared with the substance deposition and adsorption in colloidal or organic fouling. Crystallization is one of the major

mechanisms that make the mineral scale. In such a process, deposition occurs due to a higher-than-solubility concentration of ions in the vicinity of the membrane surface. Another major mechanism of deposition is caused by inverse solubility of inorganic salts, which is similar to crystallization, in convective transportation of inorganic matters.[32, 33] Typical compounds commonly seen with a low solubility are carbonate ($CaCO_3$), barium sulfate ($BaSO_4$), silica (SiO_2) and gypsum ($CaSO_4$).[34]

Last but not the least, biofouling accounts for many serious operational problems in membrane processes. The membrane is an ideal place for many microorganisms to propagate. The accumulation of microorganisms at the membrane surface is generally considered to involve surface conditioning, attachment of pioneer planktonic cell, formation of microcolonies and thus a development of mature biofilms. The biofilm can be either uniform or not and usually contains multiple layers of living and dead microorganisms and their extracellular products.[35, 36] Although the microorganisms require certain mild condition to survive, the hydrophobic membrane surface unfortunately meet such demand.[37] The microorganisms can grow, multiply and even relocate on the membrane surface while they are living, which can vastly deteriorate the membrane performance in a short time.

2.3.2 Fouling Recovery and Membrane Regeneration

Membrane fouling can be classified as reversible fouling and irreversible fouling, which are recognized by the cleaning efficiency on the fouled membranes. In general, if the fouling can be removed by physical membrane cleaning process, it is usually considered reversible, and if not, then irreversible. A typical way of membrane

cleaning the membrane is to flush the surface using water and chemicals. In pressure-driven membrane processes, backwashing is frequently used that applies hydraulic pressure to the permeate side from a normal operation. In most cases, reversible fouling can be removed through appropriate washing protocol and the membrane can be restored. However, it may sometimes require heavy chemical cleaning, which can degrade the membrane integrity and create defects on the membrane surface. When irreversible fouling happens, the water production reduces dramatically and the membrane has to be replaced. There are many studies working on the cleaning protocols and selection of rinsing chemicals to get rid of as much fouling as possible.[38-42]

On the other hand, one way to mitigate fouling and extend the membrane lifetime is to do the onsite regeneration. This idea has been given extensive attention recently.[43-45] The concept involves controllably delaminating the active layer after the membrane is fouled and then reconstruct the active layer to make the membrane back to functional again. The delaminating step is usually triggered by a special condition and then the foulants are eliminated together with the delaminated part. This process has great potential in dealing with irreversible fouling and may reduce the costs generated in membrane replacement by onsite membrane regeneration.

2.4 Current Development of FO Membranes

2.4.1 Membrane Materials

FO technology still suffers from some major challenges. The first challenge is to find the suitable membranes. In the early time people tried all kinds of materials for

separation purposes, such as bladders of animals, collodion, rubber, porcelain and many other materials that were available to them. Modern membranes for RO had been experimented and developed in 1960s and then asymmetric aromatic polyamide (PA) membranes were largely implemented in industrial membrane process.[16] In the 1970s, researchers found that they could only achieve a much lower than expected flux no matter how the membranes were designed (flat sheet or tubular). At the same time, researchers started to use cellulose acetate hollow fiber membranes for treating wastewater using FO processes. Meanwhile, people started to use RO experiments to predict the FO performance of membranes. In 1990s, Osmotek Inc. (Albany, Oregon) (currently Hydration Technologies Inc.) had developed their cellulose triacetate (CTA) membrane and demonstrated its suitability in many commercial applications of water purification. The molecular structures of PA and CTA are shown in (Figure 2.4). Unlike the PA membranes or other RO membranes, which consist of a very thin active layer (several hundreds of nanometers) and a thick porous support layer, the CTA membrane lacks the thick support layer (several hundreds of micrometers). Instead, a polyester mesh was embedded in CTA membrane to provide mechanical strength. The overall thickness of a CTA membrane can be made less than 50 μm. The significance of the CTA membrane is its support-free character, but the thickness is still not satisfactory and bears noteworthy concentration polarization. At a current stage, the PA membrane draws more attention due to its better performance in terms of both water flux and solute selectivity. Its configuration includes active and support layers is widely accepted as the general characteristics of a FO membrane.[17, 57]

Typically, the asymmetric FO membranes are required to have reasonable chemical stability, high permeability to water, and good fouling resistance for both of the active and support layers of the membranes. The material selection for the support layer is wide. Water-insoluble polymers, such as polysulfone, polyacrylonitrile, etc., are usually chosen to form the porous support layer via phase-inversion method.

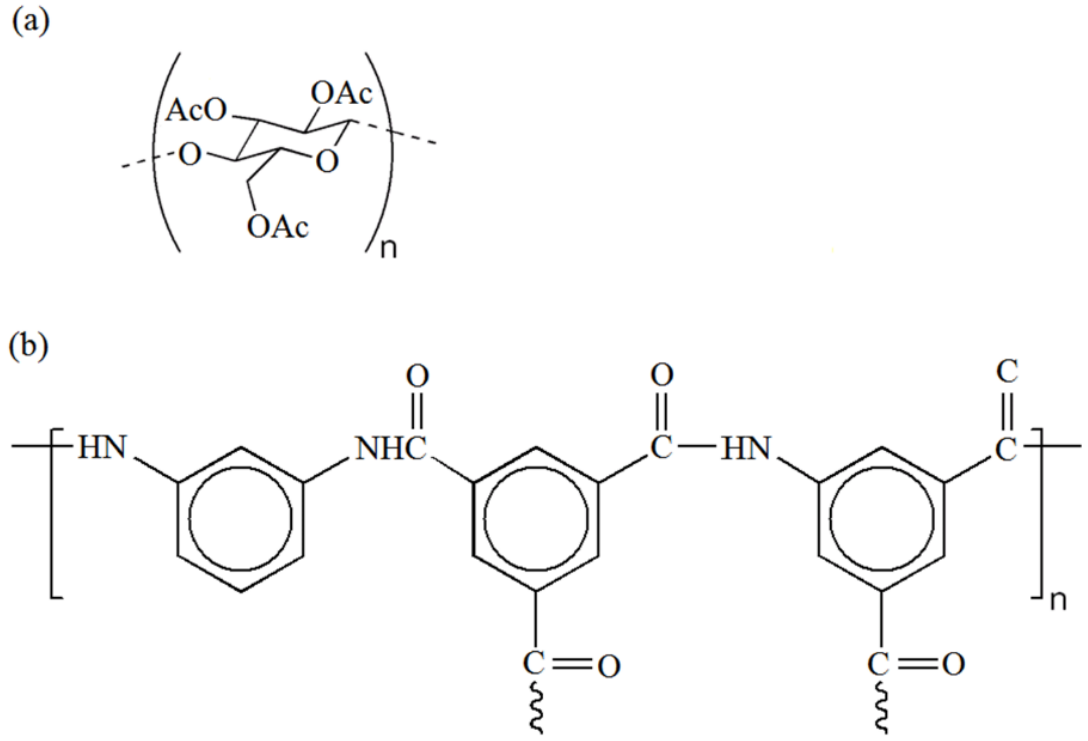

Figure 2.4. Molecular structure of (a) cellulose triacetate (CTA) and (b) polyamide (PA).

Besides the PA and CTA membranes, FO membranes whose active layer is made of polyelectrolyte have been introduced and investigated. Generally, polyelectrolyte layers are prepared via a layer-by-layer (LbL) technique in aqueous solution, which

was firstly introduced in 1997.[46-48] The LbL method involves alternating sequential attachment of polyanions and polycations on a surface. The advantage of this method is its possibility of precise thickness control and can be tuned for many applications in electrical, biomedical, optical and drug delivery.[49-52] Furthermore, this approach is facile, versatile and environmental-friendly, and it has benefited the membrane separation process for longtime.[53] In addition, polyelectrolytes usually contain reactive functional groups that can be further modified. Thus, the polyelectrolyte membrane may be potentially tailored to fit in many different water purification processes as well.

The properties of the substrate on which the polyelectrolyte adsorption initiates play a very import role. Beyond the permeability, thermal and chemical stability that are generally required for the support of a FO membrane, the prerequisites for a good support of polyelectrolyte membranes are high smoothness and high charge density. The number of polyelectrolyte layers is usually the key parameter to adjust the membrane permeability and selectivity. A better selectivity can be obtained by increasing the number of polyelectrolyte layers, but a lower flux is expected with this increasing amount of layer deposition.

The polyelectrolyte membranes have been demonstrated feasibility in many membrane separation processes recently as well. For concreteness, poly(ethyleneimine)/poly(vinyl sodium sulfonate) (PEI/PVS) and poly(vinyl amine)/PVS (PVA/PVS) after annealing have been reported to exhibit a high flux and water enrichment in pervaporation process.[54] Moreover, LbL deposition of polyelectrolyte is particularly attractive in nanofiltration (NF) process, as the

polyelectrolyte layers have the capability of separating mono and divalent ions. For example, it is reported that 5 bilayers of poly(allylamine hydrochloride)/poly(styrene sodium sulfonate) (PAH/PSS) coated on a porous alumina support showed 95% rejection of Mg^{2+} and Ca^{2+} and a selectivity of 20 for $Na^{+}/Mg^{2+}$and 50 for Na^{+}/Ca^{2+}. This is much better than many commercially available NF membranes.[55] The performance of polyelectrolyte membranes in RO process is still problematic. An ideal RO membrane should to have a high rejection to mono ions like NaCl, but polyelectrolyte membranes with good NaCl rejection usually sacrifice the permeability by annealing or making a thick active layer of polyelectrolytes. For instance, it is demonstrated that 10 to 20 bilayers of PAH/poly(acrylic acid) (PAA) exhibited 99% ion rejection, which is at the same level of conventional RO membranes, but the water permeability of this membrane is relatively low.[56] Nevertheless, polyelectrolyte membranes for FO processes still exist plenty of room for improvements and have attracted significant attention recently. Some pioneer works have been done to show the viability for using polyelectrolyte membranes in FO applications. Still, the current studies are inadequate and many unique properties of polyelectrolyte have not been fully exploited yet for FO/PRO membranes.

2.4.2 Membrane Structure

Numerous studies have been conducted on improving the hydrophilicity of both the active layer and the support layer to achieve a more reliable FO membrane. In addition to membrane materials, the membrane structure is also critical and regarded as an essential key to enhance the membrane performance. An ideal membrane

should be not only thin but also have high porosity and low tortuosity. Conventionally, for asymmetric FO membranes (like PA) the support layer is fabricated using phase inversion to achieve aligned finger-like cavities for water transport.[57] In most cases, the support layer is essentially an ultrafiltration membrane within a certain range of pore size. This type of support suffers from high tortuosity, low porosity and high tendency of fouling in PRO mode. Some efforts have been made to promote the porosity of the support layer, for example, changing the solvent or the concentration of polymer solutions during synthesis. Blending additives can also contribute to a higher porosity and thus better membrane permeability. As an example of using additives, mixing polyvinylpyrrolidone (PVP) into the polysulfone membrane during synthesis was reported to significantly enhance the membrane porosity and permeability.[58] To further improve the support layer for FO, researchers have tried to use a nonwoven web of nanofibers prepared by electrospinning technique. Through electrospinning polymer solution are stretched, dried and solidified into the shape of nanofibers with diameters in the range of 40 to 2000 nanometers at low cost.[59] This nanofiber support layer has high porosity. A polyamide membrane made with this support was reported to exhibit improved water flux.[60] The research on creating a better membrane structure and the relationship between membrane structure and membrane performance is still ongoing.

2.4.3 Strategies for Fouling Mitigation

The fouling behaviors on a membrane surface depend on many factors, including membrane surface chemistry, morphology and membrane structure. The ways to

mitigate fouling has similarity with increasing the membrane permeability. These two aims sometimes can be achieved at the same time. Although fouling mechanisms display some variation between osmotically-driven and pressure-driven membrane processes, the general beliefs for fouling mitigation are to make the membrane surface smooth, hydrophilic, and negatively charged. [61, 62, 31] Foulants, especially for organic fouling, have low tendency to cling to a hydrophilic and smooth surface. A negatively charged surface usually shows low adhesion tendency to colloidal particulates, because most of the naturally present particulates also have negatively charged surfaces. The cardinal rule of mitigating fouling for all the strategies is to weaken the interactions between foulants and membrane surface. One popular approach is to mix additives in order to change membrane surface roughness or to enhance the hydrophilicity of the raw materials during the membrane synthesis. Various materials have been investigated for this approach.[63, 64] On the other hand, coating and grafting new materials onto the membrane surface are other prevalent approaches. The foreign materials coated or grafted on the membrane surface may be monomers, polymers or inorganic nanoparticles.[65-68] Some membranes (like PA) have relatively reactive surface and may be directly used for grafting materials, including nanoparticles and polymer brushes. However for some membranes with a relatively inert surface, like most of the polymeric ultrafiltration membranes, other techniques are employed to introduce reactive sites (e.g. radicals) on the membrane surface. Some examples for such techniques include chemical initiation, photochemical radiation or plasma treatment. These techniques can be harsh which may harm the integrity of the membrane. There are a few gentle chemical treatments that are very

promising in membrane surface modification. Dopamine, for instance, is a novel bio-inspired coating material that has been proved able to attach almost any surfaces by its self-polymerization.[69] Its hydrophilic nature has been proved to enhance membrane permeability after being attached on some commercial NF membranes.[70] Progress on mitigating the PRO fouling is incomplete, but it cannot be neglected. The fouling in PRO mode is usually more severe than that in FO mode, because the large pores on the support layer can be easily penetrated in and filled with foulants.[61] The popular strategy for alleviating the PRO fouling is to form barriers on the bottom to prevent foulants from going into the pores.[71]

2.4.4 Draw Solutes

In FO/PRO operations, the concentrated draw solution provides the driving force. The desired draw solution should be inexpensive, abundant, highly soluble in water and able to generate high osmotic pressure. Some salts like NaCl satisfy all of these criteria. In some applications, seawater and salt lake water may be used as well. However, they bring another major concern in the FO process, which is the draw solute recovery. One way to deal with this issue is to implement FO and RO together, which is to reconcentrate the draw solution after diluted in the FO process. The reverse solute diffusion in this case should be noticed, and also this way is still costly. The topic on draw solute recovery has been discussed for decades. In early time, sulfur dioxide was suggested because it only needs low-grade heat to recover. Following a similar concept, a less toxic draw solute ammonium bicarbonate was evaluated as it can decompose and evaporate out upon moderate heating. This

approach can generate an osmotic pressure greater than 250 atm, displaying an unprecedented high recovery of potable water from saline feed and a significant reduction in brine discharge from desalination.[2, 11] Other concepts such as perceptible salts, magnetic nanoparticles and dendrimers were suggested for their possibility to be separate from the water after the draw solution has been diluted. [72-74] Another thought on dealing with the draw solution recovery problem is to use special draw solutions that may be utilized right after diluted. For example, a hydration bag uses sugar or beverage powder (like flavored sucrose) as the draw solution and can extract water from untreated. This is designed for military, recreational, and emergency relief situations, as the diluted draw solution after extracting is potable. Moreover, concentrated fertilizers in agriculture were employed as the draw solution and were directly applied to soils and plants after diluted.[75-77]

2.5 References

1. Low, S. C., Preliminary studies of seawater desalination using forward osmosis. Desalin Water Treat 2009, 7, (1-3), 41-46.

2. McCutcheon, J. R.; McGinnis, R. L.; Elimelech, M., A novel ammonia-carbon dioxide forward (direct) osmosis desalination process. Desalination 2005, 174, (1), 1-11.

3. Loeb, S., Osmotic Power-Plants. Science 1975, 189, (4203), 654-655.

4. Lee, K. L.; Baker, R. W.; Lonsdale, H. K., Membranes for Power-Generation by Pressure-Retarded Osmosis. J Membrane Sci 1981, 8, (2), 141-171.

5. Seppala, A.; Lampinen, M. J., Thermodynamic optimizing of pressure-retarded osmosis power generation systems. J Membrane Sci 1999, 161, (1-2), 115-138.

6. Beaudry, E. G.; Lampi, K. A., Membrane Technology for Direct-Osmosis Concentration Of Fruit Juices. Food Technol-Chicago 1990, 44, (6), 121-121.

7. Holloway, R. W.; Childress, A. E.; Dennett, K. E.; Cath, T. Y., Forward osmosis for concentration of anaerobic digester centrate. Water Res 2007, 41, (17), 4005-4014.

8. Theeuwes, F.; Yum, S. I., Principles Of Design And Operation Of Generic Osmotic Pumps for Delivery Of Semisolid Or Liquid Drug Formulations. Ann Biomed Eng 1976, 4, (4), 343-353.

9. Mehta, G. D.; Loeb, S., Internal Polarization In the Porous Substructure Of a Semipermeable Membrane under Pressure-Retarded Osmosis. J Membrane Sci 1978, 4, (2), 261-265.

10. Seppala, A.; Lampinen, M. J., On the non-linearity of osmotic flow. Exp Therm Fluid Sci 2004, 28, (4), 283-296.

11. McCutcheon, J. R.; McGinnis, R. L.; Elimelech, M., Desalination by ammonia-carbon dioxide forward osmosis: Influence of draw and feed solution concentrations on process performance. J Membrane Sci 2006, 278, (1-2), 114-123.

12. Sablani, S. S.; Goosen, M. F. A.; Al-Belushi, R.; Wilf, M., Concentration polarization in ultrafiltration and reverse osmosis: a critical review. Desalination 2001, 141, (3), 269-289.

13. Elimelech, M.; Bhattacharjee, S., A novel approach for modeling concentration polarization in crossflow membrane filtration based on the equivalence of osmotic pressure model and filtration theory. J Membrane Sci 1998, 145, (2), 223-241.

14. McCutcheon, J. R.; Elimelech, M., Influence of concentrative and dilutive internal concentration polarization on flux behavior in forward osmosis. J Membrane Sci 2006, 284, (1-2), 237-247.

15. McCutcheon, J. R.; Elimelech, M., Modeling water flux in forward osmosis: Implications for improved membrane design. Aiche J 2007, 53, (7), 1736-1744.

16. Loeb, S.; Titelman, L.; Korngold, E.; Freiman, J., Effect of porous support fabric on osmosis through a Loeb-Sourirajan type asymmetric membrane. J Membrane Sci 1997, 129, (2), 243-249.

17. Yip, N. Y.; Tiraferri, A.; Phillip, W. A.; Schiffman, J. D.; Elimelech, M., High Performance Thin-Film Composite Forward Osmosis Membrane. Environ Sci Technol 2010, 44, (10), 3812-3818.

18. Tan, C. H.; Ng, H. Y., Modified models to predict flux behavior in forward osmosis in consideration of external and internal concentration polarizations. J Membrane Sci 2008, 324, (1-2), 209-219.

19. Qin, J. J.; Chen, S. J.; Oo, M. H.; Kekre, K. A.; Cornelissen, E. R.; Ruiken, C. J., Experimental studies and modeling on concentration polarization in forward osmosis. Water Sci Technol 2010, 61, (11), 2897-2904.

20. Li, W. Y.; Gao, Y. B.; Tang, C. Y. Y., Network modeling for studying the effect of support structure on internal concentration polarization during forward

osmosis: Model development and theoretical analysis with FEM. J Membrane Sci 2011, 379, (1-2), 307-321.

21. Sagiv, A.; Semiat, R., Finite element analysis of forward osmosis process using NaCl solutions. J Membrane Sci 2011, 379, (1-2), 86-96.

22. Gruber, M. F.; Johnson, C. J.; Tang, C. Y.; Jensen, M. H.; Yde, L.; Helix-Nielsen, C., Computational fluid dynamics simulations of flow and concentration polarization in forward osmosis membrane systems. J Membrane Sci 2011, 379, (1-2), 488-495.

23. Jung, D. H.; Lee, J.; Kim, D. Y.; Lee, Y. G.; Park, M.; Lee, S.; Yang, D. R.; Kim, J. H., Simulation of forward osmosis membrane process: Effect of membrane orientation and flow direction of feed and draw solutions. Desalination 2011, 277, (1-3), 83-91.

24. Zhou, H.; Smith, D. W., Advanced technologies in water and wastewater treatment. Can J Civil Eng 2001, 28, 49-66.

25. Li, Q. L.; Elimelech, M., Organic fouling and chemical cleaning of nanofiltration membranes: Measurements and mechanisms. Environ Sci Technol 2004, 38, (17), 4683-4693.

26. Lim, A. L.; Bai, R., Membrane fouling and cleaning in microfiltration of activated sludge wastewater. J Membrane Sci 2003, 216, (1-2), 279-290.

27. Hwang, K. J.; Hsueh, C. L., Dynamic analysis of cake properties in microfiltration of soft colloids. J Membrane Sci 2003, 214, (2), 259-273.

28. Drewes, J. E.; Fox, P., Fate of natural organic matter (NOM) during groundwater recharge using reclaimed water. Water Sci Technol 1999, 40, (9), 241-248.

29. Mi, B. X.; Elimelech, M., Organic fouling of forward osmosis membranes: Fouling reversibility and cleaning without chemical reagents. J Membrane Sci 2010, 348, (1-2), 337-345.

30. Clark, M. M.; Heneghan, K. S., Ultrafiltration Of Lake Water for Potable Water Production. Desalination 1991, 80, (2-3), 243-249.

31. Fan, L. H.; Harris, J. L.; Roddick, F. A.; Booker, N. A., Influence of the characteristics of natural organic matter on the fouling of microfiltration membranes. Water Res 2001, 35, (18), 4455-4463.

32. Lee, S.; Lee, C. H., Effect of operating conditions on CaSO4 scale formation mechanism in nanofiltration for water softening. Water Res 2000, 34, (15), 3854-3866.

33. Sheikholeslami, R., Calcium sulfate fouling-precipitation or particulate: A proposed composite model. Heat Transfer Eng 2000, 21, (3), 24-33.

34. van de Lisdonk, C. A. C.; van Paassen, J. A. M.; Schippers, J. C., Monitoring scaling in nanofiltration and reverse osmosis membrane systems. Desalination 2000, 132, (1-3), 101-108.

35. Ghayeni, S. B. S.; Madaeni, S. S.; Fane, A. G.; Schneider, R. P., Aspects of microfiltration and reverse osmosis in municipal wastewater reuse. Desalination 1996, 106, (1-3), 25-29.

36. Watnick, P.; Kolter, R., Biofilm, city of microbes. J Bacteriol 2000, 182, (10), 2675-2679.

37. Kasemset, S.; Lee, A.; Miller, D. J.; Freeman, B. D.; Sharma, M. M., Effect of polydopamine deposition conditions on fouling resistance, physical properties, and permeation properties of reverse osmosis membranes in oil/water separation. J Membrane Sci 2013, 425, 208-216.

38. Ma, H. M.; Hakim, L. F.; Bowman, C. N.; Davis, R. H., Factors affecting membrane fouling reduction by surface modification and backpulsing. J Membrane Sci 2001, 189, (2), 255-270.

39. Ma, H. M.; Bowman, C. N.; Davis, R. H., Membrane fouling reduction by backpulsing and surface modification. J Membrane Sci 2000, 173, (2), 191-200.

40. Gao, W.; Liang, H.; Ma, J.; Han, M.; Chen, Z. L.; Han, Z. S.; Li, G. B., Membrane fouling control in ultrafiltration technology for drinking water production: A review. Desalination 2011, 272, (1-3), 1-8.

41. Wu, J. L.; Le-Clech, P.; Stuetz, R. M.; Fane, A. G.; Chen, V., Effects of relaxation and backwashing conditions on fouling in membrane bioreactor. J Membrane Sci 2008, 324, (1-2), 26-32.

42. Matzinos, P.; Alvarez, R., Effect of ionic strength on rinsing and alkaline cleaning of ultrafiltration inorganic membranes fouled with whey proteins. J Membrane Sci 2002, 208, (1-2), 23-30.

43. Irigoyen, J.; Politakos, N.; Murray, R.; Moya, S. E., Design and Fabrication of Regenerable Polyelectrolyte Multilayers for Applications in Foulant Removal. Macromol Chem Phys 2014, 215, (16), 1543-1550.

44. Pejman Ahmadiannamini, M. L. B., Volodymyr V. Tarabara, Sacrificial polyelectrolyte multilayer coatings as an approach to membrane fouling control: Disassembly and regeneration mechanisms. J Membrane Sci 2015, 491, 10.

45. Shazia Ilyas, J. d. G., Kitty Nijmeijer, Wiebe M. de Vos, Multifunctional polyelectrolyte multilayers as nanofiltration membranes and as sacrificial layers for easy membrane cleaning. Journal of Colloid and Interface Science 2015, 446, 8.

46. Decher, G., Fuzzy nanoassemblies: Toward layered polymeric multicomposites. Science 1997, 277, (5330), 1232-1237.

47. Decher, G.; Hong, J. D.; Schmitt, J., Buildup Of Ultrathin Multilayer Films by a Self-Assembly Process .3. Consecutively Alternating Adsorption Of Anionic And Cationic Polyelectrolytes on Charged Surfaces. Thin Solid Films 1992, 210, (1-2), 831-835.

48. Decher, G.; Eckle, M.; Schmitt, J.; Struth, B., Layer-by-layer assembled multicomposite films. Curr Opin Colloid In 1998, 3, (1), 32-39.

49. Tong, W. J.; Song, X. X.; Gao, C. Y., Layer-by-layer assembly of microcapsules and their biomedical applications. Chem Soc Rev 2012, 41, (18), 6103-6124.

50. Lutkenhaus, J. L.; Hammond, P. T., Electrochemically enabled polyelectrolyte multilayer devices: from fuel cells to sensors. Soft Matter 2007, 3, (7), 804-816.

51. Tang, Z. Y.; Wang, Y.; Podsiadlo, P.; Kotov, N. A., Biomedical applications of layer-by-layer assembly: From biomimetics to tissue engineering. Adv Mater 2006, 18, (24), 3203-3224.

52. De Koker, S.; Hoogenboom, R.; De Geest, B. G., Polymeric multilayer capsules for drug delivery. Chem Soc Rev 2012, 41, (7), 2867-2884.

53. Zhao, Q.; An, Q. F. F.; Ji, Y. L.; Qian, J. W.; Gao, C. J., Polyelectrolyte complex membranes for pervaporation, nanofiltration and fuel cell applications. J Membrane Sci 2011, 379, (1-2), 19-45.

54. Krasemann, L.; Toutianoush, A.; Tieke, B., Self-assembled polyelectrolyte multilayer membranes with highly improved pervaporation separation of ethanol/water mixtures. J Membrane Sci 2001, 181, (2), 221-228.

55. Lu, O. Y.; Malaisamy, R.; Bruening, M. L., Multilayer polyelectrolyte films as nanofiltration membranes for separating monovalent and divalent cations. J Membrane Sci 2008, 310, (1-2), 76-84.

56. Park, J.; Park, J.; Kim, S. H.; Cho, J.; Bang, J., Desalination membranes from pH-controlled and thermally-crosslinked layer-by-layer assembled multilayers. J Mater Chem 2010, 20, (11), 2085-2091.

57. Tiraferri, A.; Yip, N. Y.; Phillip, W. A.; Schiffman, J. D.; Elimelech, M., Relating performance of thin-film composite forward osmosis membranes to support layer formation and structure. J Membrane Sci 2011, 367, (1-2), 340-352.

58. Chakrabarty, B.; Ghoshal, A. K.; Purkait, A. K., Preparation, characterization and performance studies of polysulfone membranes using PVP as an additive. J Membrane Sci 2008, 315, (1-2), 36-47.

59. Reneker, D. H.; Chun, I., Nanometre diameter fibres of polymer, produced by electrospinning. Nanotechnology 1996, 7, (3), 216-223.

60. Bui, N. N.; Lind, M. L.; Hoek, E. M. V.; McCutcheon, J. R., Electrospun nanofiber supported thin film composite membranes for engineered osmosis. J Membrane Sci 2011, 385, (1-2), 10-19.

61. Mi, B.; Elimelech, M., Chemical and physical aspects of organic fouling of forward osmosis membranes. J Membrane Sci 2008, 320, (1-2), 292-302.

62. Lee, S.; Boo, C.; Elimelech, M.; Hong, S., Comparison of fouling behavior in forward osmosis (FO) and reverse osmosis (RO). J Membrane Sci 2010, 365, (1-2), 34-39.

63. Asatekin, A.; Kang, S.; Elimelech, M.; Mayes, A. M., Anti-fouling ultrafiltration membranes containing polyacrylonitrile-graft-poly (ethylene oxide) comb copolymer additives. J Membrane Sci 2007, 298, (1-2), 136-146.

64. Rahimpour, A.; Madaeni, S. S., Improvement of performance and surface properties of nano-porous polyethersulfone (PES) membrane using hydrophilic monomers as additives in the casting solution. J Membrane Sci 2010, 360, (1-2), 371-379.

65. Shaffer, D. L.; Jaramillo, H.; Castrillon, S. R. V.; Lu, X. L.; Elimelech, M., Post-fabrication modification of forward osmosis membranes with a poly(ethylene glycol) block copolymer for improved organic fouling resistance. J Membrane Sci 2015, 490, 209-219.

66. Wavhal, D. S.; Fisher, E. R., Hydrophilic modification of polyethersulfone membranes by low temperature plasma-induced graft polymerization. J Membrane Sci 2002, 209, (1), 255-269.

67. Lu, X. L.; Castrillon, S. R. V.; Shaffer, D. L.; Ma, J.; Elimelech, M., In Situ Surface Chemical Modification of Thin-Film Composite Forward Osmosis Membranes for Enhanced Organic Fouling Resistance. Environ Sci Technol 2013, 47, (21), 12219-12228.

68. Tiraferri, A.; Kang, Y.; Giannelis, E. P.; Elimelech, M., Superhydrophilic Thin-Film Composite Forward Osmosis Membranes for Organic Fouling Control: Fouling Behavior and Antifouling Mechanisms. Environ Sci Technol 2012, 46, (20), 11135-11144.

69. Lee, H.; Dellatore, S. M.; Miller, W. M.; Messersmith, P. B., Mussel-inspired surface chemistry for multifunctional coatings. Science 2007, 318, (5849), 426-430.

70. Arena, J. T.; McCloskey, B.; Freeman, B. D.; McCutcheon, J. R., Surface modification of thin film composite membrane support layers with polydopamine: Enabling use of reverse osmosis membranes in pressure retarded osmosis. J Membrane Sci 2011, 375, (1-2), 55-62.

71. Li, X.; Cai, T.; Chung, T. S., Anti-Fouling Behavior of Hyperbranched Polyglycerol-Grafted Poly(ether sulfone) Hollow Fiber Membranes for Osmotic Power Generation. Environ Sci Technol 2014, 48, (16), 9898-9907.

72. Stone, M. L.; Wilson, A. D.; Harrup, M. K.; Stewart, F. F., An initial study of hexavalent phosphazene salts as draw solutes in forward osmosis. Desalination 2013, 312, 130-136.

73. Ling, M. M.; Wang, K. Y.; Chung, T. S., Highly Water-Soluble Magnetic Nanoparticles as Novel Draw Solutes in Forward Osmosis for Water Reuse. Ind Eng Chem Res 2010, 49, (12), 5869-5876.

74. Chekli, L.; Phuntsho, S.; Shon, H. K.; Vigneswaran, S.; Kandasamy, J.; Chanan, A., A review of draw solutes in forward osmosis process and their use in modern applications. Desalin Water Treat 2012, 43, (1-3), 167-184.

75. Kim, J. E.; Phuntsho, S.; Shon, H. K., Pilot-scale nanofiltration system as post-treatment for fertilizer-drawn forward osmosis desalination for direct fertigation. Desalin Water Treat 2013, 51, (31-33), 6265-6273.

76. Phuntsho, S.; Shon, H. K.; Majeed, T.; El Saliby, I.; Vigneswaran, S.; Kandasamy, J.; Hong, S.; Lee, S., Blended Fertilizers as Draw Solutions for Fertilizer-Drawn Forward Osmosis Desalination. Environ Sci Technol 2012, 46, (8), 4567-4575.

77. Ling, M. M.; Chung, T. S., Novel dual-stage FO system for sustainable protein enrichment using nanoparticles as intermediate draw solutes. J Membrane Sci 2011, 372, (1-2), 201-209.

Chapter 3: Layer-by-layer Assembly of Zeolite/polyelectrolyte Nanocomposite Membranes

3.1 Introduction

Membrane technology has been recognized as one of the most promising candidates for solving the global water scarcity problem. The membrane industry, after growth and development for ~40 years, is still actively searching for new materials to improve membrane separation capability and energy efficiency. With the rapid advances in nanotechnology, numerous nanomaterials with superb properties have been used to improve membrane properties.[1-8] Among these nanomaterials, zeolite has exhibited many unprecedented properties that can be promisingly exploited to make novel membranes with greatly enhanced performance.[7-12] Zeolite is a nanoporous crystalline material with a well-defined framework of aluminosilicates. Because such a framework forms interconnected pores with dimensions of typically <1.0 nm, a continuous zeolite film can effectively reject small molecules and thus is often termed a molecular sieve.[13] In addition, zeolite can be tuned to be extremely hydrophilic by varying the silicon and aluminum compositions during synthesis, thus making zeolite highly permeable to water.[14, 15] Consequently, zeolite could be an ideal candidate for making water/solute separation membranes with high water permeability as well as superior selectivity. [16, 17]

Membranes made of pure zeolite crystals, however, are typically very brittle and thus can easily form cracks that are detrimental to membrane separation performance. To overcome this problem, researchers have attempted to embed zeolite nanoparticles

into polymers [e.g., polyamide, poly(ether)sulfone, and poly(vinylidene fluoride) to make composite membranes that inherit the flexibility from the polymer as well as enhanced separation capability from zeolite.[7-12, 18-20] The typical embedding approach used in these studies was to blend zeolite nanoparticles into an organic solution during the phase inversion or interfacial polymerization process.[21] However, current efforts to create novel zeolite/polymer composite membranes for water purification are severely hindered by the difficulty of achieving high zeolite loading due to the poor compatibility between the zeolite and polymer matrix. So far, zeolite/polyamide thin-film nanocomposite membranes are one of the most successful state-of-the-art zeolite membranes reported for water applications.[7-12] To make these membranes, three-dimensional (3D) zeolite nanoparticles with sizes in the range of 50–150 nm were randomly embedded in polyamide thin films using interfacial polymerization. Such synthesized nanocomposite membranes can achieve a zeolite loading of ~1 wt% (in solvent), with a water permeability nearly twice that of a control polyamide thin-film membrane.[7, 9] Although the doubled water flux is already considered remarkable progress, there is still much room to further enhance the performance of a zeolite/polymer nanocomposite membrane, because the water permeability of a zeolite/polymer nanocomposite membrane increases with increasing zeolite loading as predicted by a Maxwell mixing model.[22] Therefore, new approaches are urgently needed to significantly increase zeolite loading in membranes so that the intriguing properties of zeolite as a novel material can be fully exploited to make high-performance water purification membranes.

Herein, this study presents a highly efficient approach to significantly increase the zeolite loading in nanocomposite membranes. A novel layer-by-layer (LbL) technique was employed to sandwich zeolite nanoparticles between two different polyelectrolytes with opposite charges. The LbL-assembled polyelectrolytes have been successfully demonstrated to be ion-selective layers.[23, 24] Thus, they are currently attracting a large amount of research attention as new materials for forward osmosis (FO)/pressure-retarded osmosis (PRO) membranes,[25, 26] which represent emerging membrane processes that have a variety of important water and energy applications.[27-29] Therefore, we tested the performance of the synthesized zeolite/polyelectrolyte membranes in an FO/PRO membrane system and used polyelectrolyte membranes without zeolite as a baseline to highlight the effects of zeolite loading on the FO/PRO membrane performance.

3.2 Materials and Methods

3.2.1 Materials and Zeolite/Membrane Synthesis

Unless noted, all chemicals were obtained from Sigma-Aldrich (St. Louis, MO). The Linde type A (LTA) zeolite nanoparticles employed in this study were synthesized on the basis of the protocol described in a previous study.[30] In detail, 0.9575 g NaOH was dissolved in 89.498 g DI water in a 250 mL Teflon bottle, and 48.856 g tetramethylammonium hydroxide (TMAOH) solution (25 wt% aqueous solution) was subsequently added. Then, 6.76 g silicic acid was added to the resulting basic solution and the blended solution was kept in a convection oven at 80°C to accelerate dissolution of silicic acid. The solution was cooled to room temperature followed by

the addition of 7.353 g aluminum isopropoxide (Al (I-pro)3) after it became clear. A clear gel with a composition of $11.25SiO_2/1.8Al_2O_3/6.7(TMA)_2O/1.2Na_2O/700H_2O$ was formed after rigorous stirring at room temperature for around 1 hour. The as-made gel was transferred into a preheated convection oven for another 3 days at 70°C. The LTA nanocrystals were purified via dialysis in water for 2 days and were stored in a refrigerator for future usage.

A polyacrylonitrile (PAN; Mw = 150000) support was fabricated in our lab using a phase inversion process. Specifically, PAN (Mw 150,000) was fully dissolved in N,N-Dimethylformamide (DMF, BDH Chemicals, Radnor, PA) together with a small amount of lithium chloride (PAN/LiCl/DMF ratio is 18/2/80) and was kept in vacuum for 24 hours. The PAN solution was casted into a film (125 μm) with a stainless steel casting knife and then was immediately immersed into a water bath for 10 minutes. The PAN membranes were formed and separated from the glass plate before they were transferred to another water bath. After changing the water bath several times, the container was moved to a refrigerator for future use. The PAN surface after phase inversion facing ambient water is regarded as the "top" and the opposite surface attached to the glass plate is regarded as the "bottom".

To make the polyelectrolyte composite membrane, the PAN support was first functionalized by immersion in freshly-prepared dopamine solution (2 mg/mL in 10 mM Tris-HCl, pH 8.5) for 5 hours. Then, the membrane coated with a layer of polydopamine (PDA) was subsequently immersed in PEI (1g/L), LTA (diluted 10 times from its origin) and PAA (1g/L) combined with rinsing in deionized (DI) water before immersing the membrane into each of the three solutions. Each step of

immersion lasted 0.5 hour, expect for the first contact with PEI (1 hour).[31] In each LbL cycle, the positively charged PEI is used to electrostatically "grasp" the negative charges from hydroxyl groups on the surface of zeolite nanoparticles, and then negatively charged PAA is used to compensate the uncovered positive charges and to introduce extra charge for further LbL deposition cycles. The deposition cycles were repeated to create multiple (up to 6) trilayer membranes. Similar deposition procedures were used to prepare PEI-PAA bilayer membranes without the LTA as a control membrane. After a full cycle of the three solutions, the membrane was noted to have one "trilayer". For "bilayer" membranes, the membrane was exempted from being immersed in LTA solution.

3.2.1 Zeolite/Membrane Characterizations

The crystalline phases of the as-synthesized LTA nanoparticles were examined by the powder X-Ray diffraction (XRD), collected using a Bruker D8 Advance Lynx Powder Diffractometer (LynxEye PSD detector, sealed tube, Cu Kα radiation with Ni β-filter). Dynamic light scattering (DLS) (JDSU-model 1135P, HeNe laser with 10 mW output power at 632.8 nm wavelength) was used to investigate the particle size distribution of LTA type zeolite nanoparticles in solution. The Si/Al ratio of the LTA zeolite was determined by x-ray photoelectron spectroscopy (XPS) (Kratos AXIS 165, Kratos Analytical, UK) after the zeolite particles were fabricated into the zeolite-polyelectrolyte membrane.

The as-fabricated membranes were characterized by x-ray photoelectron spectroscopy (XPS) (Kratos AXIS 165, Kratos Analytical, UK), Fourier transform infrared (FTIR)

spectroscopy (Nicolet 6700, Thermo Scientific, Marietta, OH), scanning electron microscopy (SEM) (SU-70, Hitachi High Technologies America, Gaithersburg, MD) and quartz crystal microbalance with dissipation (QCM-D) (Q-sense, Sweden). All membrane samples were dried in an oven at 60 °C prior to characterization (XPS, FTIR, SEM). All FTIR spectra were normalized to the highest peak. A thin layer of gold nanoparticles (<10 nm) was sputtered for SEM samples. For QCM-D experiments, the effective surface of a gold sensor first came in contact with fresh dopamine solution (2 mg/mL, 10 mM Tris-HCl pH 8.5) for 5 hours and then was put in a flow cell after rinsing. This flow cell allows for the pipetting of coating solutions directly onto the sensor surface and the sensor vibration frequency and dissipation were recorded. The sequence of solution, duration of contact time, and solution composition were kept the same as that for membrane synthesis. A viscoelastic model from the Q-Tools software (Q-sense, Sweden) was used to convert the frequency and dissipation data to the amount of mass deposition on the sensor surface.

3.2.2 Membrane Performance Tests

Membrane performance was tested in a lab-scale, cross-flow FO membrane system.[32] The water flux was tested at room temperature, using a cross-flow rate of 8.5 cm/s, deionized (DI) water as the feed solution, and 1 M magnesium chloride ($MgCl_2$) and 0.5 M trisodium citrate (TSC) solutions as the draw solution. A membrane was tested with its top surface facing the feed solution (i.e., FO mode) and the draw solution (i.e., PRO mode). The solute fluxes for $MgCl_2$ and TSC were monitored by measuring the solution conductivity in the feed solution using a conductivity meter.

3.3 Results and Discussion

3.3.1 Membrane Characterizations and Validations of Zeolite Incorporation

The X-ray diffraction (XRD) pattern of the as-synthesized LTA zeolite is shown in Figure 3.1. The structure of the LTA can thus be confirmed. The LTA nanoparticles demonstrate an average particle size of 90 nm in diameter, as confirmed by SEM (Figure 3.2a) and DLS (Figure 3.2b). The PAN support has a thickness of ~60 μm and pore sizes of around 10 and 20–50 nm on the front and back sides, respectively, as shown in Figure 3.3.

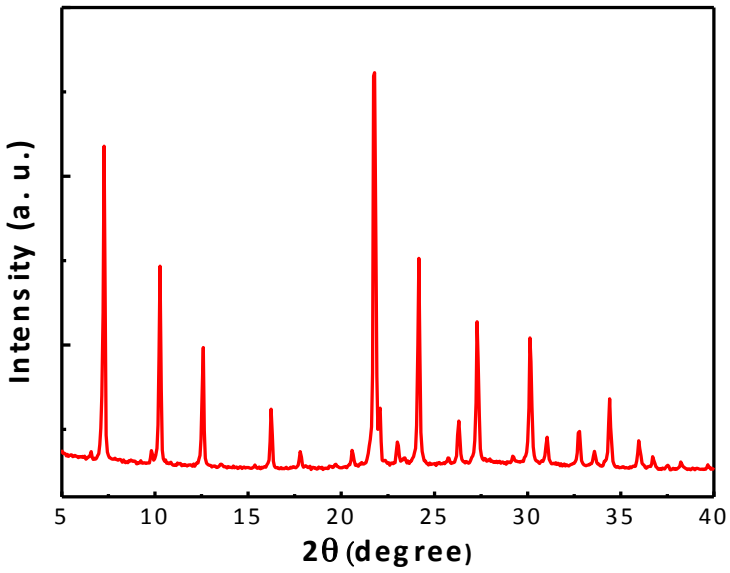

Figure 3.1. XRD pattern of the synthesized LTA zeolite particles.

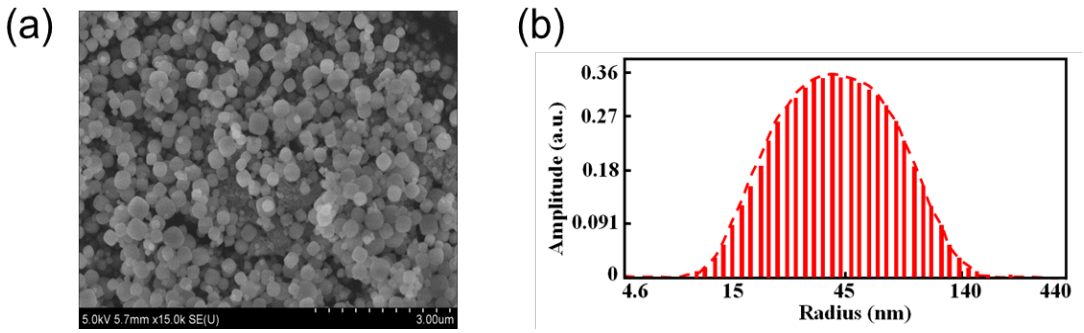

Figure 3.2. (a) The morphology of the LTA nanoparticles characterized by SEM and (b) the size distribution measured by DLS.

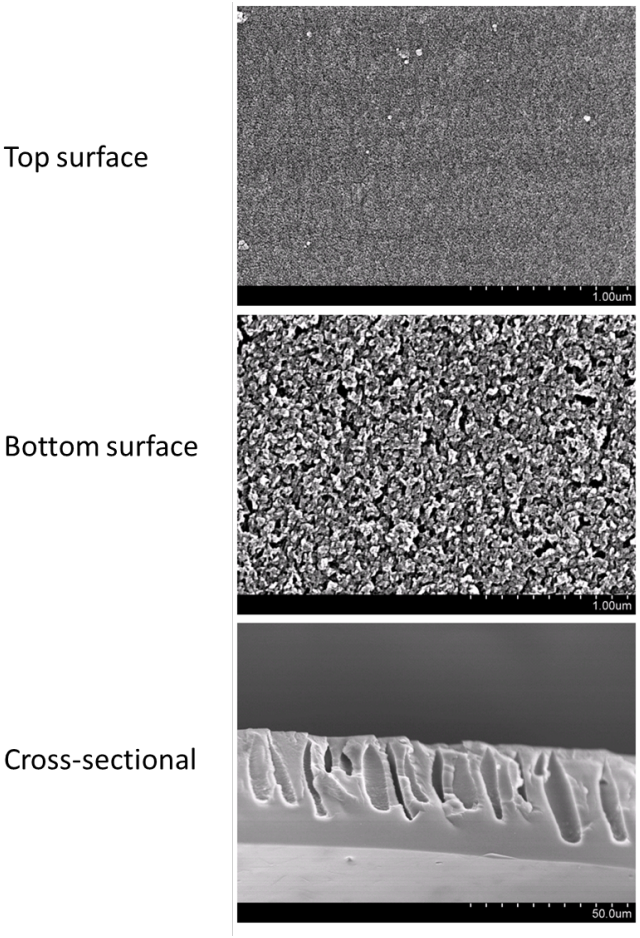

Figure 3.3. SEM images of the pristine PAN support. The top surface has a pore size of ~10 nm and the bottom surface has pore size up to 50 nm. The thickness is around 60 μm.

As schematically illustrated in Figure 3.4, LbL assembly was used to prepare the PEI–LTA–PAA trilayer membranes by sandwiching LTA zeolite nanoparticles between PEI and PAA layers. In the LbL assembly process, the positively charged PEI was first deposited on both sides of a PDA-treated PAN support. The PEI layer electrostatically attracted a layer of slightly negatively charged LTA zeolite nanoparticles onto the surface, and the remaining un-neutralized charges on PEI further drew another layer of PAA on top, thus completing one cycle of trilayer deposition. It is believed that the last PAA layer also introduced extra negative charges on the outside surface for subsequent PEI–LTA–PAA trilayer deposition cycles. The bilayer PEI–PAA membranes without LTA zeolite were assembled and used as a control in this study to elucidate the effects of zeolite loading on membrane performance.

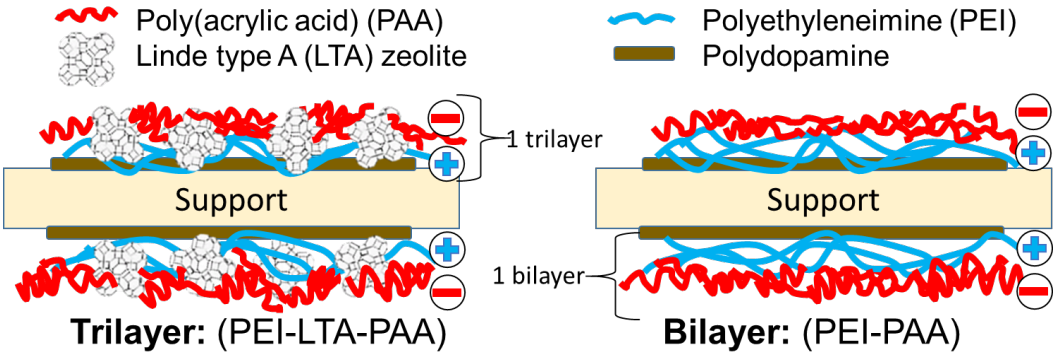

Figure 3.4. Schematic of layer-by-layer assembly of trilayer and bilayer membranes using polydopamine-treated PAN as a support. Only one trilayer or bilayer on each side of the support is shown for the sake of clarity.

Comparison of the SEM images of the trilayer and bilayer membranes clearly demonstrates the successful incorporation of zeolite nanoparticles into the trilayer membrane. Note that as the PAN support before and after PDA coating had very similar surface morphology, the images of a PDA-treated PAN support are not shown. As shown in Figure 3.5, both top and bottom surfaces of the trilayer membrane exhibit rough, particle-like features, especially in the first two deposition cycles, while the bilayer membrane consistently appears smooth and featureless. It is interesting to note that, when the number of trilayers reaches three or more, the trilayer membrane starts to lose its roughness and particle-like features and looks almost as smooth as the bilayer membrane. This is most likely because the LbL assembly incorporated a smaller and smaller amount of LTA zeolite nanoparticles as the number of deposition cycles increased.

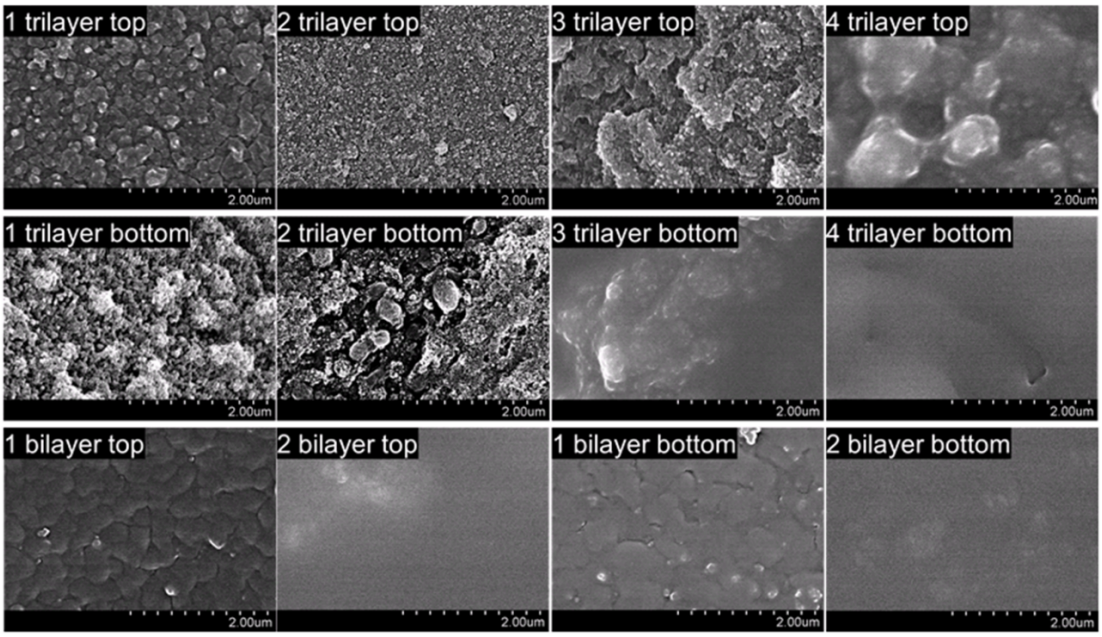

Figure 3.5. SEM images of the top and bottom surfaces of membranes with different numbers of trilayers or bilayers.

3.3.2 Extremely High Zeolite Loading Enabled by Trilayer Assembly

Several techniques were employed to further verify and quantify the incorporation of LTA into the trilayer membranes. FTIR was first used to examine the changes caused by each single deposited layer during the process of making trilayer or bilayer membranes. As shown in Figure 3.6a, a characteristic peak for −COOH (~1720 cm^{-1}) appears upon deposition of PAA, and when LTA is incorporated, an obvious peak (between 1000 and 1100 cm^{-1}) that is typically attributed to the −Si−O bond vibration can be observed. Further FTIR characterization (Figure 3.6b) shows that when the number of deposition cycles increases, the peak (~2250 cm^{-1}) that represents −C≡N from the PAN support has a diminishing trend, indicating an increasing thickness of the bilayer or trilayer membrane. Correspondingly, the characteristic peaks for PAA

in bilayer membranes and LTA in trilayer membranes clearly become stronger with an increasing number of deposition cycles.

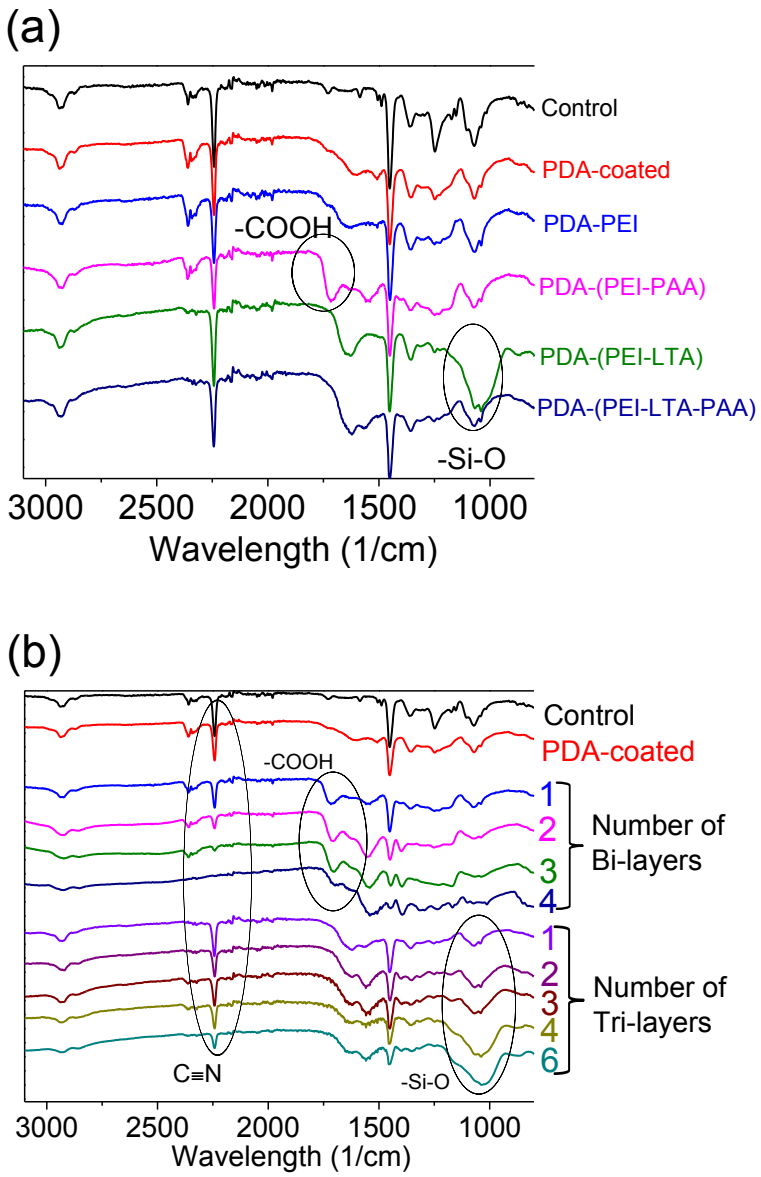

Figure 3.6. FTIR spectra of (a) trilayer or bilayer membranes after each deposition step and (b) bilayer and trilayer membranes with different numbers of layers.

To further understand how effectively each layer was deposited during the LbL assembly of the trilayer membrane, XPS was used to characterize the elemental composition of the membrane surface (typically within 10 nm depth) after each step of layer deposition. As shown in Figure 3.7, the elemental composition of the membrane surface varied significantly when the last deposition layer changed among PEI, LTA, and PAA. For instance, silicon and aluminum signals could always be observed when LTA was the last deposition layer, demonstrating effective LTA deposition. The signals for these two elements, however, almost disappeared after the subsequent PAA deposition, indicating that one layer of PAA was able to almost fully cover the previously deposited LTA zeolite nanoparticles. It is also noteworthy that the amount of deposited LTA (represented by silicon and aluminum concentrations) started to decrease after the third trilayer deposition, indicating a lower percentage of zeolite nanoparticles in the trilayers with more deposition cycles. This observation is consistent with the SEM images in Figure 3.5 showing smoother, less particle-like surfaces on membranes with a large number (four to six) of trilayers. Additionally, the XPS analysis (Table 3.1) of the zeolite/polyelectrolyte membrane showed an average Si/Al ratio of 3.12, which is consistent with the Si/Al ratio of 3.14 used in the LTA zeolite synthesis gel [$11.3SiO_2/1.8Al_2O_3/6.7(TMA)_2O/1.2Na_2O/700H_2O$].

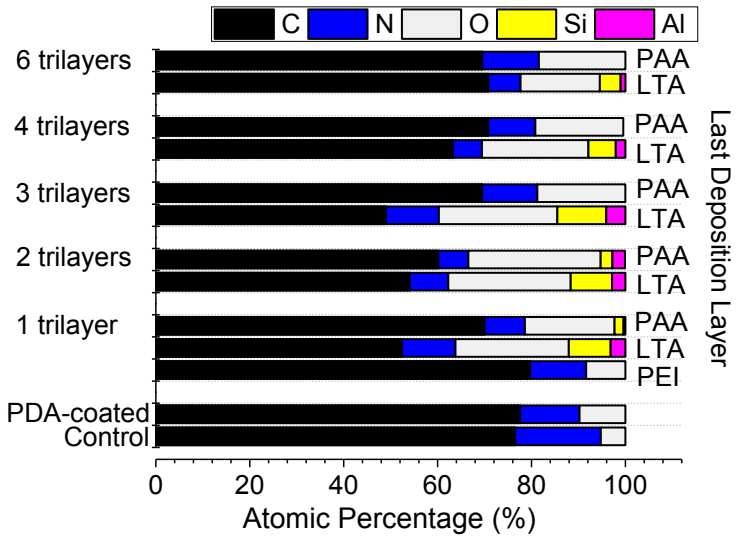

Figure 3.7. Surface elemental composition obtained by XPS analysis for the bottom surface of trilayer membranes.

Table 3.1. Atomic percentage of silicon and aluminum in the trilayer membrane characterized by XPS analysis.

	Si (%)	**Al (%)**	**Si/Al ratio**
1 trilayer	8.90	3.15	2.83
2 trilayers	8.81	2.84	3.10
3 trilayers	10.42	4.08	2.55
4 trilayers	5.81	2.06	2.82
6 trilayers	4.43	1.03	4.30
Average	7.67	2.63	**3.12**

To accurately quantify the zeolite loading in the trilayer membrane, QCM-D was used to measure the mass of deposited PEI, LTA, and PAA during the LbL assembly of trilayer membranes. Note that the same LbL protocol was used on the QCM-D sensor so that the real bilayer or trilayer membrane synthesis could be fully simulated.

As shown in Figure 3.8a, the mass of deposited LTA nanoparticles was higher than that of PEI and PAA in the first trilayer deposition, but the mass of PEI and PAA increased much faster as the number of deposition cycles increased. The zeolite loading (expressed as the weight percentage for LTA zeolite nanoparticles) in the trilayer membranes is plotted in Figure 3.8b. The zeolite loading reached as high as 66 wt % in the one-trilayer membrane and remained above 30 wt % even in a six-trilayer membrane, despite an apparent decreasing trend with an increasing number of trilayers. Therefore, the LbL approach presented here provides a promising route to high zeolite loading in nanocomposite membranes. The dramatic increase in zeolite loading is attributed to the enhanced compatibility between zeolite and the polyelectrolyte film due to the electrostatic interactions introduced during the assembly of alternately charged layers.

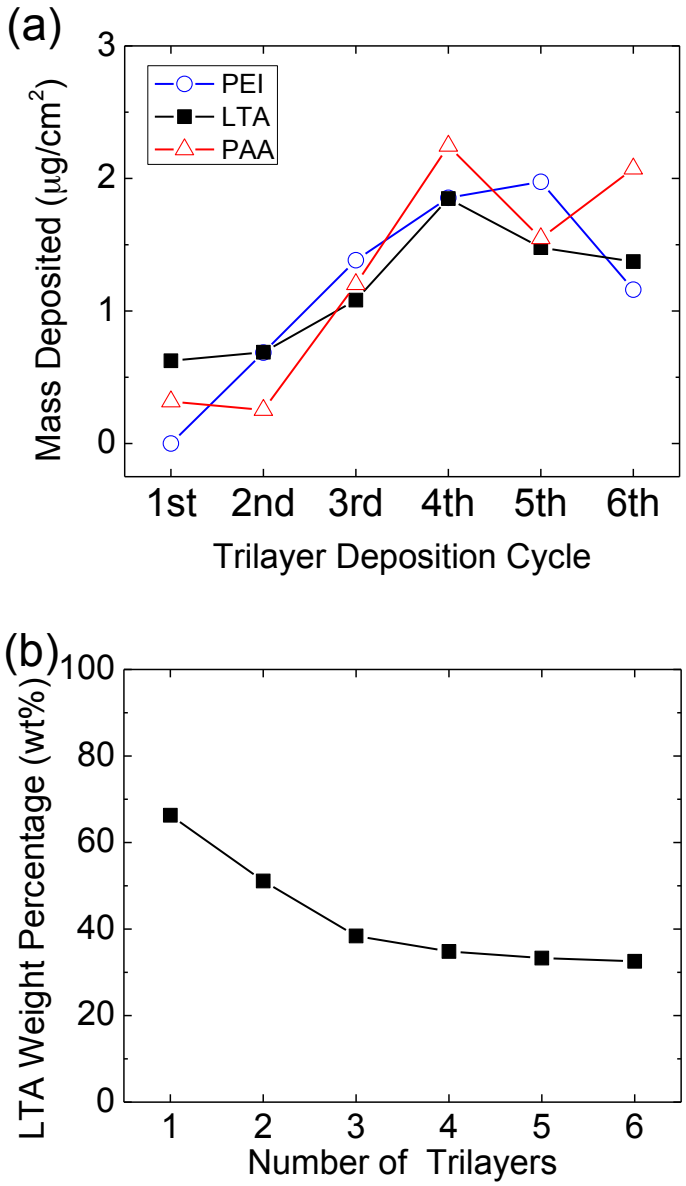

Figure 3.8. (a) Mass of deposited PEI, LTA zeolite nanoparticles, and PAA within each deposition cycle during the LbL assembly of trilayer membranes, obtained by QCM-D measurement. (b) Weight percentage for LTA zeolite nanoparticles in the trilayer membranes.

3.3.3 Effects of Zeolite Incorporation on Membrane Performance

The performance of bilayer and trilayer membranes was tested in an FO system using 1 M $MgCl_2$ or 0.5 M TSC as the draw solution and DI water as the feed solution. Both the bilayer and trilayer membranes demonstrated excellent stability by maintaining constant water and solute flux after being repeatedly tested in the system with a cross-flow rate of 8.5 cm/s. As shown in panels a and b of Figure 3.9, the membrane consisting of two to three trilayers performed the best with the highest water flux and lowest reverse solute flux. This is most likely because the one-trilayer membrane could carry imperfections from incomplete bridging over a few relatively large PAN pores, thus decreasing the osmotic-driven water flux and increasing the reverse solute flux. When more than three trilayers were assembled, however, the water flux decreased again because of the increased membrane thickness, which naturally causes more resistance and hence hinders water transport.

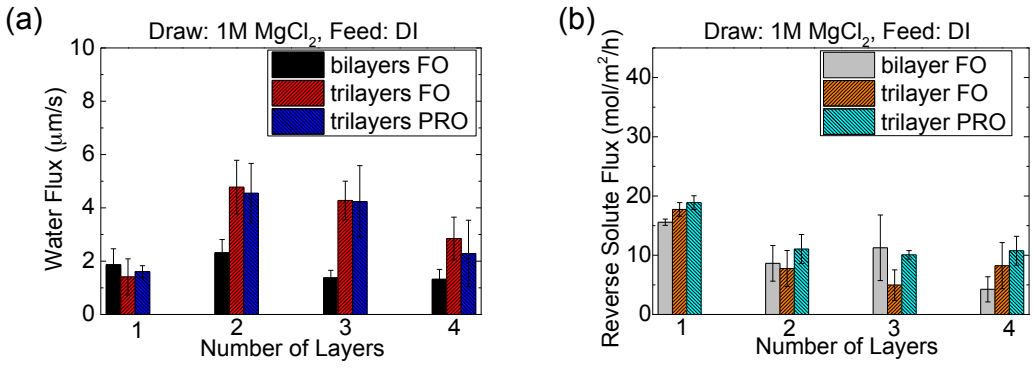

Figure 3.9. (a) Water flux data for trilayer and bilayer membranes in FO and PRO modes. (b) Reverse solute flux data for trilayer and bilayer membranes in FO and PRO modes.

Incorporation of zeolite nanoparticles significantly enhanced membrane water flux without sacrificing membrane selectivity. As revealed in Figure 3.9a, the water flux of the two-trilayer membrane is 4.8 μm/s (17.3 LMH), more than twice that of the bilayer membrane flux of 2.2 μm/s (7.9 LMH). In the meantime, comparison of the reverse solute fluxes in Figure 3.9b demonstrates a similar or even slightly improved solute rejection for the trilayer membrane, indicating that the membrane integrity was not compromised by the incorporation of zeolite nanoparticles. The dramatic increase in water flux without a decrease in selectivity suggests that the incorporation of extremely hydrophilic, porous zeolite nanoparticles into the polyelectrolyte layers creates paths for fast water transport, dramatically increasing the membrane permeability. At this stage, the actual major paths of fast water transport, whether through the porous structure of zeolite or around the hydrophilic zeolite nanoparticles, remain unclear. Nevertheless, it is expected that the membrane performance can be further improved by cross-linking the polyelectrolytes and enforcing more transport paths through the zeolite nanoparticles.

Another unique property of the synthesized trilayer membrane is the double-sided coating on the membrane support, which was designed to minimize internal concentration polarization within the support layer. To examine the effectiveness of the double-sided coating, we tested water and solute fluxes of the membrane in opposite orientations (i.e., FO and PRO modes). As shown in panels a and b of Figure 3.9, both the water flux and reverse solute flux were similar for the two modes, indicating that the active layers created on the top and bottom sides of the membrane support are almost non-differentiable. Such double-sided coating is very beneficial

for membrane fouling control in PRO mode, because the coating on the bottom side can effectively prevent foulants from entering the internal structure of the membrane support.

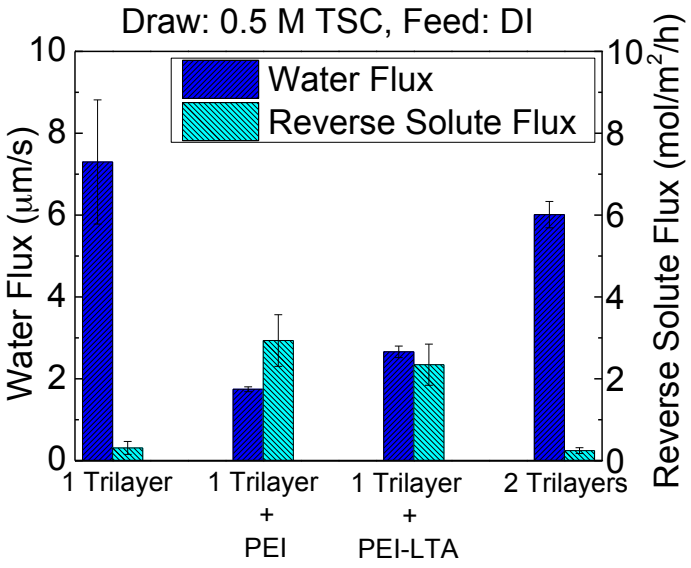

Figure 3.10. Water flux and reverse solute flux for trilayer membranes (with different last layers) in FO mode. The negatively charged surface (PAA) shows better membrane performance for its strong repulsive force to citrates.

Another important advantage of using LbL for membrane synthesis was validated as well: membrane surface properties (e.g., charge, hydrophilicity, and functionality) can be conveniently tailored by altering the last deposition layer to achieve better water flux, selectivity, and fouling resistance. As an illustration, the surface charge of the trilayer membrane was altered by changing the last deposition layer. As shown in Figure 3.10, a complete trilayer membrane was negatively charged by having PAA as the outermost layer, and the membrane surface became positively charged when an

additional PEI layer was deposited as the last layer. As the membrane surface charge changed from negative to positive, the water flux (using TSC as draw solutes in FO modes) was severely reduced and the reverse solute flux was considerably increased. The reverse solute flux varied correspondingly with the surface charges. Sucrose, a neutral molecule with a similar hydraulic radius with TSC, was also used to further validate the charge effect, as shown in Figure 3.11. The reverse solute flux using sucrose was not meaningfully higher, but the water flux was obviously lower. This phenomenon indicates that the citrate ions (negatively charged) used as the draw solute are heavily repulsed by the negatively charged PAA, resulting in less reverse solute transport and hence a higher osmotic driving force. Likewise, other surface properties can also be effectively tailored to enhance the separation performance of the trilayer membrane.

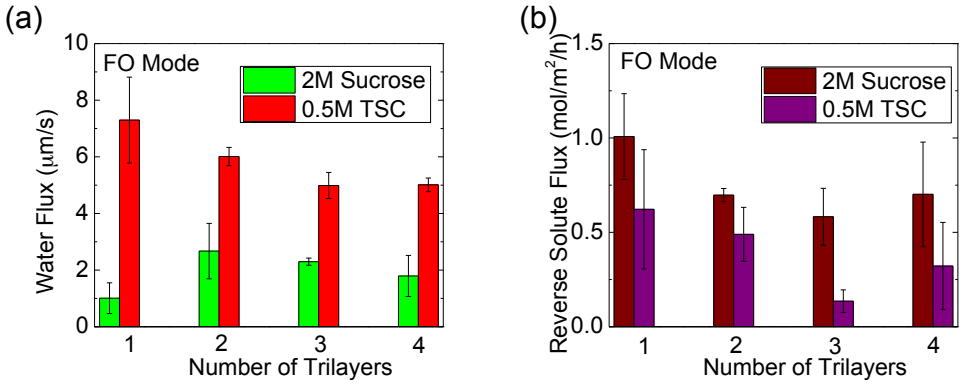

Figure 3.11. (a)Water flux and (b)reverse solute flux for trilayer membranes using TSC or sucrose as draw solutes in FO mode. The two draw solutions generate a similar osmotic pressure according to the Morse equation. The water flux using sucrose as draw solutes is lower than that using TSC but the reverse solute flux is comparable.

Finally, the performance of the synthesized trilayer membrane was compared with a commercially available CTA membrane in FO mode. As shown in Figure 3.12, the water flux of the one-trilayer membrane is ~4 times that of the CTA membrane, while the TSC rejections by the one-trilayer and CTA membranes are 95.3 and 99%, respectively. Therefore, this zeolite/polyelectrolyte nanocomposite represents a promising material for FO and PRO membranes.

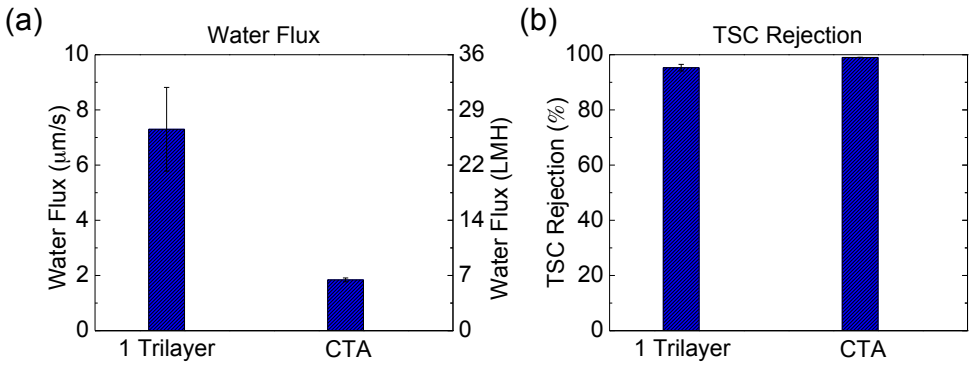

Figure 3.12. Comparison of the performance of the 1-trilayer zeolite membrane and a commercial citrate triacetate (CTA) FO membrane in terms of (a)water flux and (b)TSC rejection.

3.4 Conclusions

This study proves that incorporating zeolite nanoparticles into nanocomposite membranes is advantageous with respect to enhancing membrane permeability by providing preferential water flow paths (possibly through the subnanometer porous structure of zeolite) while maintaining excellent separation capability. It is found that a layer-by-layer assembly approach can effectively incorporate zeolite nanoparticles

into nanocomposite membranes. Negatively charged Linde type A (LTA) zeolite nanoparticles were sandwiched between two different polyelectrolyte layers, negatively charged poly(acrylic acid) (PAA) and positively charged poly(ethyleneimine) (PEI), to form a PEI–LTA–PAA trilayer. The zeolite loading in the multitrilayer membranes was between 30 and 60 wt %, which is attributed to the drastically improved compatibility between zeolite and polymers, a direct result of electrostatic interactions. The performance of the trilayer membrane was compared with that of a control PEI–PAA bilayer membrane in a forward osmosis membrane system. The incorporation of zeolite nanoparticles was found to enhance membrane water permeability by >2-fold without compromising the membrane selectivity for tested species.

3.5 Acknowledgements

This material is based on work supported by the National Science Foundation (NSF) under Grant CBET-1154572 and a University of Maryland ADVANCE Program for Inclusive Excellence Interdisciplinary and Engaged Research Seed Grant. The support is gratefully acknowledged. We also acknowledge the facility support of the Maryland NanoCenter and Nipple. The NispLab is supported in part by the NSF as a Materials Research Science and Engineering Center shared experimental facility.

3.6 References

1. Tiraferri, A.; Kang, Y.; Giannelis, E. P.; Elimelech, M., Superhydrophilic Thin-Film Composite Forward Osmosis Membranes for Organic Fouling Control: Fouling Behavior and Antifouling Mechanisms. *Environ Sci Technol* **2012,** *46*, (20), 11135-11144.

2. Bui, N. N.; McCutcheon, J. R., Hydrophilic Nanofibers as New Supports for Thin Film Composite Membranes for Engineered Osmosis. *Environ Sci Technol* **2013,** *47*, (3), 1761-1769.

3. Hu, M.; Mi, B., Enabling Graphene Oxide Nanosheets as Water Separation Membranes. *Environ Sci Technol* **2013,** *47*, (8), 3715-3723.

4. Gao, Y.; Hu, M.; Mi, B. X., Membrane surface modification with TiO2-graphene oxide for enhanced photocatalytic performance. *J Membrane Sci* **2014,** *455*, 349-356.

5. Perreault, F.; Tousley, M. E.; Elimelech, M., Thin-Film Composite Polyamide Membranes Functionalized with Biocidal Graphene Oxide Nanosheets. *Environmental Science & Technology Letters* **2013,** *1*, 71-76.

6. Liu, Y.; Rosenfield, E.; Hu, M.; Mi, B., Direct observation of bacterial deposition on and detachment from nanocomposite membranes embedded with silver nanoparticles. *Water Res* **2013,** *47*, (9), 2949-2958.

7. Jeong, B. H.; Hoek, E. M. V.; Yan, Y. S.; Subramani, A.; Huang, X. F.; Hurwitz, G.; Ghosh, A. K.; Jawor, A., Interfacial polymerization of thin film nanocomposites: A new concept for reverse osmosis membranes. *J Membrane Sci* **2007,** *294*, (1-2), 1-7.

8. Lind, M. L.; Jeong, B. H.; Subramani, A.; Huang, X. F.; Hoek, E. M. V., Effect of mobile cation on zeolite-polyamide thin film nanocomposite membranes. *J Mater Res* **2009,** *24*, (5), 1624-1631.

9. Ma, N.; Wei, J.; Liao, R. H.; Tang, C. Y. Y., Zeolite-polyamide thin film nanocomposite membranes: Towards enhanced performance for forward osmosis. *J Membrane Sci* **2012,** *405*, 149-157.

10. Fathizadeh, M.; Aroujalian, A.; Raisi, A., Effect of added NaX nano-zeolite into polyamide as a top thin layer of membrane on water flux and salt rejection in a reverse osmosis process. *J Membrane Sci* **2011,** *375*, (1-2), 88-95.

11. Kong, C. L.; Shintani, T.; Tsuru, T., "Pre-seeding"-assisted synthesis of a high performance polyamide-zeolite nanocomposite membrane for water purification. *New J Chem* **2010,** *34*, (10), 2101-2104.

12. Lind, M. L.; Ghosh, A. K.; Jawor, A.; Huang, X. F.; Hou, W.; Yang, Y.; Hoek, E. M. V., Influence of Zeolite Crystal Size on Zeolite-Polyamide Thin Film Nanocomposite Membranes. *Langmuir* **2009,** *25*, (17), 10139-10145.

13. Davis, M. E.; Lobo, R. F., Zeolite and Molecular-Sieve Synthesis. *Chem Mater* **1992,** *4*, (4), 756-768.

14. Kawai, T.; Tsutsumi, K., Evaluation of Hydrophilic-Hydrophobic Character of Zeolites by Measurements of Their Immersional Heats in Water. *Colloid Polym Sci* **1992,** *270*, (7), 711-715.

15. Castillo, J. M.; Silvestre-Albero, J.; Rodriguez-Reinoso, F.; Vlugt, T. J. H.; Calero, S., Water adsorption in hydrophilic zeolites: experiment and simulation. *Phys Chem Chem Phys* **2013,** *15*, (40), 17374-17382.

16. Li, L. X.; Dong, J. H.; Nenoff, T. M.; Lee, R., Desalination by reverse osmosis using MFI zeolite membranes. *J Membrane Sci* **2004,** *243*, (1-2), 401-404.

17. Duke, M. C.; O'Brien-Abraham, J.; Milne, N.; Zhu, B.; Lin, J. Y. S.; da Costa, J. C. D., Seawater desalination performance of MFI type membranes made by secondary growth. *Sep Purif Technol* **2009,** *68*, (3), 343-350.

18. Liu, F.; Ma, B. R.; Zhou, D.; Xiang, Y. H.; Xue, L. X., Breaking through tradeoff of Polysulfone ultrafiltration membranes by zeolite 4A. *Micropor Mesopor Mat* **2014,** *186*, 113-120.

19. Pendergast, M. T. M.; Nygaard, J. M.; Ghosh, A. K.; Hoek, E. M. V., Using nanocomposite materials technology to understand and control reverse osmosis membrane compaction. *Desalination* **2010,** *261*, (3), 255-263.

20. Liao, C. J.; Yu, P.; Zhao, J. Q.; Wang, L. M.; Luo, Y. B., Preparation and characterization of NaY/PVDF hybrid ultrafiltration membranes containing silver ions as antibacterial materials. *Desalination* **2011,** *272*, (1-3), 59-65.

21. Perego, C.; Bagatin, R.; Tagliabue, M.; Vignola, R., Zeolites and related mesoporous materials for multi-talented environmental solutions. *Micropor Mesopor Mat* **2013,** *166*, 37-49.

22. Pendergast, M. M.; Hoek, E. M. V., A review of water treatment membrane nanotechnologies. *Energy Environ. Sci.* **2011,** *4*, (6), 1946-1971.

23. Cheng, C.; White, N.; Shi, H.; Robson, M.; Bruening, M. L., Cation separations in electrodialysis through membranes coated with polyelectrolyte multilayers. *Polymer* **2014,** *55*, (6), 1397-1403.

24. Liu, G. Q.; Dotzauer, D. M.; Bruening, M. L., Ion-exchange membranes prepared using layer-by-layer polyelectrolyte deposition. *J Membrane Sci* **2010,** *354*, (1-2), 198-205.

25. Saren, Q.; Qiu, C. Q.; Tang, C. Y. Y., Synthesis and Characterization of Novel Forward Osmosis Membranes based on Layer-by-Layer Assembly. *Environ Sci Technol* **2011,** *45*, (12), 5201-5208.

26. Duong, P. H. H.; Zuo, J.; Chung, T. S., Highly crosslinked layer-by-layer polyelectrolyte FO membranes: Understanding effects of salt concentration and deposition time on FO performance. *J Membrane Sci* **2013,** *427*, 411-421.

27. Cath, T. Y.; Childress, A. E.; Elimelech, M., Forward osmosis: Principles, applications, and recent developments. *J Membrane Sci* **2006,** *281*, (1-2), 70-87.

28. Zhao, S. F.; Zou, L.; Tang, C. Y. Y.; Mulcahy, D., Recent developments in forward osmosis: Opportunities and challenges. *J Membrane Sci* **2012,** *396*, 1-21.

29. Alsvik, I. L.; Hagg, M. B., Pressure Retarded Osmosis and Forward Osmosis Membranes: Materials and Methods. *Polymers-Basel* **2013,** *5*, (1), 303-327.

30. Jawor, A.; Jeong, B. H.; Hoek, E. M. V., Synthesis, characterization, and ion-exchange properties of colloidal zeolite nanocrystals. *J Nanopart Res* **2009,** *11*, (7), 1795-1803.

31. Zhang, R. N.; Su, Y. L.; Zhao, X. T.; Li, Y. F.; Zhao, J. J.; Jiang, Z. Y., A novel positively charged composite nanofiltration membrane prepared by bio-inspired adhesion of polydopamine and surface grafting of poly(ethylene imine). *J Membrane Sci* **2014,** *470*, 9-17.

32. Liu, Y. L.; Mi, B. X., Effects of organic macromolecular conditioning on gypsum scaling of forward osmosis membranes. *J Membrane Sci* **2014,** *450*, 153-161.

Chapter 4: Fouling Study on Zeolite/polyelectrolyte Nanocomposite Membranes

4.1 Introduction

Membrane technologies, especially the emerging forward osmosis (FO) process, for water treatment are promising in solving the escalating water crises. Unlike the conventional reverse osmosis (RO) process, which demands tremendous amount of energy input, the FO process is considered energy-efficient, because the driving force for water transport originates from the concentration gradient established between the two sides of a semi-permeable membrane. This process is spontaneous and can potentially reduce the monstrous operation costs of a membrane system.[1, 2] However, the application of FO has been severely hindered by membrane fouling. Membrane fouling in FO depicts a process that substances in the feed water deposit on the membrane surface or in the membrane pores. This process can severely degrade the membrane performance by heavily declining water flux or even affecting the quality of the produced water.[3]

In general, there are several types of foulants: colloidal, biological, organic and inorganic scaling. A typical way to recover a fouled membrane is to use chemical cleaning or intense flushing, but in practice such recovering methods become ineffective when irreversible fouling occurs.[4, 5] The replacement for a fouled membrane accounts for a large portion of the operating costs. Thus, a membrane with better fouling resistance and low fouling tendency is highly desired. The fouling mechanisms of membranes for both osmotically-driven FO and pressure-driven RO

processes have been extensively investigated recently.[6-10] According to these studies, unfortunately, most of the FO membranes are made of hydrophobic polymers, which show strong affinity to organic matters. Furthermore, the fouling is usually more severe in the FO-related pressure-retarded osmosis (PRO) process in which the more hydrophobic support layer with large pores of the asymmetric membrane is exposed to foulants. Foulants can easily penetrate and stay in the pores to block the water transport.[10]

As a general belief, prohibiting the initial attachment of foulants is critical, which means to alleviate the interactions between the foulants and the membrane surface. A popular way to address this issue is to make the membrane surface hydrophilic and negatively charged by mixing or grafting foreign materials.[11-15] Recently, the polyelectrolyte film fabricated via a layer-by-layer (LbL) has been proved feasible and effective in composing a FO membrane. This method utilizes charged and water-soluble polymers, which are expected to provide good fouling resistance. However, fouling behaviors of polyelectrolyte FO membranes have not been concretely studied.[16, 17]

Moreover, a novel way to embed zeolite nanoparticles within the polyelectrolyte layers to make a composite FO membrane has been demonstrated previously. This composite membrane has active layer of polyelectrolytes on both sides. It is expected this composite membrane will demonstrate better resistance to organic fouling due to the hydrophilicity of zeolite nanoparticles and also in PRO process.[18] Furthermore, this zeolite-embedded composite membrane may encounter severe silica scaling, a common type of inorganic fouling, because zeolites are aluminosilicate-based and the

abundant hydroxyl-terminals on zeolite nanoparticles can provide reactive sites for silica-based substances to condense and grow.[19] Given that there are no reports that have illustrated the silica scaling on zeolite-contained membranes and few reports on the organic fouling behaviors of polyelectrolyte films, the aim of this study is to supply evidence to the following issues: (1) polyelectrolyte membranes show good fouling resistance to organic matters; (2) the zeolite-embedded composite membrane has deteriorated resistance to silica scaling; (3) creating active layers on both sides of the FO membrane has the potential to mitigate the fouling in PRO mode.

4.2 Materials and Methods

4.2.1 Membrane Synthesis

Unless specified, all chemicals are obtained from Sigma-Aldrich (St. Louis, MO) and used as received. Two module polyelectrolytes, poly(acrylic acid) (PAA) and polyethyleneimine (PEI), are used to demonstrate this work. The zeolite nanoparticles used is Linde Type A (LTA), one of the most common and important zeolites. The support layer was made of polyacrylonitrile (PAN). The membrane synthesis procedure was followed the same approach as described previously. A trilayer indicates each coating cycle contains (PEI-LTA-PAA) while a bilayer means the layers were build up by (PEI-PAA). The one-sided coating membrane was made the same way except for a special device was employed to constrain the coating solution (dopamine, polyelectrolytes, LTA) from contacting the bottom surface. The way to identify top and bottom follows the same way in the previous work as well.[18]

According to some earlier results, membranes with 2 bilayers or 2 trilayers were selected for evaluation under presence of two organic foulants and silica scaling. The two organic foulants used in this study are alginate and bovine serum albumin (BSA), which are widely used as representatives in the membrane society for creating organic fouling environment.[10, 11, 20] Trisodium citrate (TSC, Alfa Aesar, Ward Hill, MA) was used as the draw solute. The feed solution for organic fouling experiments contained 50 mM sodium chloride (NaCl) and 0.5 mM calcium chloride ($CaCl_2$) as the presence of Ca^{2+} is proven to aggravate the organic fouling.[9] The concentration of organic foulants present during the fouling process was 200 mg/L. For silica scaling experiments, the feed was composed of 115 mM NaCl and 19 mM magnesium chloride ($MgCl_2$). Sodium metasilicate was selected as the seed of silica scaling which present with a concentration of 4.2 mM (a saturation index of 2.2 for amorphous silica).[21]

4.2.2 Fouling Experiments

The fouling experiments were conducted in a bench-scale cross-flow system.[20] All the fouling experiments were made to start at around the same initial flux by adjusting the concentration of draw solution. A baseline experiment without foulant presence was always collected prior to introducing the foulants for correcting water flux decline caused by dilution of draw solution. The membranes were flushed by pure water for 20 minutes as a rising step after 18 hours of contacting with foulants, and then water flux of the membranes were measured again to access the flux recovery ability after fouled. Comparisons were firstly made between one-sided coating and double-sided

coating trilayer membranes in PRO mode for demonstrating the effects of double-sided coating on mitigating PRO fouling, because the coating on the bottom side is expected to effectively prevent foulants from entering the internal structure of the membrane support. Comparisons were then made between the bilayer and trilayer membranes under the presence of different foulants for demonstrating the pros and cons of having zeolite nanoparticles incorporated.

The fouling processes were also repeated on QCM-D sensors in an open channel. The sensors were coated with polydopamine, LTA, and polyelectrolyte to construct 2 bilayers or trilayers following the same protocol as used for membrane synthesis. Then the sensors were flushed and stabilized in water after the layers were deposited. The sensors were further rinsed with an ionic solution with the same compositions of the feed but foulants. The sensors were rinsed and stabilized in water again before the frequencies were recorded. Next, these sensors were contacted with the fouling solution that composed of exactly the same compositions used for fouling the membrane. The contacting period of time was also 18 hours. The fouling solutions were rinsed off gently, and the sensors stabilized in pure water before they were analyzed using QCM-D again. A viscoelastic model was created using the built-in Q-Tools software (Q-sense, Sweden) to convert the frequency to the amount of mass deposition on the sensor surface.

4.3 Results and Discussion

4.3.1 Effects of One-sided and Double-sided Coating

The one-side and double-side coated trilayer membranes were tested in FO and PRO modes. As depicted in Figure 1, it can be observed that the trilayer membranes coated on both sides exhibit similar fouling behaviors for both BSA and alginate fouling. Specifically, in FO mode where the top surface facing the feed solution and thus the foulants, the water flux of the membrane coated with 2 trilayers on both sides dropped to ~88% of the initial water flux after fouled and gave a recovered flux at ~93% of the initial flux in BSA fouling experiments. The trilayer membrane held ~92% of the initial flux after fouled by BSA and its flux was recovered to ~96% in PRO mode. When alginate was present as the foulants, the flux of such membranes dropped to 77%~78% of the initial flux when running in the FO or PRO modes, but the recovered water flux can reach more than 92%. The small water flux decline after having been fouled and the high flux recovery after a simple flushing step indicate a good organic fouling resistance of the trilayer membranes. These results also prove that the two sides of coating are not significantly varied in the perspective of fouling, which is a good supplement to the previous work.[18]

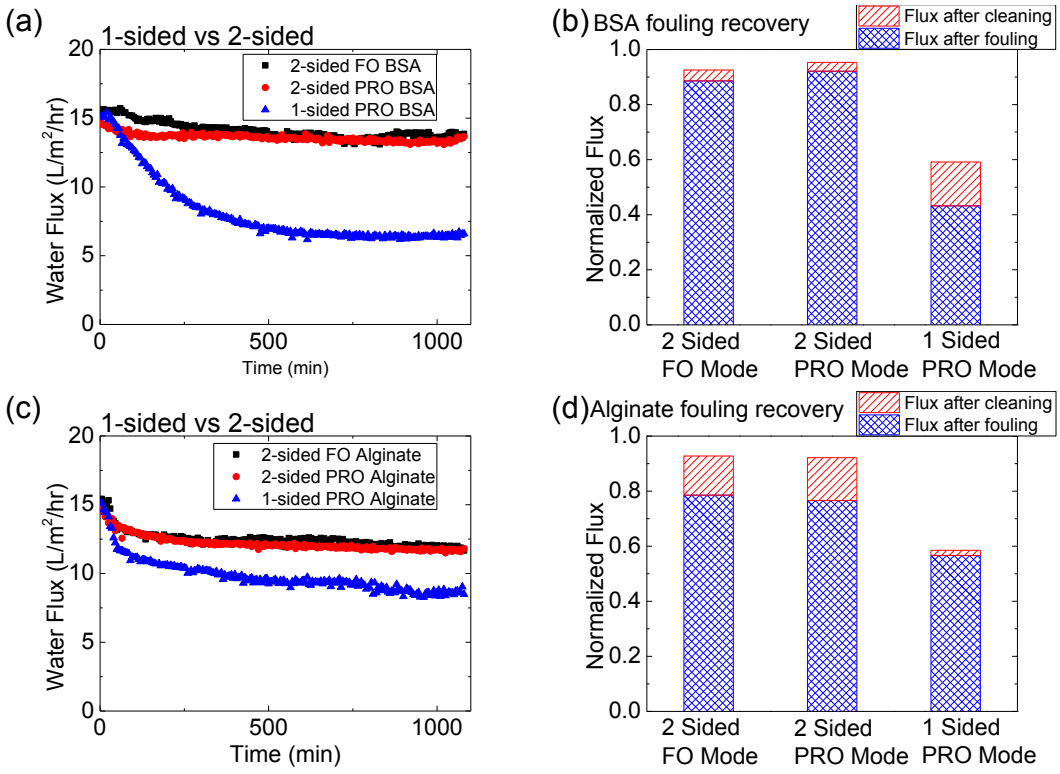

Figure 4.1. Membrane performance and the flux recovery rates of double-sided trilayer membranes (FO and PRO modes) and one-sided trilayer membrane (PRO mode) under (a, b) BSA or (c, d) alginate fouling. The one-sided membranes showed much less resistance to the organic foulants in PRO mode.

The membranes coated with 2 trilayers only on the top surface were also tested under the identical condition. When such membranes were operated in PRO mode, the PAN support layer was exposed directly to the foulants. In this scenario, the water flux only preserved ~43% of the starting flux under BSA fouling, and the water flux after the rinsing step was recovered to ~58%. The alginate fouling reduced the water flux to ~54% and the fouled membrane showed almost no recovery (~2% recovered), indicating that the PAN support was extremely vulnerable to organic foulants.

Therefore, the strategy of depositing a dense coating on the bottom side of the FO membrane is beneficial in mitigating organic fouling in PRO mode. It is expected that the coating could prevent the foulants from attaching to the support and penetrating into the inner membrane. The dopamine chemistry with polyelectrolytes utilized for making the membranes in this study can be extended to any kind of membranes. The pore covering effects can also be visualized by SEM, as illustrated in Figure 4.2. The pores, especially those at the bottom, were well covered after 2 bilayers or trilayers deposition. The 2-bilayer coating illustrated a smooth and featureless morphology while the 3-bilayer coating illustrated particle-like features that can be attributed to the LTA presence.

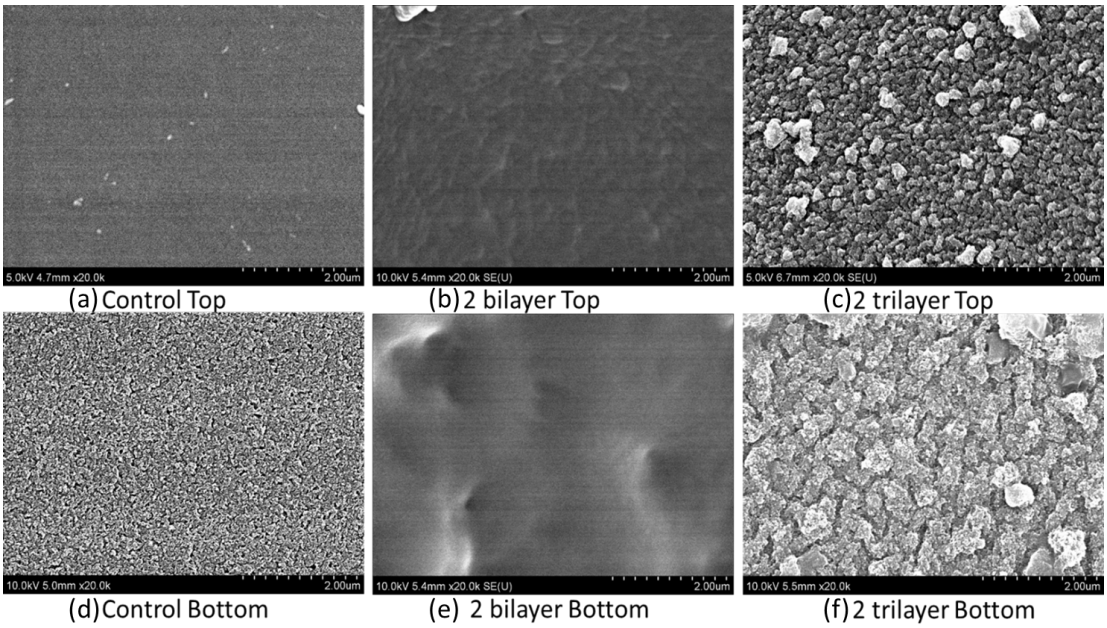

Figure 4.2. SEM images for both top and bottom surfaces of the (a, d) control PAN support and membranes coated with (b, e) 2 bilayers (smooth) or (c, f) 2 trilayers (rough). The multilayers can fully cover the pores of the support.

The zeolite-embedded polyelectrolyte composite membranes showed limited resistance to silica scaling. Figure 4.3 depicts the membrane performance and the flux recovery rate under silica scaling. The trilayer membranes showed a flux decline to ~68% and ~66% in FO and PRO, respectively. As a comparison, the flux decrease for the one-sided coating membrane in PRO mode was ~84%. The water fluxes were recovered to ~73% in FO mode and ~75% in PRO mode whereas the water flux recovery for the one-side coating membrane was ~98%. In other words, the bottom PAN support layer performed significantly better than the polyelectrolyte active layer with LTA incorporation. These phenomena meet the expectation as the LTA nanoparticles have high tendency for the occurrence of silica scaling.

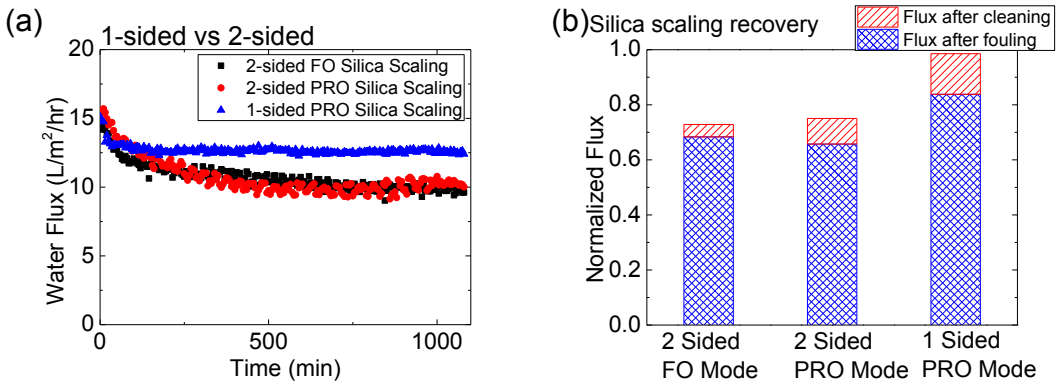

Figure 4.3. (a) Membrane performance and (b) the flux recovery rates of double-sided trilayer membranes (FO and PRO modes) and one-sided trilayer membrane (PRO mode) under silica scaling. The LTA-embedded layers showed lower resistance to the silica scaling.

4.3.2 Fouling on Bilayers and Trilayers

The silica scaling performance on bilayer membranes without LTA incorporation was conducted in FO mode and then compared with the trilayer membranes, as illustrated in Figure 4.4. The bilayer membranes showed almost no silica scaling. The water flux held ~98% after the membrane had been contacted with the scaling solution for 18 hours and the recovery rate was nearly 100%. This proves that the polyelectrolytes are extremely resistant to the scaling. The trilayer membranes were, as mentioned above, degraded significantly by the silica scaling. The LTA presence is hence identified as the primary cause of the severe silica scaling formation.

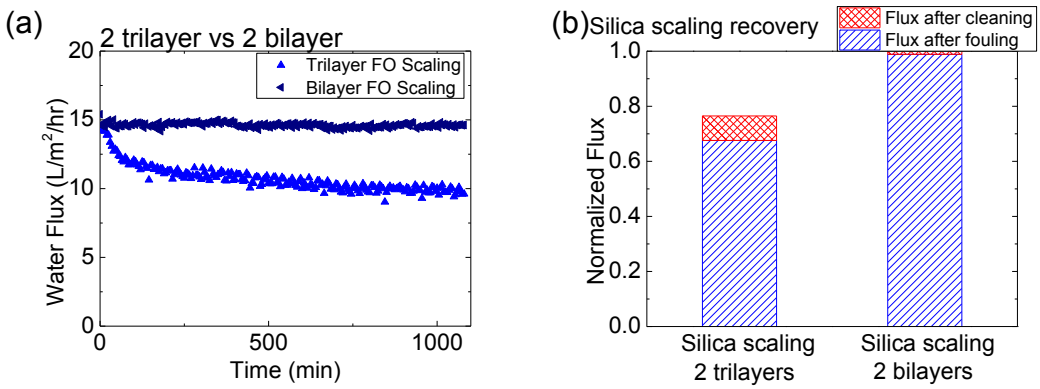

Figure 4.4. (a) Membrane performance and (b) the flux recovery rates of bilayer and trilayer membranes under silica scaling (FO mode). The bilayers without LTA incorporation was almost free of silica scaling.

Under the presence of the two organic foulants, as shown in Figure 4.5, the bilayer and trilayer membranes performed very similarly. The water flux of the bilayer membranes declined to ~88% under BSA fouling and ~86% under alginate fouling. The recovered fluxes by the simple rinsing step were ~96% and ~99% after BSA and

alginate fouled, respectively in FO mode. The LTA did not show meaningful improvements to the membrane fouling. Considering the hydrophilic nature of LTA nanoparticles and its in-between position, it is plausible that the LTA incorporation did not obviously affect the interactions between foulants and the membrane surface. The little lower resistance of trilayer membranes in terms of the flux decline and recovery rate could be attributed to the increased surface roughness of the membrane, as portrayed in Figure 4.2. Some organic foulants like BSA and alginate could be trapped in the cavities and voids that created by the embedded LTA nanoparticles underneath the polyelectrolytes.

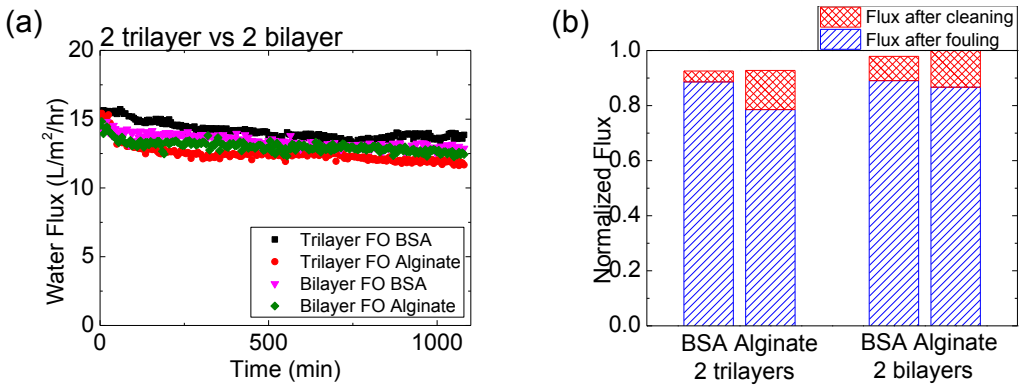

Figure 4.5. (a) BSA and alginate fouling profiles and (b) the recovery rates on 2-bilayer and 2-trilayer membranes. The trilayer membranes performed similarly to the bilayer membranes in organic fouling experiments.

4.3.3 QCM-D Measurements of Fouling Process

In QCM-D measurements, the sensors coated with 2 trilayers of PEI-LTA-PAA were focused to quantitatively model the deposited mass of foulants. The frequency of each sensor after dopamine coating was set as the baseline with zero mass. The frequencies

were converted to mass using the built-in software. Figure 4.6 describes the percentage of mass change after the layer deposition and after fouling. After treated with BSA foulants, the mass of the sensor coated with 2 trilayers was found increased by 7.9% referenced to the mass of trilayers. The mass increase after alginate fouling was about 12.6%. The larger mass deposition of alginate than that of BSA may explain the greater water flux reduction in alginate fouling experiments than the reduction under BSA fouling condition. The silica scaling produced a much higher mass increase on the sensor, which was about 23.0%, indicating a considerable scaling layer formed. Collectively, these results are corresponding with the fouling behaviors measured in the FO system.

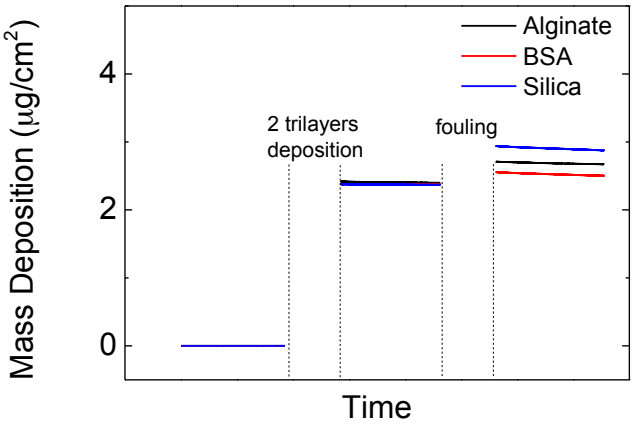

Figure 4.6. Weight deposition of different foulants (alginate, BSA, and silica scaling) on 2 trilayers measured via QCM-D.

4.4 Conclusions

This study demonstrates the fouling behaviors of a novel polyelectrolyte-zeolite composite FO membrane. Unlike the traditional FO membranes that are asymmetric, the polyelectrolyte membranes have active layers on both sides and have been proven helpful in mitigating PRO fouling. Moreover, this composite membrane showed good fouling resistance to organic foulants, but it is susceptible to the silica scaling. The reason is believed to be the zeolite incorporation, as zeolites are essentially aluminosilicates and highly compatible with silica-based matters. To further confirm the observation, fouling experiments on a polyelectrolyte membrane without zeolite incorporation were conducted, and the silica scaling was found negligible. The whole fouling procedures were also repeated on QCM-D sensors to access the mass deposition of the foulants, revealing the scaling does result in a substantial mass deposition. This work may help to define the advantages and limitations of using zeolite/polyelectrolyte-based membranes for diverse water treatment processes.

4.5 Acknowledgements

This material is based on work supported by the National Science Foundation (NSF) under Grant CBET-1154572 and a University of Maryland ADVANCE Program for Inclusive Excellence Interdisciplinary and Engaged Research Seed Grant. The support is gratefully acknowledged. We also acknowledge the facility support of the Maryland NanoCenter and NispLab. The NispLab is supported in part by the NSF as a Materials Research Science and Engineering Center shared experimental facility.

4.6 References

1. Cath, T. Y.; Childress, A. E.; Elimelech, M., Forward osmosis: Principles, applications, and recent developments. *J Membrane Sci* **2006,** *281*, (1-2), 70-87.

2. Alsvik, I. L.; Hagg, M. B., Pressure Retarded Osmosis and Forward Osmosis Membranes: Materials and Methods. *Polymers-Basel* **2013,** *5*, (1), 303-327.

3. Belfort, G.; Davis, R. H.; Zydney, A. L., The Behavior Of Suspensions And Macromolecular Solutions In Cross-Flow Microfiltration. *J Membrane Sci* **1994,** *96*, (1-2), 1-58.

4. Kimura, K.; Hane, Y.; Watanabe, Y.; Amy, G.; Ohkuma, N., Irreversible membrane fouling during ultrafiltration of surface water. *Water Res* **2004,** *38*, (14-15), 3431-3441.

5. Wu, J. L.; Le-Clech, P.; Stuetz, R. M.; Fane, A. G.; Chen, V., Effects of relaxation and backwashing conditions on fouling in membrane bioreactor. *J Membrane Sci* **2008,** *324*, (1-2), 26-32.

6. Fan, L. H.; Harris, J. L.; Roddick, F. A.; Booker, N. A., Influence of the characteristics of natural organic matter on the fouling of microfiltration membranes. *Water Res* **2001,** *35*, (18), 4455-4463.

7. Lee, S.; Boo, C.; Elimelech, M.; Hong, S., Comparison of fouling behavior in forward osmosis (FO) and reverse osmosis (RO). *J Membrane Sci* **2010,** *365*, (1-2), 34-39.

8. Li, Q. L.; Elimelech, M., Organic fouling and chemical cleaning of nanofiltration membranes: Measurements and mechanisms. *Environ Sci Technol* **2004,** *38*, (17), 4683-4693.

9. Mi, B.; Elimelech, M., Chemical and physical aspects of organic fouling of forward osmosis membranes. *J Membrane Sci* **2008,** *320*, (1-2), 292-302.

10. Mi, B. X.; Elimelech, M., Organic fouling of forward osmosis membranes: Fouling reversibility and cleaning without chemical reagents. *J Membrane Sci* **2010,** *348*, (1-2), 337-345.

11. Asatekin, A.; Kang, S.; Elimelech, M.; Mayes, A. M., Anti-fouling ultrafiltration membranes containing polyacrylonitrile-graft-poly (ethylene oxide) comb copolymer additives. *J Membrane Sci* **2007,** *298*, (1-2), 136-146.

12. Lu, X. L.; Castrillon, S. R. V.; Shaffer, D. L.; Ma, J.; Elimelech, M., In Situ Surface Chemical Modification of Thin-Film Composite Forward Osmosis Membranes for Enhanced Organic Fouling Resistance. *Environ Sci Technol* **2013,** *47*, (21), 12219-12228.

13. Ma, H. M.; Hakim, L. F.; Bowman, C. N.; Davis, R. H., Factors affecting membrane fouling reduction by surface modification and backpulsing. *J Membrane Sci* **2001,** *189*, (2), 255-270.

14. Shaffer, D. L.; Jaramillo, H.; Castrillon, S. R. V.; Lu, X. L.; Elimelech, M., Post-fabrication modification of forward osmosis membranes with a poly(ethylene glycol) block copolymer for improved organic fouling resistance. *J Membrane Sci* **2015,** *490*, 209-219.

15. Tiraferri, A.; Kang, Y.; Giannelis, E. P.; Elimelech, M., Superhydrophilic Thin-Film Composite Forward Osmosis Membranes for Organic Fouling Control: Fouling Behavior and Antifouling Mechanisms. *Environ Sci Technol* **2012,** *46*, (20), 11135-11144.

16. Duong, P. H. H.; Zuo, J.; Chung, T. S., Highly crosslinked layer-by-layer polyelectrolyte FO membranes: Understanding effects of salt concentration and deposition time on FO performance. *J Membrane Sci* **2013,** *427*, 411-421.

17. Qiu, C. Q.; Qi, S. R.; Tang, C. Y. Y., Synthesis of high flux forward osmosis membranes by chemically crosslinked layer-by-layer polyelectrolytes. *J Membrane Sci* **2011,** *381*, (1-2), 74-80.

18. Kang, Y.; Emdadi, L.; Lee, M. J.; Liu, D. X.; Mi, B. X., Layer-by-Layer Assembly of Zeolite/Polyelectrolyte Nanocomposite Membranes with High Zeolite Loading. *Environmental Science & Technology Letters* **2014,** *1*, (12), 504-509.

19. Kawai, T.; Tsutsumi, K., Reactivity of silanol groups on zeolite surfaces. *Colloid Polym Sci* **1998,** *276*, (11), 992-998.

20. Liu, Y. L.; Mi, B. X., Effects of organic macromolecular conditioning on gypsum scaling of forward osmosis membranes. *J Membrane Sci* **2014,** *450*, 153-161.

21. Mi, B. X.; Elimelech, M., Silica scaling and scaling reversibility in forward osmosis. *Desalination* **2013,** *312*, 75-81.

Chapter 5: Membrane Regeneration of Polyelectrolyte Membranes

5.1 Introduction

Membrane-based technologies have remarkably benefited separation processes for water purification and treatment. Ultrafiltration (UF), nanofiltration (NF), reverse osmosis (RO) and the emerging forward osmosis (FO) are among the most effective approaches to purifying water, especially for non-traditional water sources.[1, 2] Typically, these membrane processes involve semipermeable membranes, in which thin-film composite polyamide (PA) and cellulose triacetate (CTA) have been largely applied due to their good separation capability and reasonable chemical resistance.[3-6] In addition, polyelectrolyte multilayers fabricated via the versatile layer-by-layer (LbL) technique have been developed and proven effective as separation barriers in various membrane processes.[7-10] The polyelectrolyte membranes show relatively good performance and have great potential for working in complicated circumstances, as they can meet special needs by adjusting the fabrication conditions, altering surface charge and functionality, and/or selecting different polyelectrolyte species.[8, 11-14]

These water treatment membranes, like all other diverse membranes for separation, concentration and recovery processes, still face many technical limitations. One of the biggest obstacles that hinder the wide utilization of membrane technologies in water treatment is membrane fouling.[15-21]

All kinds of pre- and post-treatments during membrane synthesis have been extensively investigated for improving the membrane fouling resistance, such as grafting a hydrophilic coating and reducing surface roughness.[22-25] Furthermore, backwashing and chemical rinsing are the most commonly used methods to mitigate membrane fouling. However, when irreversible fouling occurs on the membrane surface, conventional membrane cleaning protocols become ineffective and thus membrane replacements are required.[26, 27] Therefore, there is a need to extend the membrane lifetime and cut the costs from membrane replacement.

Interestingly, the polyelectrolyte layer created via LbL assembly can be controlled to be released under certain conditions.[28, 29] This unique property of polyelectrolytes offers the possibility of removing the active layer of a polyelectrolyte membrane as a sacrificial layer along with the irreversible foulants deposited on the membrane surface. The polyelectrolyte layer can be then regenerated on-site and sent back to functional through the LbL assembly. Several studies have discussed the possibility of using strong acids or bases to disassemble and rebuild the polyelectrolyte active layer in a NF or UF process for fouling control. A few combinations of weak polyelectrolytes, such as poly(allylamine) hydrochloride (PAH)/poly(acrylic acid) (PAA), poly(sodium 4-styrenesulfonate) (PSS)/PAH, and poly(diallylmethyl-ammonium chloride) (PDADMAC)/PSS, were used for demonstration.[30-32] Since fouling mechanisms are different between pressure-driven processes and osmotically-driven processes, the effectiveness and efficiency of the polyelectrolyte-based membranes in FO operation need to be examined as well.[17, 33]

In this study, the membrane regenerability of a polyelectrolyte membrane composed of PAA and polyethyleneimine (PEI) was investigated in FO process. Using this formula of (PEI-PAA), the polyelectrolyte bilayers were fabricated on the top of a polydopamine-functionalized polysulfone (PSf) support. A unique phenomenon of the water transport mechanism was observed and briefly discussed. The bilayer membranes were characterized through several tools to understand the regenerating process. The membrane regenerability was evaluated using alginate as the representative foulant and using strong acid to trigger the release of polyelectrolyte layers.

5.2 Materials and Methods

5.2.1 Membrane Synthesis

All materials and chemicals were purchased from Sigma-Aldrich (St. Louis, MO) and were used as received unless specified. The polysulfone (PSF, M_w 22,000) support was made by a conventional phase-inversion method with polyvinylpyrrolidone (PVP, M_w 55,000) for pore forming. PSf and PVP were fully dissolved in 1-Methyl-2-pyrrolidone (NMP) with a PSf/PVP/NMP ratio of 16/4/80 and kept in vacuum for 48 hour. The as-prepared solution was cast into a 125-μm film with a stainless steel casting knife on a glass plate, and the glass plate was then immediately immersed into a water bath for 10 minutes. The PSf membranes were afterwards transferred to another water bath after they were separated from the glass plate. The water bath was refreshed several times and was stored in a refrigerator for future use. Bilayers of poly(acrylic acid) (PAA, M_v 450,000) and polyethyleneimine (PEI, M_w 750,000)

were created through a layer-by-layer assembly on a polydopamine-coated PSf. Specifically, the PSf support was treated by soaking in a freshly-prepared dopamine solution (2 mg/mL dopamine in 10mM Tris-HCl, pH 8.5) for 5 hour. Then the polydopamine-coated PSf was subsequently immersed in PEI (1 g/L) and PAA (1 g/L) solutions. Each dipping step lasted for 20 minutes except for the first PEI immersion (1 hour). Deionized (DI) water was used to rinse the membrane between any two dipping steps.

5.2.2 Membrane Performance and Regeneration Tests

Hydrochloric acid (HCl) was used in this study for disassembling and triggering the release of the polyelectrolyte bilayers. HCl solutions at different pHs were prepared and the pH was determined by a pH meter (Accumet Excel XL15, Thermo Scientific, Marietta, OH). As a releasing step, the bilayer membranes were immersed in HCl solution for 0.5 hour and thoroughly rinsed with DI water. The membrane was then stabilized in DI water for 1 hour before any further treatment.

The regeneration process followed exactly the same conditions as used in the synthesis process, including soaking the acid-treated and DI-stabilized membrane alternatively into PEI and PAA solutions for a new layer deposition. A schematic drawing of the regenerating process is illustrated in Figure 5.1. The membrane flux before and after fouling/regeneration was evaluated using a lab-scale FO system.[34] The membrane was installed in a cross-flow cell at a constant flow rate of 8.5 cm/s and tested in both FO and PRO modes. Trisodium citrate (TSC, Fisher Scientific, Pittsburgh, PA) was used as the draw solute. The conductivity change in feed solution

after the water flux reached steady state was monitored using a conductivity meter (Accumet Excel XL30, Thermo Scientific, Marietta, OH). The conductivity records were converted to solute concentration based on an established standard curve for calculating the reverse solute flux. For fouling the membrane, alginate (200 mg/L) was mixed into the feed solution, which also contained 50 mM NaCl and 0.5 mM $CaCl_2$.[17] The fouling duration is 18 hour for allowing the sufficient deposition of foulants.

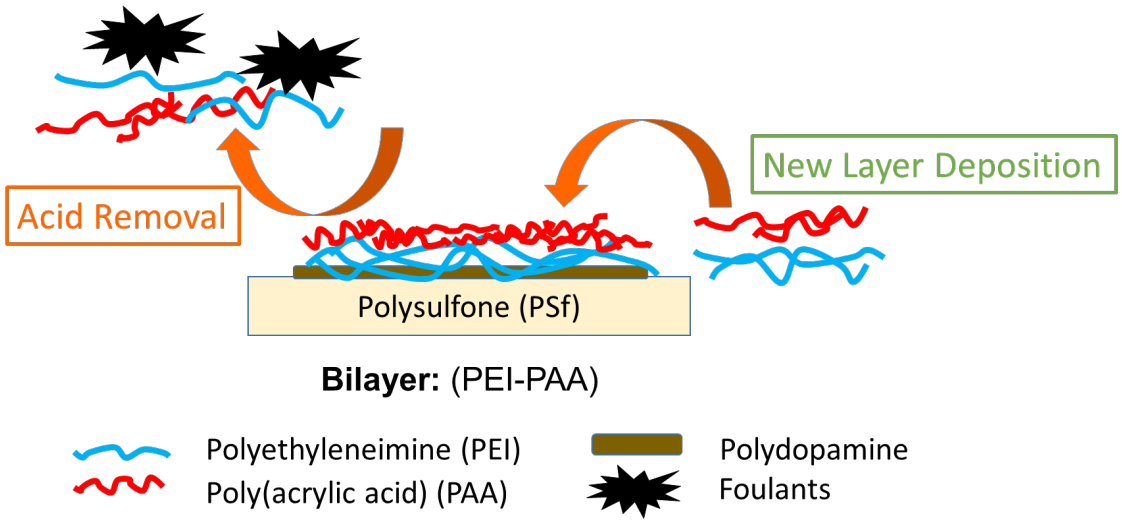

Figure 5.1. A schematic drawing of the regenerating process that involves removal of the fouled layer by acid treatment and deposition of new polyelectrolyte layers.

5.2.3 Membrane Characterizations

The bilayer membranes were characterized by Fourier transform infrared (FTIR) spectroscopy (Nicolet 6700, Thermo Scientific, Marietta, OH), scanning electron microscopy (SEM, SU-70, Hitachi High Technologies America, Gaithersburg, MD)

and quartz crystal microbalance with dissipation (QCM-D, Q-sense E4 system, Sweden). For FTIR and SEM, the samples were dried overnight at room temperature and put into an oven at 60 °C for 30 minutes to eliminate moisture before characterization. The SEM samples were sputtered with a thin layer of gold nanoparticles (<10 nm) on top for eliminating the electron-charging effect. The treatment procedures for the QCM-D sensors, including the dipping sequence, dipping duration, and treating solutions, were kept the same as that used for the membrane synthesis. A flow-chamber at a flow rate of 0.1 mL/min was used for monitoring the variations of vibration frequency and dissipation, which were modeled using the Q-Tools software (Q-sense, Sweden) to analyze the amount of mass deposited and released on the sensor surface. Transmission electron microscopy (TEM, JEOL JEM 2100, Peabody, MA) was also employed for examining the structural change caused by the acid treatment. The polyelectrolyte solutions were dipped onto a TEM carbon grid following the same sequence of membrane synthesis.

5.3 Results and Discussion

5.3.1 Membrane Characterizations and Performance

A number of PEI-PAA bilayers (2, 4, and 6) were created on the PSf support. The top surface is defined based on the PSf support after phase inversion, which the surface facing ambient water is considered as the top while the surface attached to the glass plate is the bottom. The contact of polyelectrolyte solutions was not merely constrained on one surface. SEM gives the top surface morphology of the bilayer membranes (Figure 5.2). Except for the sample right after dopamine functionalization

that shows some polydopamine aggregations, the pristine control PSf support and bilayer-coated membranes illustrate relatively smooth and featureless characteristics. The increasing number of bilayers can be differentiated from the FTIR spectra (Figure 5.3a). Compared with the pristine control PSf, the background support characteristic peaks ranging 700 - 1250 cm^{-1} becomes less intensive. The 2-bilayer membrane shows a small characteristic peak of carboxyls from PAA near 1700 cm^{-1}. With the increasing number of bilayers, two broad peaks at around 1410 and 1550 cm^{-1} becomes predominant which represents the asymmetric carboxylate stretching from PEI-PAA binding.[35]

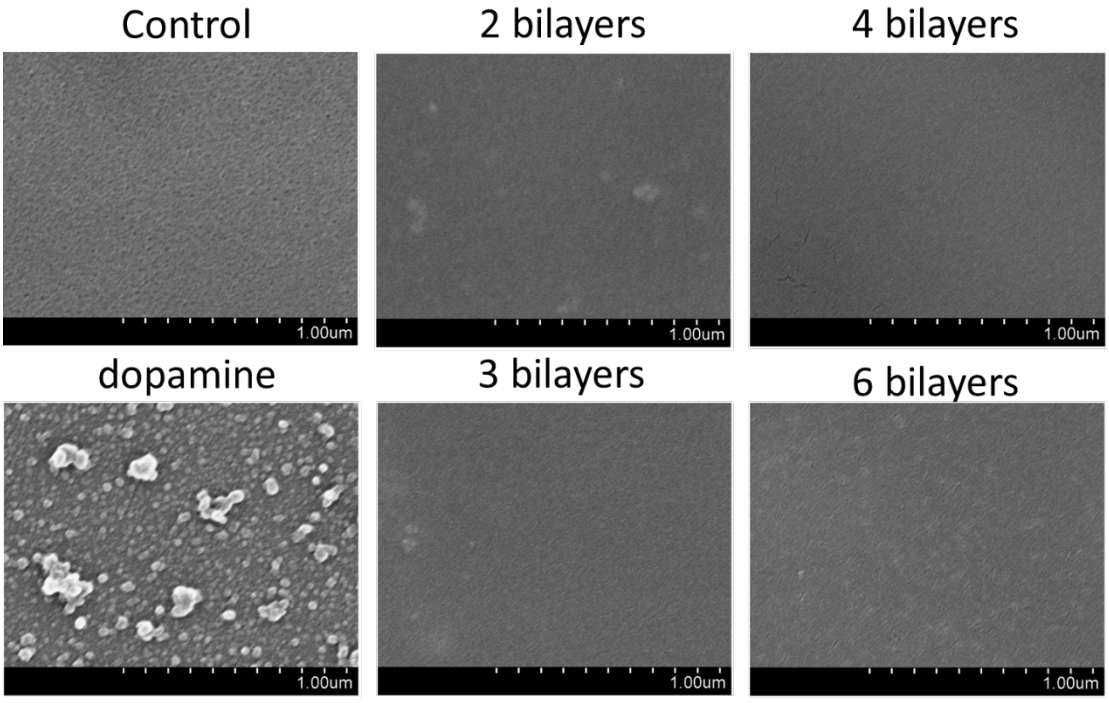

Figure 5.2. SEM images of the PSf support before and after different number of bilayers deposition.

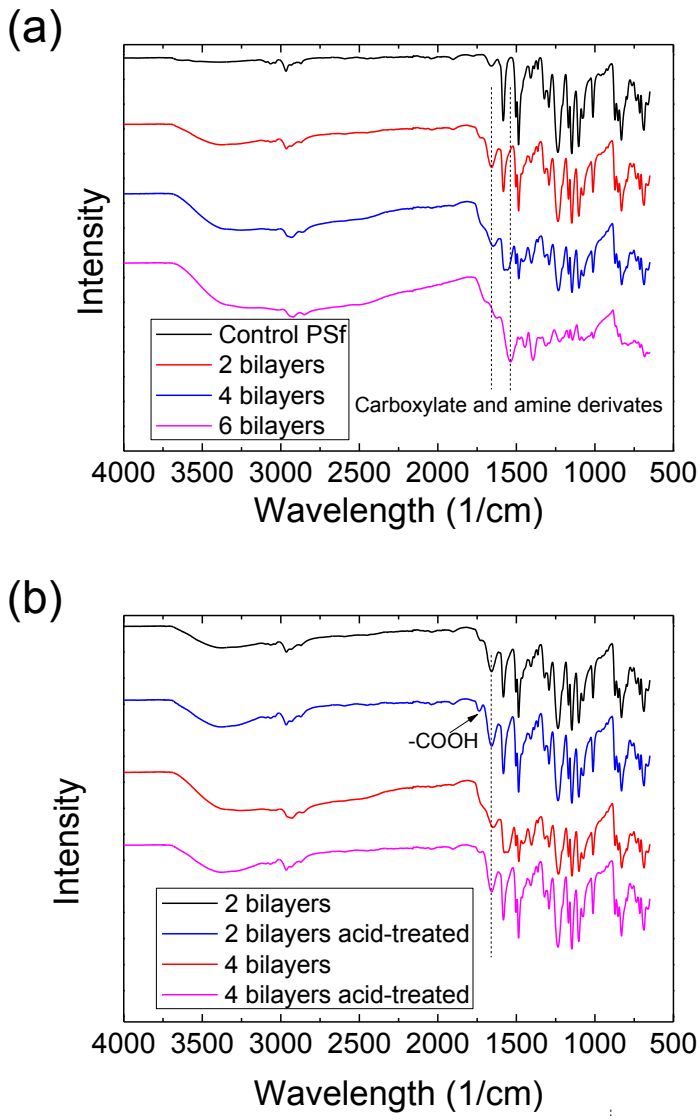

Figure 5.3. FTIR spectra of (a) the polyelectrolyte membranes with different number of bilayers and (b) 2-bilayer and 4-bilayer membranes before and after acid treatment.

Membrane flux (Figure 5.4a) and reverse solute flux (Figure 5.4b) were measured in the FO system with both membrane directions, namely FO (top layer facing feed solution) and PRO (top layer facing draw solution) modes. The FO flux decreased with increasing number of bilayers for both FO and PRO modes, which is mainly

attributed to the thicker layer causing a stronger permeation resistance. The reverse solute flux was lower as well when more bilayers were deposited, as the rejection to solute was enhanced with a thicker active layer. The 2-bilayer membranes present the highest water flux at ~6.1 μm/s (22.0 LMH) with a reasonable reverse solute flux of ~0.06 MMH when using 0.5M TSC as draw solution and DI water as feed. As a result, the 2-bilayer membranes were selected for the following regenerating tests.

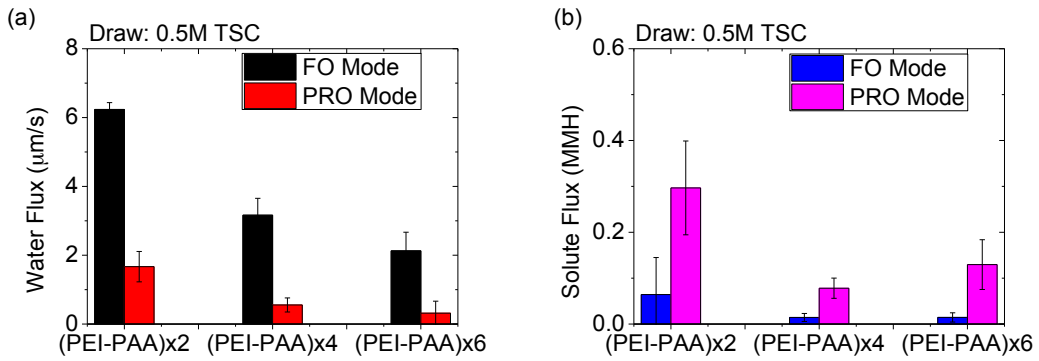

Figure 5.4. (a) Water flux and (b) reverse solute flux for the polyelectrolyte membranes with different number of bilayers (2, 4 or 6).

Interestingly, we observed a phenomenon in which the water flux in PRO mode is significantly smaller than that in FO mode, which contradicts the behaviors of asymmetric PA- or CTA-based FO membranes. For those membranes, PRO flux is typically higher than FO flux, because of a greater effective osmotic gradient in PRO mode after subtracting the influence of internal concentration polarization.[36, 37] A model (Figure 5.5) was established to explain this observation. Unlike PA or CTA, polyelectrolyte layers will significantly swell under ionic strength, resulting in a lower solute rejection and thus a lower osmotic gradient. Although the bilayer

depositing process was conducted on both surfaces, the bottom surface of PSf support could not maintain an integral layer of polyelectrolyte deposition because it has large pores (~400 nm), but the top can hold a complete layer of polyelectrolytes (Figure 5.6). In FO mode, the top surface facing the feed solution (low ionic strength) is relatively dense and can work as an effective barrier, and the bottom does not contribute to rejecting solutes. Comparatively in PRO mode, the top integrated polyelectrolyte layer (in high ionic strength) swells and becomes a less effective barrier, leading to higher solute flux and lower water flux. Still, the bottom surface provides little contribution for rejecting solutes. Our previous work on polyacrylonitrile (PAN) support showed a comparable FO and PRO fluxes, which can be also explained by this mode, noting that the bottom of PAN support has much smaller pore size and can maintain the integrity of the polyelectrolyte layer.[13] Briefly, when using PAN as the support, which is barely distinguished after the trilayer deposition on both sides, the top layer in FO mode and the bottom layer in PRO mode play the major and similar role of separation. (Figure 5.5b).

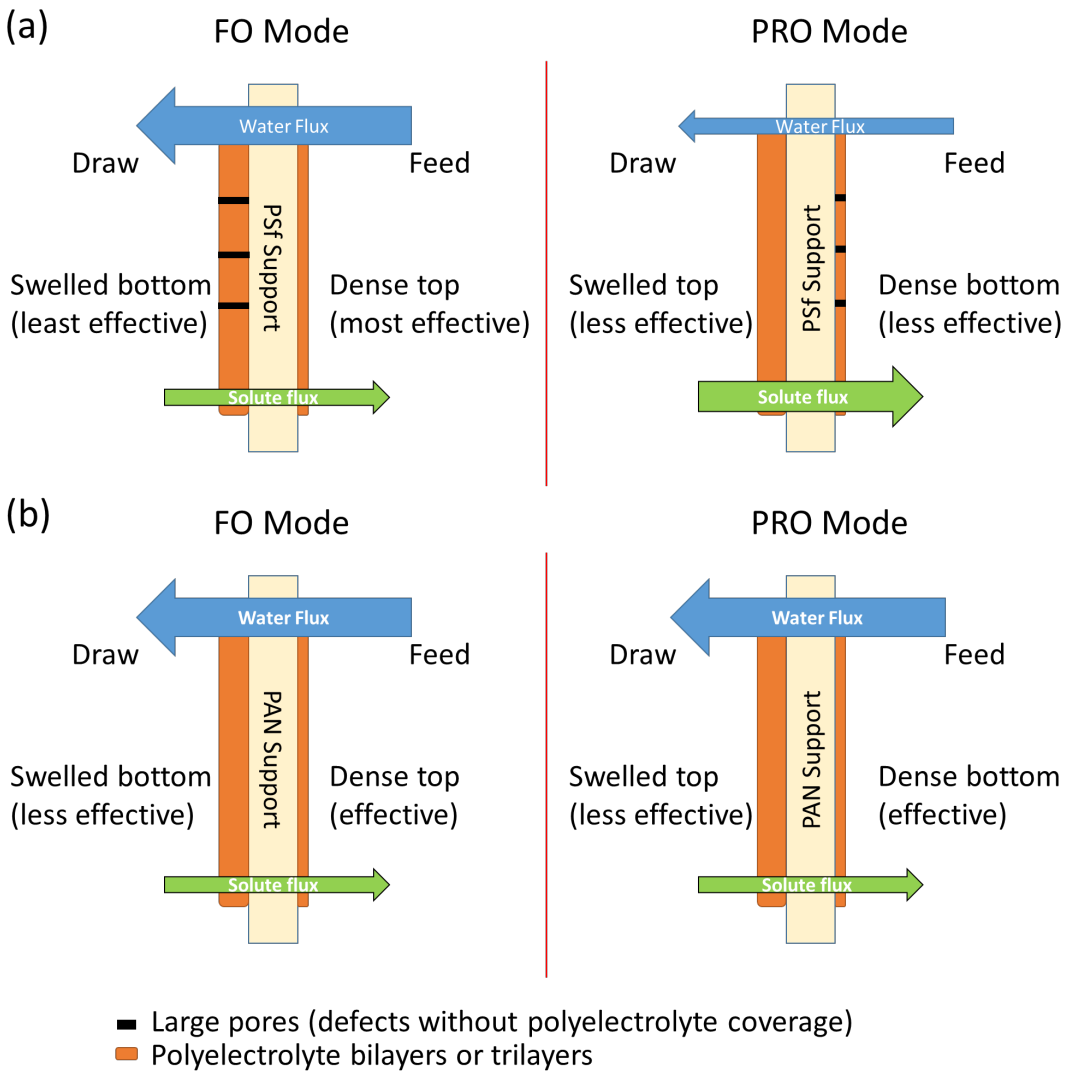

Figure 5.5. A schematic model of the proposed transport mechanism to explain the unique water flux behavior of (a) PSf-supported and (b) PAN-supported membranes. The effectiveness of each active layer is noted for different settings.

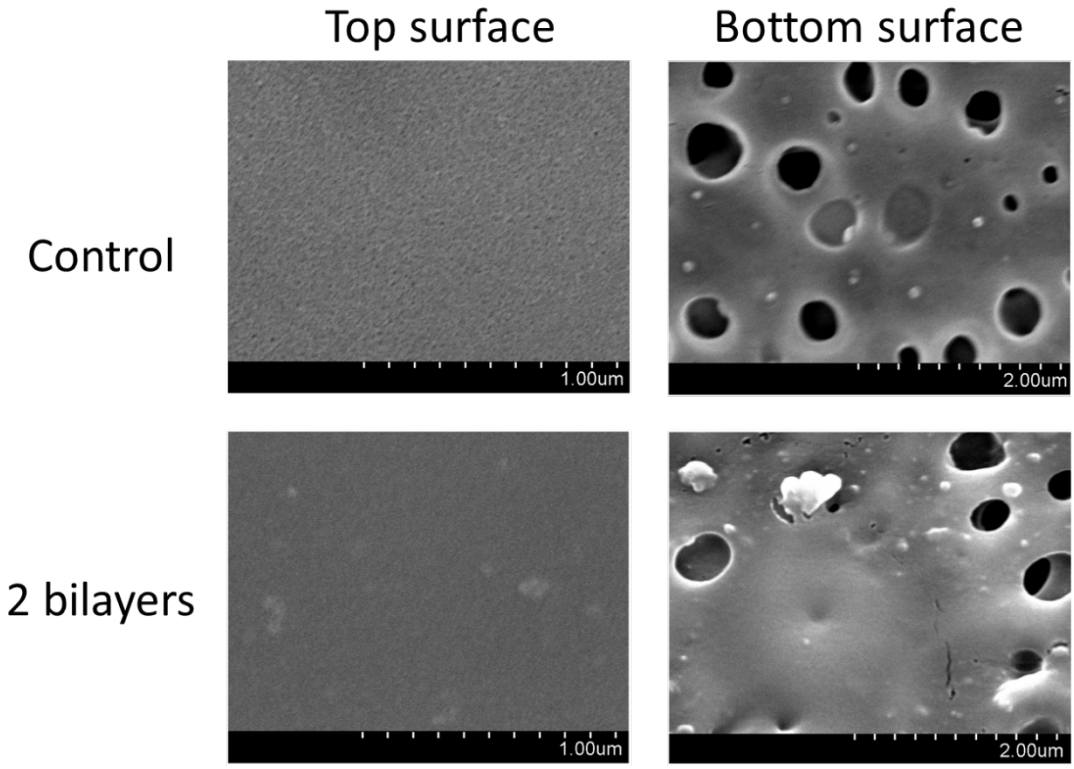

Figure 5.6. SEM images for top and bottom surfaces of PSf support before and after 2-bilayer polyelectrolyte deposition.

5.3.2 Effects of Acid Treatment

Strong acid can protonate carboxyl groups of PAA and neutralize the charges for deconstructing the polyelectrolyte binding. Release of polyelectrolyte layers under acidic condition was firstly simulated using QCM-D. Two bilayers of PEI-PAA were first created on the QCM-D sensor and subsequently treated with HCl solutions from pH3 to pH2 (Figure 5.7). The polyelectrolyte layers were not severely damaged, as the vibration frequency remained almost unchanged. The pKa for carboxyl groups is around 4.5, but when those groups are localized and constrained on a surface instead of free-moving, the "effective pKa" can be varied.[38] The integrity of polyelectrolyte

layers almost maintained even at pH 2, therefore HCl solution at pH 1 is chosen to delaminate the polyelectrolyte layers.

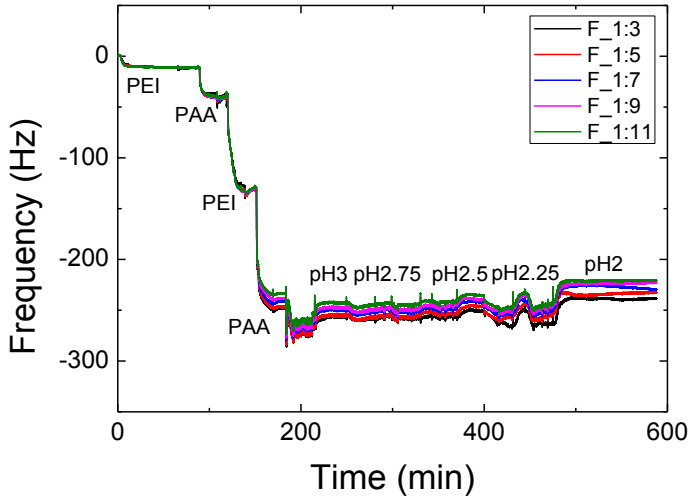

Figure 5.7. The effects of acid treatment ranging between pH 3 and pH 2 on a 2-bilayer film coated on a QCM-D sensor. The mass (frequency) change was not obvious within such pH range.

In the QCM-D measurements of the pH 1 effects on the polyelectrolyte layers (Figure 5.8a), it can be found that a large portion but not all of the layers was removed. A little more than one bilayer was left. The residual mass was also previously reported for the NF membranes.[31, 32] Unlike the previous reports that the residual mass was mainly attributed to adsorption, the first layer of PEI is designed to covalently bond with the polydopamine layer through nucleophilic addition.[39, 40] The releasing part was mostly the second bilayer. The left first bilayer could benefit the regeneration, because it could help to prevent the acid-foulant mixture during the releasing step

from penetrating and blocking the support. Cross-sectional SEM images of the 6-bilayer membranes and the 2-bilayer membranes (Figure 5.9) also illustrate the thickness change, illustrating the removal and residual of polyelectrolytes by the acid treatment. The thickness was reduced from ~3 μm to less than 1 μm for the 6-bilayer membranes after the acid treatment. The compositions of the membrane, according to the FTIR spectroscopy (Figure 5.3b), were similar after the acid treatment. The membrane after acid-treatment exhibits changes at around 1700 ~ 1720 cm^{-1}, which is attributed to the disassociation of carboxylates and appearance of carboxyls.

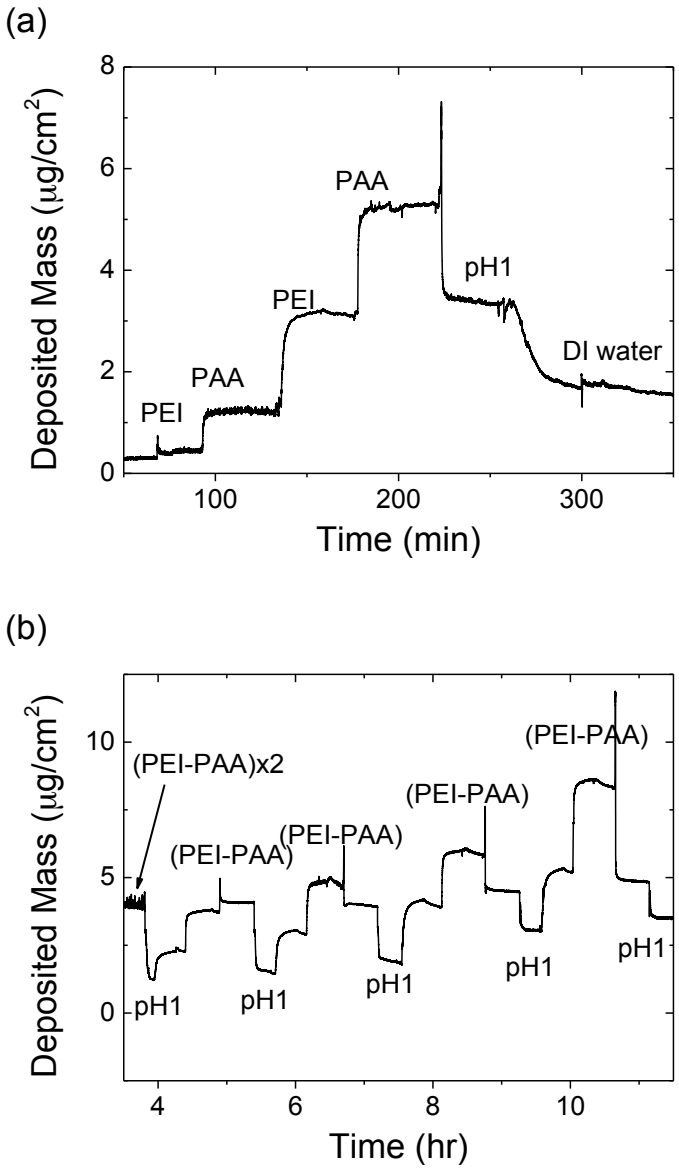

Figure 5.8. Mass deposition measured via QCM-D: (a) mass removal effect of acid on 2-bilayer film and (b)the regenerating process with constructing the new bilayer for 4 cycles.

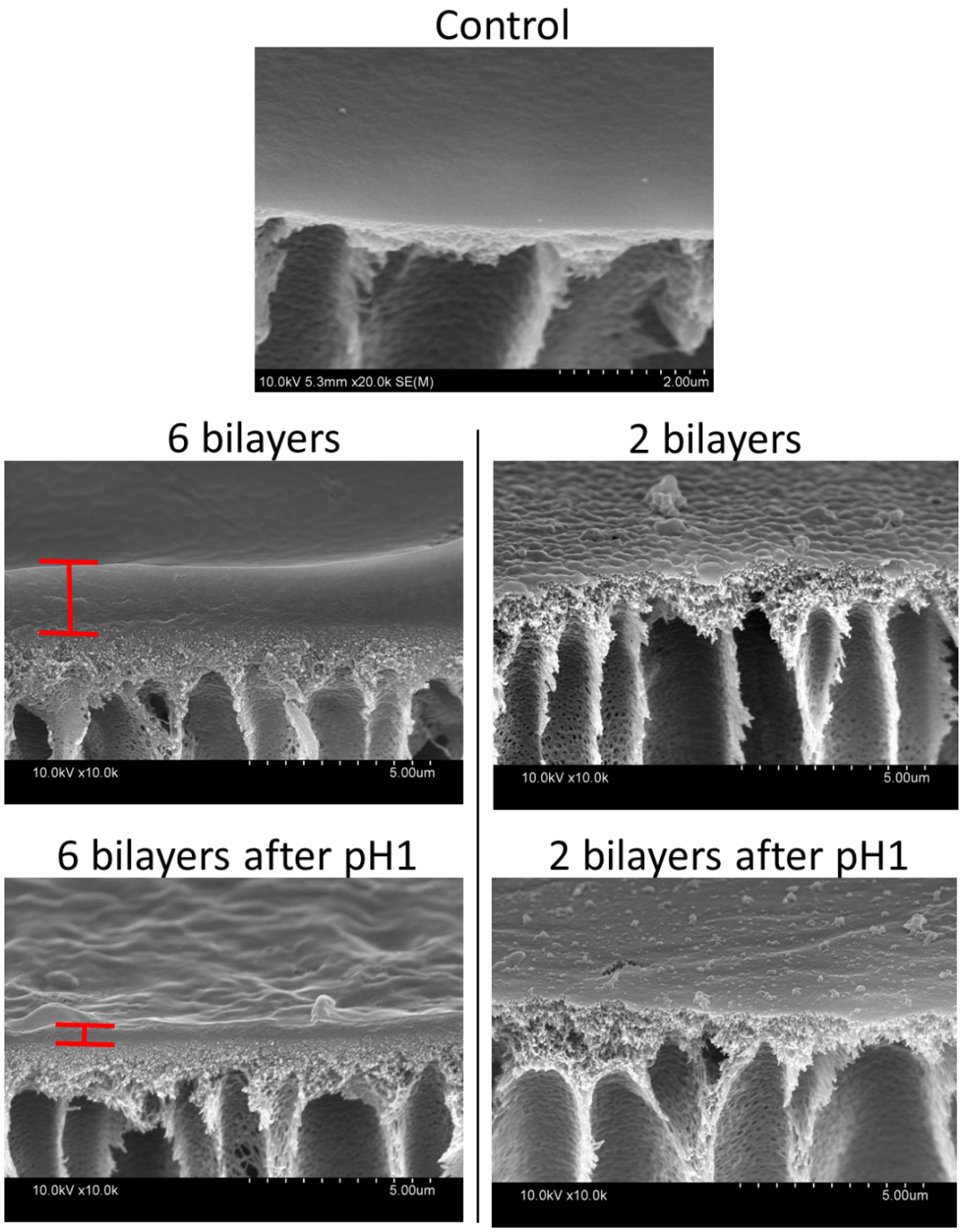

Figure 5.9. Cross-sectional SEM for 6-bilayer and 2-bilayer membranes to illustrate the reduced thickness of polyelectrolyte layer after acid treatment.

The release and regeneration processes were also modeled using QCM-D (Figure 5.8b). It can be found that the amount of residual mass after acid treatment increased along with increasing regeneration cycles. In other words, the regenerated layers are observed to contain more mass (a thicker polyelectrolyte layer) than the original layers, although the increase of residual mass after acid treatment (~0.5 μg/cm^2/cycle) and the increased mass of regenerated layer (~0.4 μg/cm^2/cycle) are minimal. This additional mass may be caused by a structural change after the strong acid treatment.[41] To elucidate this phenomenon, 2 bilayers were created on a TEM carbon grid and characterized (Figure 5.10). The as-prepared 2-bilayer-coated grid presents a smooth featherless surface similar to the SEM images, however after the acid-treatment, the sample presents a much rougher surface. This implies that the acid does not evenly remove the polyelectrolyte layers and some areas show better acid resistance possibly due to a tighter structure or a higher density of polyelectrolyte molecules. At a higher magnification, a few small areas with aligned features are observed. TEM diffraction patterns for these features present a bright ring, suggesting the existence of some alignments of polyelectrolytes, which are not observed in the untreated samples. Figure 5.10b presents the EDX spectrum for the acid-treated sample. Except for the copper (Cu) and silicon (Si) peaks that were collected from the TEM grid due to an insufficient coverage of sample, carbon (C), oxygen (O) and chlorine (Cl) could be all detected. Given that nitrogen (N) was absent, it seems like the major component left on the TEM grid was PAA rather than the blend of PEI and PAA. The alignment observed is likely due to the precipitation of PAA after the acid protonated the carboxylates and reduced the solubility of PAA. This observation that

the acid treatment has removed most of PEI and left PAA from the 2 bilayers on TEM grid is agreed with the QCM-D results (Figure 5.8a). In the QCM-D analysis, the sensor coated with polydopamine (TEM grid was not treated with polydopamine) was covalently bonded with PEI, so most of the PEI stayed on the sensor. The PAAs left after acid treatment consisted of two parts: associated with PEIs before the acid treatment and precipitated on the surface after the acid treatment, eventually forming the more than one residual bilayer. It is hypothesized that after the regenerating step the membrane may retain a similar state because the available sites on the residual layer for the extensive PAA have certain capacity. This implies that the mass of residual layer after acid treatment is not likely to keep growing unlimitedly.

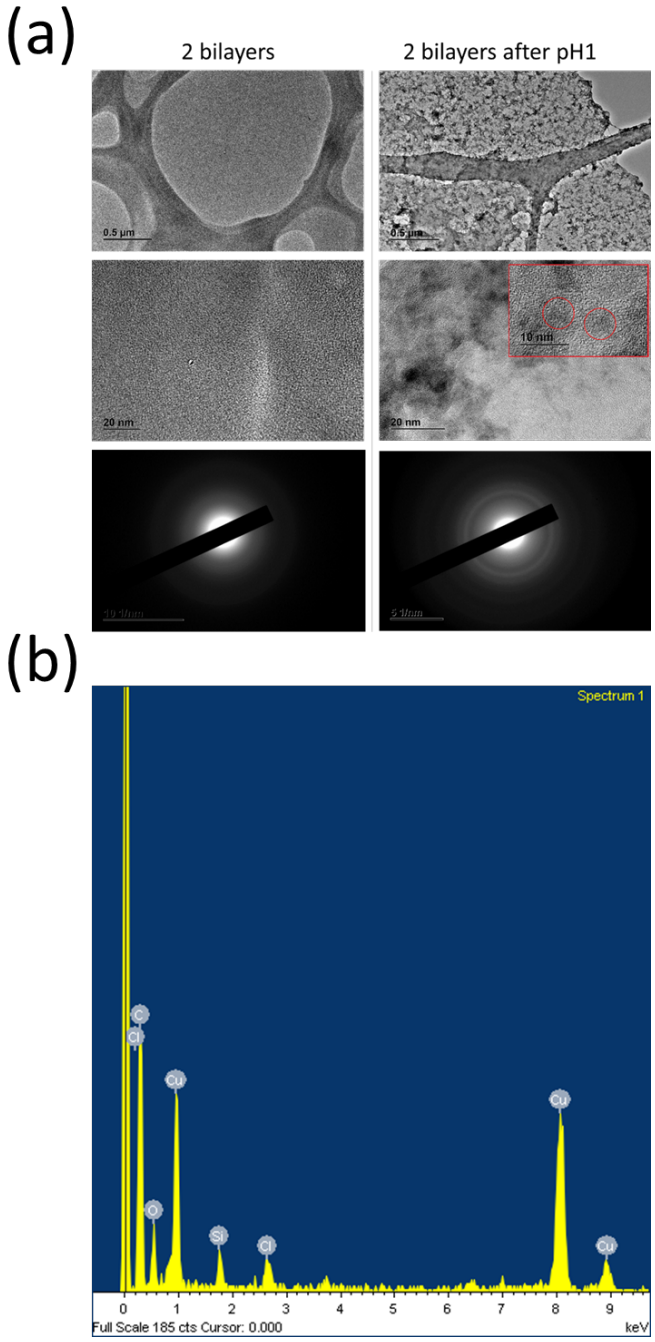

Figure 5.10. (a)TEM images for a 2-bilayer film before and after acid treatment (pH 1) and (b) EDX spectrum of the treated sample. The Cu and Si came from the TEM copper grid and the detector.

5.3.3 Regeneration Process in FO

The 2-bilayer membranes were tested in FO mode. The water flux (Figure 5.11a) was measured after acid treatment and a new bilayer of PEI-PAA deposition. The water flux was significantly increased after the acid removal, from ~20 LMH to ~24 LMH, which is likely due to a smaller permeation resistance of the thinner polyelectrolyte layer. After the new bilayer was deposited, the water flux returned to about 15 LMH. With the repeating of regeneration cycles, the flux fluctuated at around 15 LMH, as an indirect proof for the heterogeneous removal and deposition of polyelectrolyte layers.

The membrane was evaluated following the same procedure when alginate foulants was present. The fluxes after fouling, acid treatment and regeneration were recorded and compared (Figure 5.11c). The fouled flux was taken after about 1.5-hour fouling when the flux decline was steady. Then another fouling experiment started after a new bilayer was generated. The water flux was also monitored for a few cycles for the regenerating steps under fouling condition (Figure 5.11b). The water flux can be recovered to ~90% on average for 4 cycles. Some areas, as discussed above, could not be fully removed by the acid treatment. When irreversible fouling occurred on such areas, they might stay and gradually deteriorate the membrane performance. Also, during the releasing step, some foulants could still attach the residual first bilayer and degrade the membrane performance. Nevertheless, this regenerable polyelectrolyte membrane has an extended lifetime and is a good candidate to control membrane fouling.

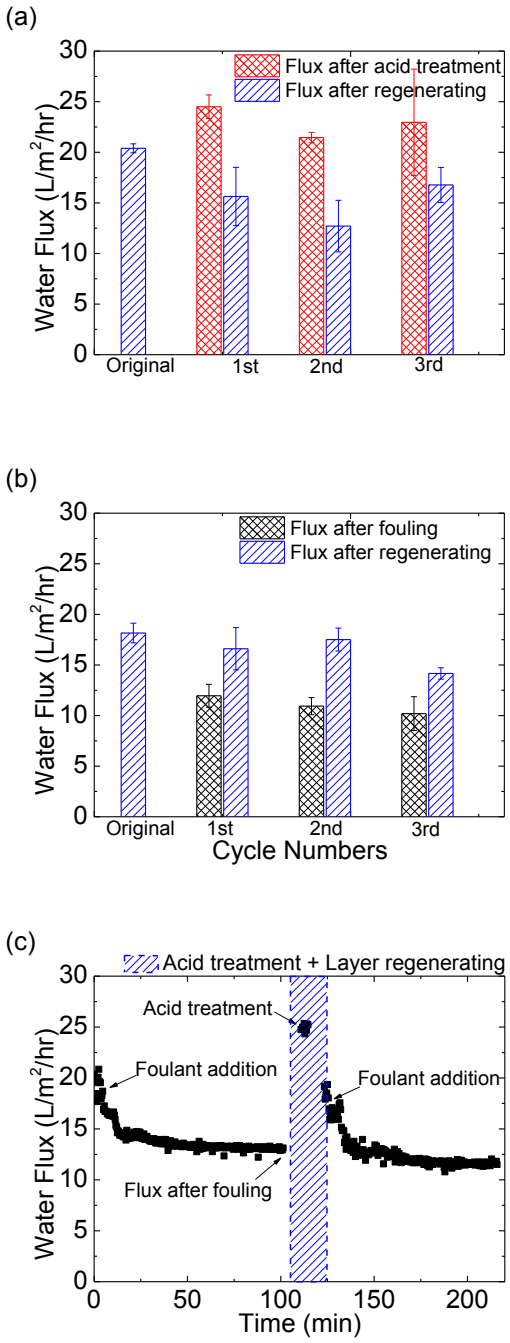

Figure 5.11. (a)The pure water flux of the clean polyelectrolyte membranes treated by acid and regenerated for 3 cycles without fouling presence. (b)Water flux of the fouled and regenerated membranes for 3 cycles (c)An example of data collection in fouling experiments. All data were collected in FO mode, draw: 0.5M TSC, feed: 20 mM NaCl, 0.5 M $CaCl_2$, and 200 mg/L alginate for fouling experiments).

5.4 Conclusions

Polyelectrolyte membranes are in a category of their own uniqueness and properties. Their water transport phenomena and mechanisms are quite different. They have great potential for meeting a wide range of requirements in all kinds of applications for their versatility. In this study, a regenerable polyelectrolyte membrane for fouling control in forward osmosis (FO) process has been proposed. The membrane was made using poly(acrylic acid) (PAA) and polyethyleneimine (PEI) via a layer-by-layer technique to make bilayers on a polydopamine-functionalized polysulfone support. The membrane shows a water flux of ~ 6.1 μm/s (22.0 LMH) in FO mode (active layer facing feed solution) using 0.5 M trisodium citrate as the draw solution and a water flux of ~1.7 μm/s (6.1 LMH) in PRO mode (active layer facing draw solution). This unique phenomenon is likely attributed to the swelling of polyelectrolyte layers. Strong acid was used successfully in the regenerating process to deconstruct and to trigger the release of the (PEI-PAA) bilayers, and the polyelectrolyte membrane was able to regenerate by depositing fresh bilayers again via the layer-by-layer assembly. The alginate was used to foul the membrane to evaluate the regenerating efficiency, and a regenerating efficiency of ~90% is obtained. The membrane may have beard structure change and uneven removal during the acid treatment, leading to the incomplete efficiency. Several tools were employed to characterize the regenerating process, which reveals that the removal was not complete.

Regenerable membranes can be used regardless of the type of foulants. The regenerable polyelectrolyte membrane in this study is promising in converting the

cost from membrane replacement to the cost of creating new active layer, which is an economical solution to save the membrane support and module. As for future work, regeneration efficiency may be further promoted by finely controlling the resided membrane structure after the removal process.

5.5 Acknowledgements

This study is based upon work supported by the National Science Foundation (NSF) under Grant Nos. CBET-1158601 and CBET-1154572. These supports are gratefully acknowledged. The authors also acknowledge the facility support of the Maryland NanoCenter and AIMLab.

5.6 References

1. Elimelech, M.; Phillip, W. A., The Future of Seawater Desalination: Energy, Technology, and the Environment. *Science* **2011,** *333*, (6043), 712-717.

2. Shannon, M. A.; Bohn, P. W.; Elimelech, M.; Georgiadis, J. G.; Marinas, B. J.; Mayes, A. M., Science and technology for water purification in the coming decades. *Nature* **2008,** *452*, (7185), 301-310.

3. Gu, Y. S.; Wang, Y. N.; Wei, J.; Tang, C. Y. Y., Organic fouling of thin-film composite polyamide and cellulose triacetate forward osmosis membranes by oppositely charged macromolecules. *Water Res* **2013,** *47*, (5), 1867-1874.

4. Su, J. C.; Yang, Q.; Teo, J. F.; Chung, T. S., Cellulose acetate nanofiltration hollow fiber membranes for forward osmosis processes. *J Membrane Sci* **2010,** *355*, (1-2), 36-44.

5. Tiraferri, A.; Yip, N. Y.; Phillip, W. A.; Schiffman, J. D.; Elimelech, M., Relating performance of thin-film composite forward osmosis membranes to support layer formation and structure. *J Membrane Sci* **2011,** *367*, (1-2), 340-352.

6. Yip, N. Y.; Tiraferri, A.; Phillip, W. A.; Schiffman, J. D.; Elimelech, M., High Performance Thin-Film Composite Forward Osmosis Membrane. *Environ Sci Technol* **2010,** *44*, (10), 3812-3818.

7. Jin, W. Q.; Toutianoush, A.; Tieke, B., Use of polyelectrolyte layer-by-layer assemblies as nanofiltration and reverse osmosis membranes. *Langmuir* **2003,** *19*, (7), 2550-2553.

8. Stanton, B. W.; Harris, J. J.; Miller, M. D.; Bruening, M. L., Ultrathin, multilayered polyelectrolyte films as nanofiltration membranes. *Langmuir* **2003,** *19*, (17), 7038-7042.

9. Saren, Q.; Qiu, C. Q.; Tang, C. Y. Y., Synthesis and Characterization of Novel Forward Osmosis Membranes based on Layer-by-Layer Assembly. *Environ Sci Technol* **2011,** *45*, (12), 5201-5208.

10. Pardeshi, P.; Mungray, A. A., Synthesis, characterization and application of novel high flux FO membrane by layer-by-layer self-assembled polyelectrolyte. *J Membrane Sci* **2014,** *453*, 202-211.

11. Hong, S. U.; Lu, O. Y.; Bruening, M. L., Recovery of phosphate using multilayer polyelectrolyte nanofiltration membranes. *J Membrane Sci* **2009,** *327*, (1-2), 2-5.

12. Duong, P. H. H.; Zuo, J.; Chung, T. S., Highly crosslinked layer-by-layer polyelectrolyte FO membranes: Understanding effects of salt concentration and deposition time on FO performance. *J Membrane Sci* **2013,** *427*, 411-421.

13. Kang, Y.; Emdadi, L.; Lee, M. J.; Liu, D. X.; Mi, B. X., Layer-by-Layer Assembly of Zeolite/Polyelectrolyte Nanocomposite Membranes with High Zeolite Loading. *Environmental Science & Technology Letters* **2014,** *1*, (12), 504-509.

14. Liu, C.; Shi, L.; Wang, R., Crosslinked layer-by-layer polyelectrolyte nanofiltration hollow fiber membrane for low-pressure water softening with the presence of SO42- in feed water. *J Membrane Sci* **2015,** *486*, 169-176.

15. Howe, K. J.; Clark, M. M., Fouling of microfiltration and ultrafiltration membranes by natural waters. *Environ Sci Technol* **2002,** *36*, (16), 3571-3576.

16. Le-Clech, P.; Chen, V.; Fane, T. A. G., Fouling in membrane bioreactors used in wastewater treatment. *J Membrane Sci* **2006,** *284*, (1-2), 17-53.

17. Mi, B.; Elimelech, M., Chemical and physical aspects of organic fouling of forward osmosis membranes. *J Membrane Sci* **2008,** *320*, (1-2), 292-302.

18. Tijing, L. D.; Woo, Y. C.; Choi, J. S.; Lee, S.; Kim, S. H.; Shon, H. K., Fouling and its control in membrane distillation-A review. *J Membrane Sci* **2015,** *475*, 215-244.

19. Padaki, M.; Murali, R. S.; Abdullah, M. S.; Misdan, N.; Moslehyani, A.; Kassim, M. A.; Hilal, N.; Ismail, A. F., Membrane technology enhancement in oil-water separation. A review. *Desalination* **2015,** *357*, 197-207.

20. Yip, N. Y.; Elimelech, M., Influence of Natural Organic Matter Fouling and Osmotic Backwash on Pressure Retarded Osmosis Energy Production from Natural Salinity Gradients. *Environ Sci Technol* **2013,** *47*, (21), 12607-12616.

21. Shaffer, D. L.; Chavez, L. H. A.; Ben-Sasson, M.; Castrillon, S. R. V.; Yip, N. Y.; Elimelech, M., Desalination and Reuse of High-Salinity Shale Gas Produced Water: Drivers, Technologies, and Future Directions. *Environ Sci Technol* **2013,** *47*, (17), 9569-9583.

22. Diagne, F.; Malaisamy, R.; Boddie, V.; Holbrook, R. D.; Eribo, B.; Jones, K. L., Polyelectrolyte and Silver Nanoparticle Modification of Microfiltration Membranes To Mitigate Organic and Bacterial Fouling. *Environ Sci Technol* **2012,** *46*, (7), 4025-4033.

23. Mo, Y. H.; Tiraferri, A.; Yip, N. Y.; Adout, A.; Huang, X.; Elimelech, M., Improved Antifouling Properties of Polyamide Nanofiltration Membranes by Reducing the Density of Surface Carboxyl Groups. *Environ Sci Technol* **2012,** *46*, (24), 13253-13261.

24. Tiraferri, A.; Kang, Y.; Giannelis, E. P.; Elimelech, M., Superhydrophilic Thin-Film Composite Forward Osmosis Membranes for Organic Fouling Control: Fouling Behavior and Antifouling Mechanisms. *Environ Sci Technol* **2012,** *46*, (20), 11135-11144.

25. Li, X.; Cai, T.; Chung, T. S., Anti-Fouling Behavior of Hyperbranched Polyglycerol-Grafted Poly(ether sulfone) Hollow Fiber Membranes for Osmotic Power Generation. *Environ Sci Technol* **2014,** *48*, (16), 9898-9907.

26. Katsoufidou, K.; Yiantsios, S. G.; Karabelas, A. J., A study of ultrafiltration membrane fouling by humic acids and flux recovery by backwashing: Experiments and modeling. *J Membrane Sci* **2005,** *266*, (1-2), 40-50.

27. Ang, W. S.; Yip, N. Y.; Tiraferri, A.; Elimelech, M., Chemical cleaning of RO membranes fouled by wastewater effluent: Achieving higher efficiency with dual-step cleaning. *J Membrane Sci* **2011,** *382*, (1-2), 100-106.

28. Sukhishvili, S. A.; Granick, S., Layered, erasable, ultrathin polymer films. *J Am Chem Soc* **2000,** *122*, (39), 9550-9551.

29. Dubas, S. T.; Schlenoff, J. B., Polyelectrolyte multilayers containing a weak polyacid: Construction and deconstruction. *Macromolecules* **2001,** *34*, (11), 3736-3740.

30. Irigoyen, J.; Politakos, N.; Murray, R.; Moya, S. E., Design and Fabrication of Regenerable Polyelectrolyte Multilayers for Applications in Foulant Removal. *Macromol Chem Phys* **2014,** *215*, (16), 1543-1550.

31. Pejman Ahmadiannamini, M. L. B., Volodymyr V. Tarabara, Sacrificial polyelectrolyte multilayer coatings as an approach to membrane fouling control: Disassembly and regeneration mechanisms. *J Membrane Sci* **2015,** *491*, 10.

32. Shazia Ilyas, J. d. G., Kitty Nijmeijer, Wiebe M. de Vos, Multifunctional polyelectrolyte multilayers as nanofiltration membranes and as sacrificial layers for easy membrane cleaning. *Journal of Colloid and Interface Science* **2015,** *446*, 8.

33. Lee, S.; Boo, C.; Elimelech, M.; Hong, S., Comparison of fouling behavior in forward osmosis (FO) and reverse osmosis (RO). *J Membrane Sci* **2010,** *365*, (1-2), 34-39.

34. Liu, Y. L.; Mi, B. X., Combined fouling of forward osmosis membranes: Synergistic foulant interaction and direct observation of fouling layer formation. *J Membrane Sci* **2012,** *407*, 136-144.

35. Socrates, G.; Socrates, G., *Infrared and Raman characteristic group frequencies : tables and charts*. 3rd ed.; Wiley: Chichester ; New York, 2001; p xv, 347 p.

36. Cath, T. Y.; Childress, A. E.; Elimelech, M., Forward osmosis: Principles, applications, and recent developments. *J Membrane Sci* **2006,** *281*, (1-2), 70-87.

37. Alsvik, I. L.; Hagg, M. B., Pressure Retarded Osmosis and Forward Osmosis Membranes: Materials and Methods. *Polymers-Basel* **2013,** *5*, (1), 303-327.

38. Burke, S. E.; Barrett, C. J., Acid-base equilibria of weak polyelectrolytes in multilayer thin films. *Langmuir* **2003,** *19*, (8), 3297-3303.

39. LaVoie, M. J.; Ostaszewski, B. L.; Weihofen, A.; Schlossmacher, M. G.; Selkoe, D. J., Dopamine covalently modifies and functionally inactivates parkin. *Nat Med* **2005,** *11*, (11), 1214-1221.

40. Gu, J. E.; Lee, S.; Stafford, C. M.; Lee, J. S.; Choi, W.; Kim, B. Y.; Baek, K. Y.; Chan, E. P.; Chung, J. Y.; Bang, J.; Lee, J. H., Molecular Layer-by-Layer Assembled Thin-Film Composite Membranes for Water Desalination. *Adv Mater* **2013,** *25*, (34), 4778-4782.

41. Lutkenhaus, J. L.; McEnnis, K.; Hammond, P. T., Nano- and microporous layer-by-layer assemblies containing linear poly(ethylenimine) and poly(acrylic acid). *Macromolecules* **2008,** *41*, (16), 6047-6054.

Chapter 6: Crosslinking of Polyelectrolyte-Zeolite Composite Membranes

6.1 Introduction

The global water scarcity issues have bothered for decades. Approaches to purify water, especially non-traditional water sources, are urgently needed. The use of membrane technology is one of the most promising approaches for addressing the issues, as membranes have been proven reliable in performance and suitable for many water treatment processes.[1, 2] The most common membrane processes, like reverse osmosis (RO), are pressure-driven, which requires huge energy input. Given the membrane fouling can exaggerate the required pressure and thus the energy demand, the costs from membrane system operation and maintenance can be tremendous, which hinders a broader usage of membrane process. Forward osmosis (FO), an emerging membrane process, has drawn significant attention recently, because it has great potential to reduce the operation costs. Instead of using hydraulic pressure, the FO process utilizes concentration gradient between the solutions on the different side of the membrane, which are named draw and feed solutions. The water molecules can transport spontaneously through the membrane from the feed side to the draw side. Some successful pilot work involves FO process has been demonstrated already.[3-8, 9] However, there are several technical challenges in operating the FO process. One critical challenge is the lack of a suitable membrane. After decades of exploration on membrane materials, two types of membranes are most commonly used nowadays – polyamide (PA) thin-film composite membrane and cellulose triacetate (CTA)

membranes.[10] However, these two membranes still suffer from those universal problems in all membrane processes, such as unsatisfactory water flux and membrane fouling, but the research progress begins to slow down for a few bottleneck problems. On the other hand, membranes made of polyelectrolytes arise and have been proved efficient in FO process.[11-13] The polyelectrolyte layer is typically fabricated via a layer-by-layer (LbL) method, which is versatile and provides many possibilities to further enhance membrane performance.[14-16]

It was previously demonstrated that combining the polyelectrolytes and zeolite nanoparticles into a composite membrane could significantly enhance its FO performance. The zeolite nanoparticles were sandwiched between polycations and polyanions. The transport mechanism of water molecules has not been clear in this composite membrane yet. The water molecules are likely passing through and around zeolite bulks at the same time, which needs further elucidations.[12] Also, it was found that the polyelectrolyte swelling in aqueous solutions plays a crucial role in membrane process, which indicates a different transport mechanism from traditional asymmetric FO membrane.[17] Herein, a better understanding of such zeolite-polyelectrolyte composite membranes in the FO process is needed. A simple approach to understand the water transport mechanism is to modify the transport paths in the membrane active layers. Constraining water transport in polyelectrolyte layers and forcing transport through zeolites by crosslinking the polyelectrolytes may help to reveal some of the intrinsic transport characteristics of the polyelectrolyte-zeolite composite membranes.

The scope of this work is to examine the performance of the polyelectrolyte-zeolite FO membrane after a partial crosslinking step. As previously described, Linda Type A zeolite nanoparticles were used as a representative of the zeolites, and the polyelectrolytes selected in this study are poly(acrylic acid) (PAA) and polyethyleneimine (PEI) for fabricating the composite membrane. Colloidal silica nanoparticles were used as a substitution of the LTA to fabricate the composite membrane, which may also help to elucidate the role of zeolites. There are multiple ways reported to crosslink the two polyelectrolytes to amide bonds.[18-20] Unfortunately, most of the ways to form the amide bonds are not suitable for membranes, because membranes are usually vulnerable to organic solvent and high temperature. Consequently, this study emphasizes an approach to achieve the crosslinking by crosslinking the PEIs using glutaraldehyde (GA). The GA can crosslink the amines on PEI under a mild condition, which is a highly desired condition for membranes.[11, 13, 21]

6.2 Materials and Methods

6.2.1 Membrane Synthesis and Crosslinking

Unless specified, all the chemicals were received from Sigma-Aldrich (St. Louis, MO) and used without any pretreatments. Two different support layers were used in this study using the conventional phase inversion method. Explicitly, polysulfone (PSf, M_w 22,000, Solvay Advanced Polymers LLC, Alpharetta, Georgia) and polyvinylpyrrolidone (PVP, Mw 55,000) were dissolved in 1-Methyl-2-pyrrolidone (NMP) to form a blend solution (PSf/PVP/NMP ratio of 16/4/80). Polyacrylonitrile

(PAN, Mw 150,000) and lithium chloride (LiCl) were dissolved in N,N-Dimethylformamide (DMF, BDH Chemicals, Radnor, PA) with a PAN/LiCl/DMF ratio of 18/2/80. Both polymer solutions were casted into a 125-μm film using a stainless steel casting rod on glass plates before coagulation in a water bath.

Both support were treated with a freshly-prepared dopamine solution (2 mg/mL dopamine, 10mM Tris-HCl, pH 8.5) for 5 hours before depositing polyelectrolyte and zeolite as the active layer. The depositing follows a layer-by-layer technique, using poly(acrylic acid) (PAA, M_v 450,000) and polyethyleneimine (PEI, M_w 750,000). The synthesis of LTA nanoparticles and layer deposition procedures followed the same protocol as described somewhere else.[22] A bilayer indicates a combination of the two polyelectrolytes PEI-PAA while a trilayer means a combination of PEI-LTA-PAA that contains LTA in the middle of the two polyelectrolytes. For experiments replacing the LTA with silica, colloidal silica nanoparticles (SnowtexXL, Nissan Chemical, Houston, TX) were diluted to the same concentration of LTA (~0.13 g/L, pH 7.4 ~ 7.8).

Two bilayers or trilayers were focused in this study. After the layers were created on the support, the membranes were soaked in fresh 0.5% glutaraldehyde (GA) solution for 1 hour at room temperature for the partial crosslinking. The membrane were then thoroughly rinsed and stabilized in pure water for at least 12 hours before tested.

6.2.2 Membrane Performance Tests

The membranes were tested in a lab-scale FO system. Trisodium citrate (TSC, Alfa Aesar, Ward Hill, MA) was performed as the draw solutes and pure water were used

as the feed solution. The solute fluxes TSC were calculated by converting the solution conductivity in the feed solution measured via a conductivity meter. The “top” and “bottom” surface are identified based on the direction of the support layer during phase inversion where the “bottom” indicates the surface attached to the glass plates. FO mode refers to the topside of the membrane facing the feed solution and PRO mode indicates the topside facing the draw solution.

6.2.3 Membrane Characterizations

Fourier transform infrared (FTIR) spectroscopy (Nicolet 6700, Thermo Scientific, Marietta, OH), scanning electron microscopy (SEM) (SU-70, Hitachi High Technologies America, Gaithersburg, MD) and quartz crystal microbalance with dissipation (QCM-D) (Q-sense, Sweden) were employed to validate the effects of crosslinking. The membrane samples were dried at room temperature instead of in an oven to avoid further crosslinking caused by heat. The SEM samples were supported a thin layer of gold nanoparticles (<10 nm) for eliminating the charging effect under electron gun. For QCM-D experiments, bilayers or trilayers were deposited on the sensors following the same protocol as on the membranes. The frequency data were measured in an open channel and then converted to mass using the QCM-D built-in software.

6.3 Results and Discussion

6.3.1 Crosslinking Validation

The FTIR spectra on bilayer and trilayer membranes with different supports (PAN or PSf) were firstly employed to examine the changes after GA treatment. For both the bilayer and trilayer membranes with PAN support, which is depicted in Figure 6.1a, a peak at ~1710 cm^{-1} becomes stronger after the GA treatment. This is attributed to an increasing number of free carboxyl groups, which were released after the amine groups on PEI chains got crosslinked by GA. Also, the spectra intensity was enhanced at around 1240 cm^{-1}, which could be caused by the addition of GA chains. The FTIR spectra of PSf-supported bilayer and trilayer membranes are present in Figure 6.1b. The most predominant change is the disappearance of peaks at ~1720 cm^{-1} when the sets of bilayers and trilayers are compared. This missing peak is more likely due to a less amount of PAA deposited under the presence of LTA. Another minor change can be observed is the relatively enhanced intensity at ~1100 cm^{-1}, which is also caused by the LTA incorporation. Two possible reasons that may explain the undetectable changes after GA treatment for the PSf-supported composite membranes: (1) PSf has a relatively complicated structure that gives many strong hybrid peaks, which covers the change caused by GA addition. (2) the active layer on PSf is too thin to give sufficient IR signal for the GA treatment. The SEM confirms the thickness difference of the deposited active layers. The 2-bilayer membranes on PSf support, as shown in Figure 6.2a, have a less than 200 nm active layer. As a comparison, the active layer of the 2-bilayer membrane on PAN support is more than 400 nm, as illustrated in Figure 6.2b.

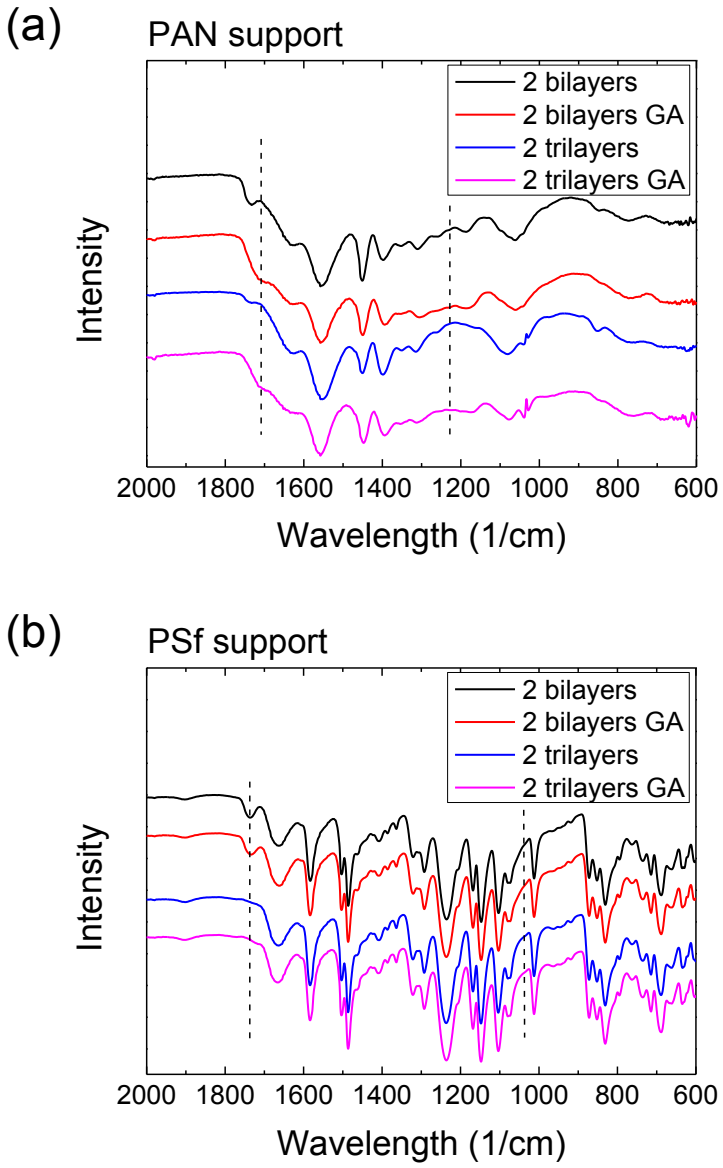

Figure 6.1. FTIR spectra of GA treatment on 2-bilayer and 2-trilayer membranes using (a) PAN or (b) PSf support. GA effects are more obvious in PAN-supported membranes.

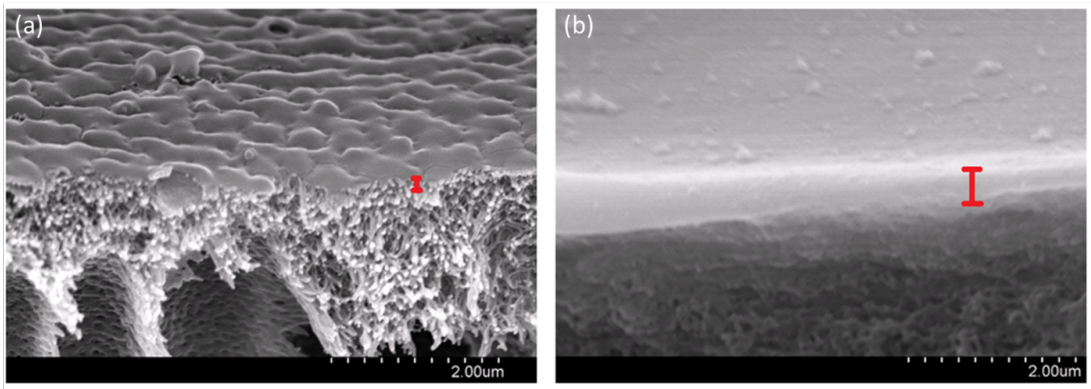

Figure 6.2. Cross-sectional SEM images of 2 bilayers on (a) PAN and (b) PSf support. The estimated thickness of the active layers was noted in red bar.

The GA addition to 2 bilayers was conducted on QCM-D sensors. Figure 6.3a presents the mass increases in three stages: after dopamine-coated (set as baseline with zero mass), after deposited 2 bilayers of PEI-PAA, and after GA treatment. The mass from the addition of 2 bilayers is around 5.2 μg/cm^2, which shows good consistency on duplicate experiments (not shown). Based on our previous QCM-D measurements, the PEI content is at around 39.2% in the bilayers. The mass increased to about 5.4 μg/cm^2 after the sensors were treated with GA solution. Hence, the GA addition roughly accounts for ~9.8% of the PEI mass.

It is expected that the crosslinking can enhance the stability of the polyelectrolyte layers, which is also a major concern with the polyelectrolyte films. The mass change of the polyelectrolyte layers after soaking in ionic solutions was examined using QCM-D. Figure 6.3b depicts the mass change of the multilayers on the sensors. The three curves represent uncrosslinked, crosslinked 2 bilayers and crosslinked 2 trilayers, respectively. The crosslinked 2 bilayers contained more mass than the uncrosslinked 2 bilayers because of the GA addition. All three sensors were soaked in

20 mM NaCl for 24 hours after the layer deposition step and exhibited minor mass loss (less than 4%), which is likely attributed to the delamination of some loosely attached materials. Then, all the sensors were measured again using QCM-D after they had soaked in 2 M NaCl for another 24 hours before they were stabilized in pure water. The crosslinked multilayers, either bilayers or trilayers, did not further lose mass. Comparatively, the uncrosslinked 2-bilayer experienced another considerable mass loss, about 14%. Nevertheless, the mass did not keep losing, as soaking the sensor in 2M NaCl for another week did not further diminish the mass number (not shown in the figure).

Collectively, the bilayers experienced some initial loss under ionic strength regardless of the GA crosslinking, but further material loss in higher ionic solutions can be secured by the crosslinking. This proves that the effective crosslinking created by GA promotes the stability of polyelectrolyte layers. Some redundant and loosely attached polyelectrolytes are believed to constitute the initial minor loss. This minor loss was independent on whether the polyelectrolytes were crosslinked. Additional materials can be released in the uncrosslinked samples when encountered a solution with higher ionic strength, but the loss was not continuous and reached an equilibrium state. Hence, the polyelectrolyte membranes can maintain good integrity, even without the crosslinking, but crosslinking can help preserve more materials in the active layers.

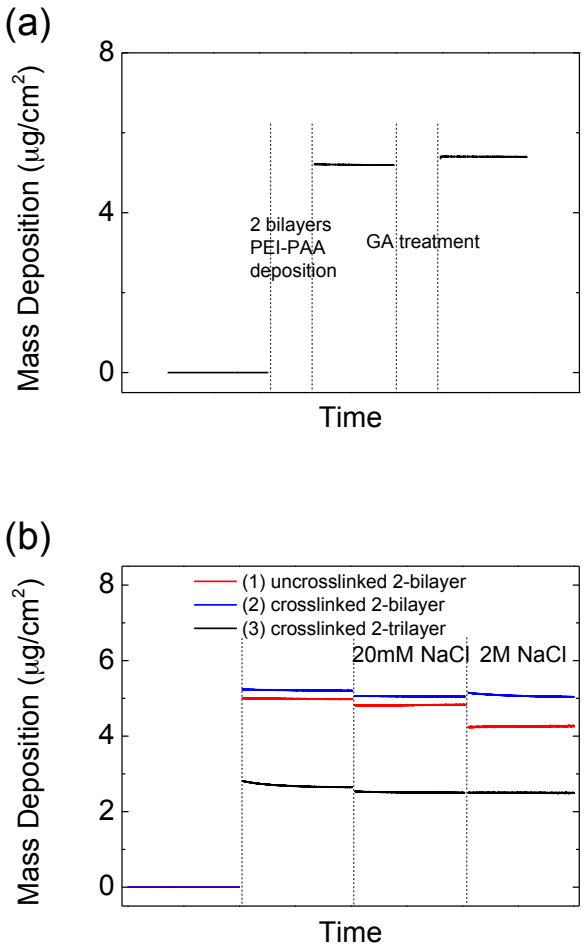

Figure 6.3. (a)Mass addition from GA treatment. (b) the mass loss of 2-bialyer or 2-trialyer films in NaCl solutions measured by QCM-D. The sensors were soaked in each solution for 24 hours and then stabilized in pure water. All mass numbers were measured in pure water environment.

6.3.2 Crosslinking Effects on PAN-supported Trilayer Membranes

The FO tests were firstly run on the membranes that consist of 2 bilayers or trilayers on the PAN support. Figure 6.4 depicts the water flux and reverse solute flux before and after GA treatment. The membrane with 2 bilayers of PEI-PAA showed a flux at

~7.2 μm/s (25.9 LMH) in FO mode and ~5.8 μm/s (20.9 LMH) in PRO mode. After the GA treatment of crosslinking, the water flux reduced to ~1.6 μm/s (5.8 LMH), ~77.8% reduction in FO mode and ~72.4% reduction in PRO mode. The reverse solute fluxes did not change so significantly, which remained around 0.1 MMH. The unchanging reverse solute flux was likely governed by membrane defects. The flux decline suggests that the GA treatment has effectively created barriers for water transport by crosslinking the PEIs. For the PAN membrane coated with 2 trilayers of PEI-LTA-PAA, the water flux varied slightly. In FO mode, the water flux was ~8.0 μm/s (28.8 LMH) and the flux after GA treatment was ~7.8 μm/s (28.1 LMH). In PRO mode, the membrane water flux before the GA treatment was ~6.5 μm/s (23.4 LMH) and then became ~5.9 μm/s (21.2 LMH). Similarly, the reverse solute fluxes varied slightly and could be attributed to some defective areas on the membrane. These results of water flux reveal that the water transport in the trilayer membranes was undisturbed by crosslinking and mainly through the zeolite areas, either penetrating through or flowing around the particles. The zeolite could work as the rejecting barriers in this scenario, but the wrapping polyelectrolyte layers could still play a role of rejecting solutes.

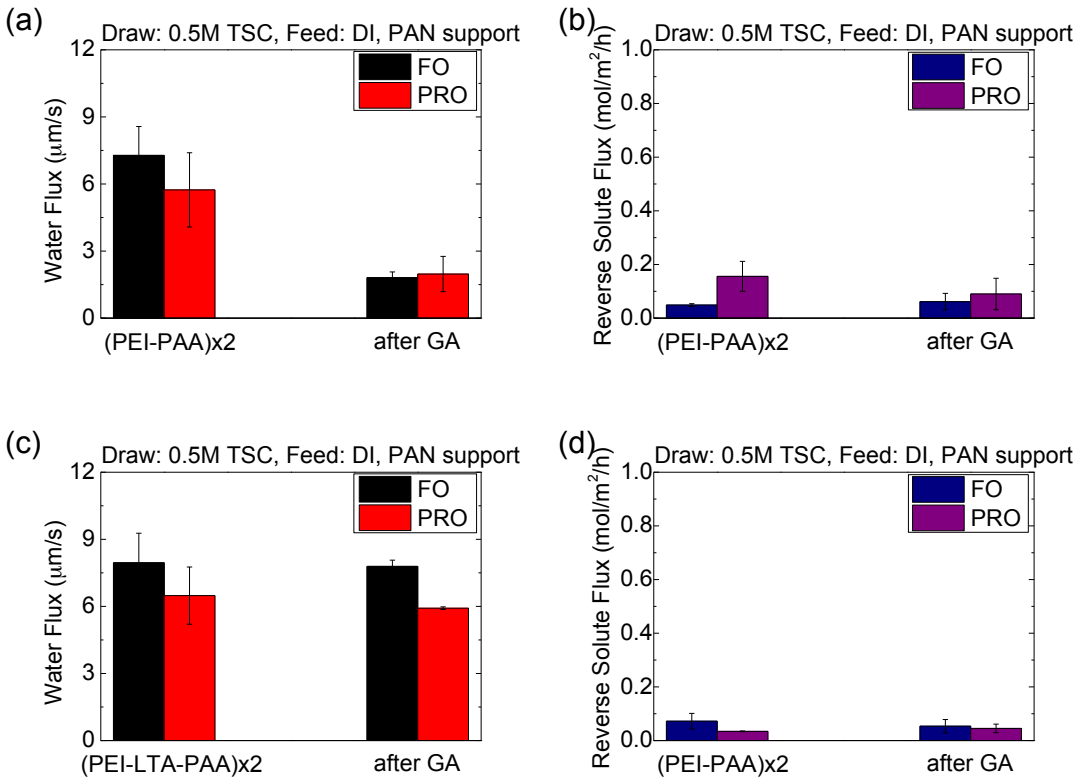

Figure 6.4. (a, b) Water flux and reverse solute flux for PAN-supported 2-bilayer and (c, d) for 2-trilayer membrane before and after GA treatment.

6.3.3 Crosslinking Effects on Silica Trilayer Membranes

To better evaluate the function of LTA nanoparticles, colloidal silica was used to replace the LTA nanoparticles during the membrane synthesis on PAN support. The particle size of the silica nanoparticles selected was 40-60 nm in diameter, as confirmed by SEM (Figure 6.5). The silica nanoparticles were smaller than the size of the LTA nanoparticles, because larger silica nanoparticles (similar size with LTA) were found poorly dispersed and flocculated when immersed the charged membrane. Two trilayers of PEI-Silica-PAA were made for demonstrating the difference. The water fluxes of the silica-embedded trilayer membranes, as shown in Figure 6.6a,

were ~5.4 μm/s (19.4 LMH) in FO mode and ~5.7 μm/s (20.5 LMH) in PRO mode, which are smaller than the LTA-embedded trilayer membranes (Figure6.4a). After GA treatment, the water fluxes were down to ~3.0 μm/s (10.8 LMH) and ~4.0 μm/s (14.4 LMH), respectively in FO and PRO. The PRO reverse solute flux is reduced insignificantly. The percentages of the flux reduction were around 44.4% in FO mode and 29.8% in PRO mode. The water flux of silica-embedded membrane was smaller than the LTA-embedded membrane. Moreover, the reduction caused by GA crosslinking was less predominant than that for the bilayer membranes. Unlike the LTA, the silica nanoparticles were solid and disallow inside water transport, so the water very likely passed through the bare polyelectrolyte layers and the adjacent area in between of the silica and the polyelectrolytes. The GA crosslinking heavily reduced the water permeability of the polyelectrolyte layers and forced the water to go around silica, giving an overall effect that the water flux was influenced moderately by GA crosslinking. On the other hand, the reverse solute flux of silica-embedded membrane was fairly greater than LTA-embedded membrane. As the solid silica nanoparticles was unable to reject solutes, it demonstrates that the LTA could improve membrane rejection and more likely result from its unique interconnected structure.

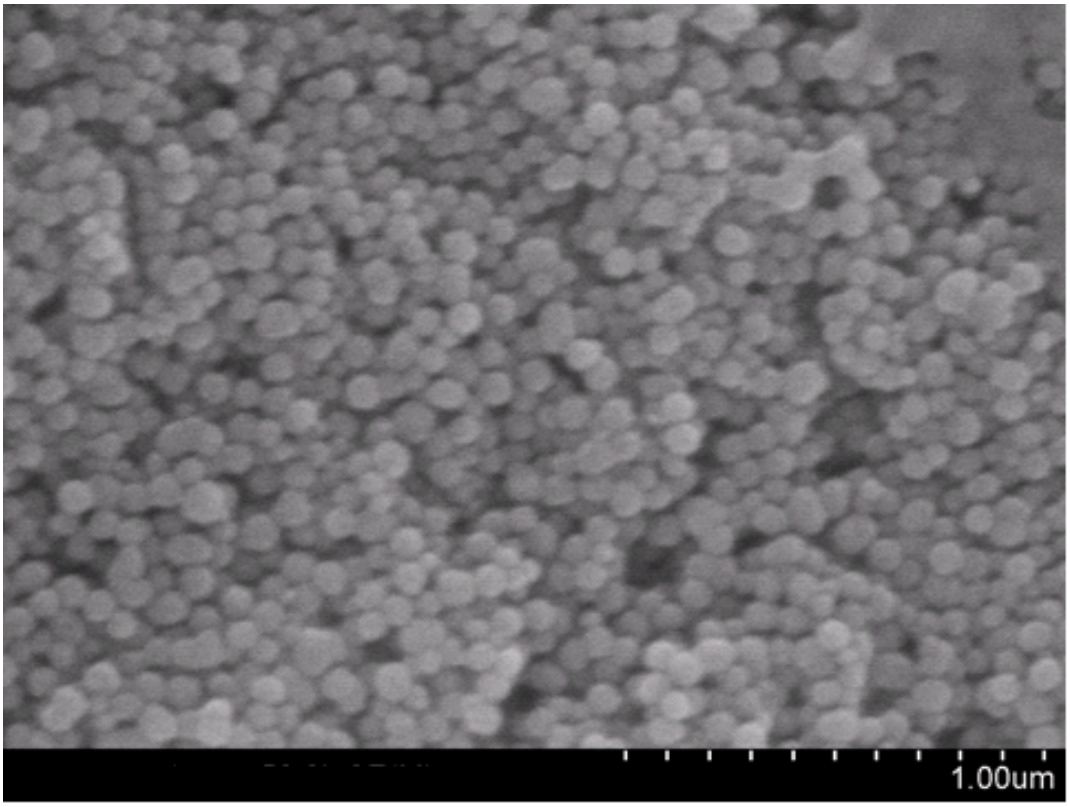

Figure 6.5. SEM image of bare silica nanoparticles. The nanoparticles have a diameter in range of 40-60 nm.

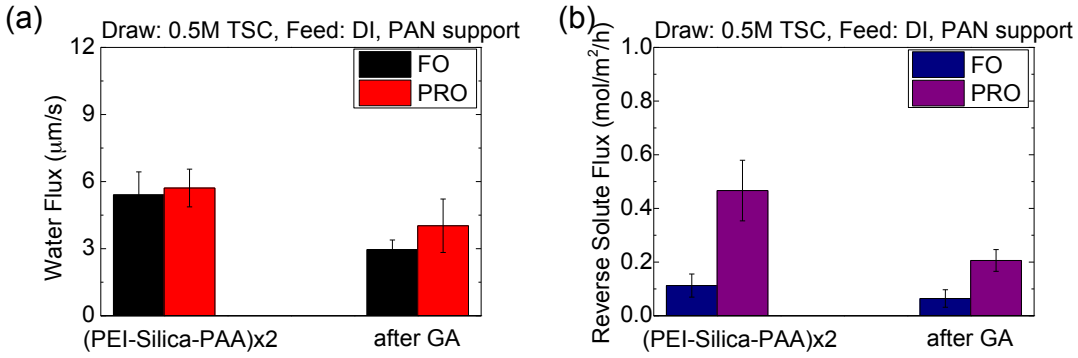

Figure 6.6. (a) Water flux and (b) reverse solute flux of trilayer silica membranes (PEI-Silica-PAA) before and after GA treatment. The trilayer membranes showed less response to the GA treatment.

The morphology of the membrane coated with 1 trilayer or 2 trilayers of PEI-Silica-PAA was examined using SEM, as present in Figure 6.7. The top and bottom surfaces display almost the same appearance. It can be seen that a uniform layer with particle-like features are present for both 1-trilayer and 2-trilayer silica membranes apart from some micron-sized particles. Most likely, those large particles came from the severe aggregation of silica nanoparticles during the synthesis. As what was just mentioned, the dispensability of colloidal silica nanoparticles can be easily disturbed. The highly charged surface, especially after the polyelectrolytes were deposited, would cause the silica nanoparticles to form aggregates.

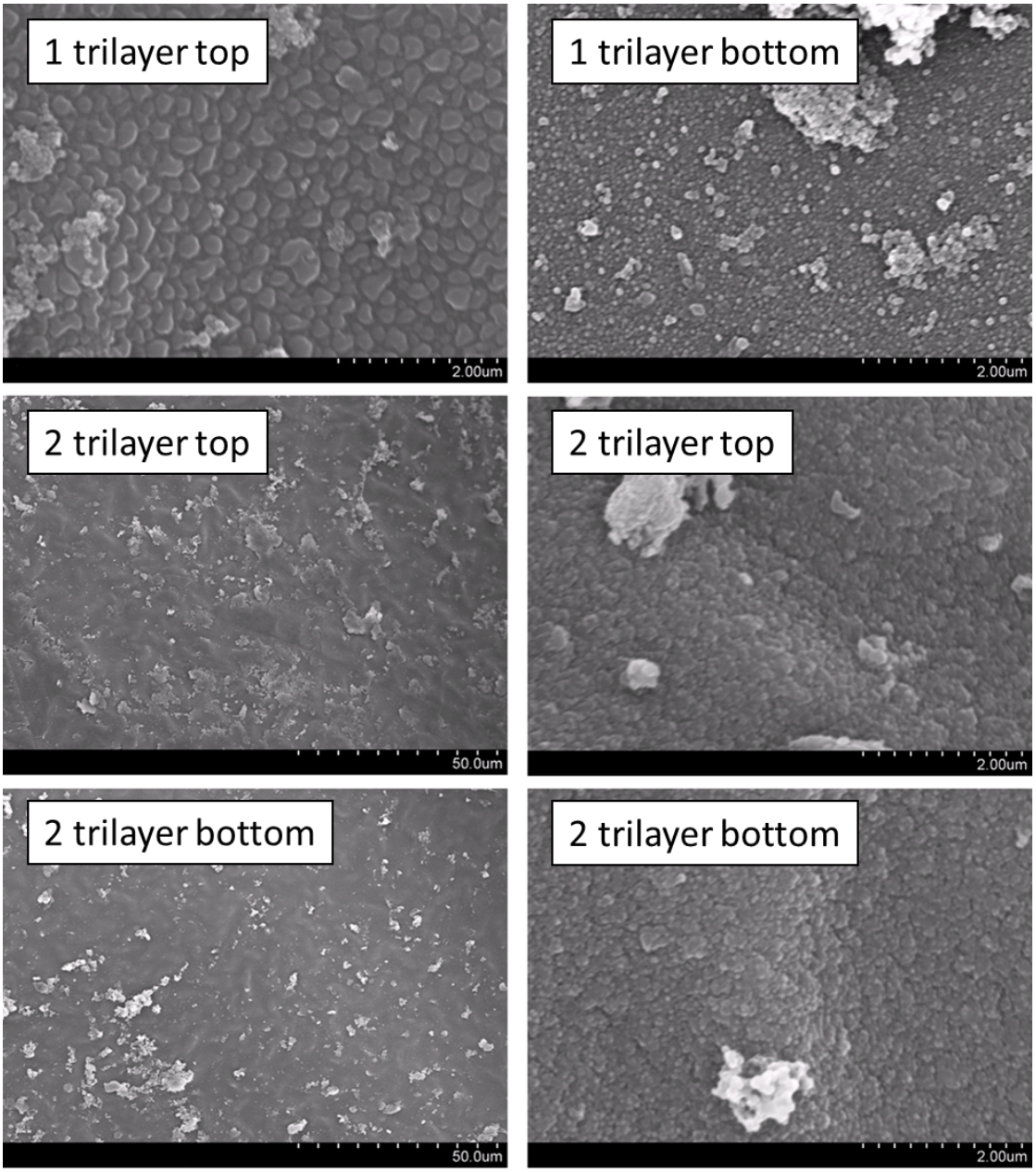

Figure 6.7. SEM images of silica-embedded 1-trilayer and 2-trilayer (at different magnifications) membranes on the PAN support.

QCM-D was used to analyze the silica deposition process (Figure 6.8). Silica nanoparticles were largely incorporated in the deposition of first trilayer, giving a higher mass number than a LTA trilayer. But in the second layer deposition, a

significant amount of polyelectrolytes rather than silica were added. This excessive deposition of polyelectrolytes is dissimilar with the LTA deposition. The mass after two trilayers of PEI-Silica-PAA, which is around 22.5 μg/cm^2, is approximately in equivalent of 3 bilayers of PEI-PAA (not shown). This composition is more like a "1 trilayer + 2 bilayer", which further explains the mediocre flux behaviors encountered with GA treatment (Figure 6.6a). The silica nanoparticles were less charged than LTA and consumed fewer charges during the layer deposition process. The second trilayer of PEI-Silica-PAA absorbed more polyelectrolytes.

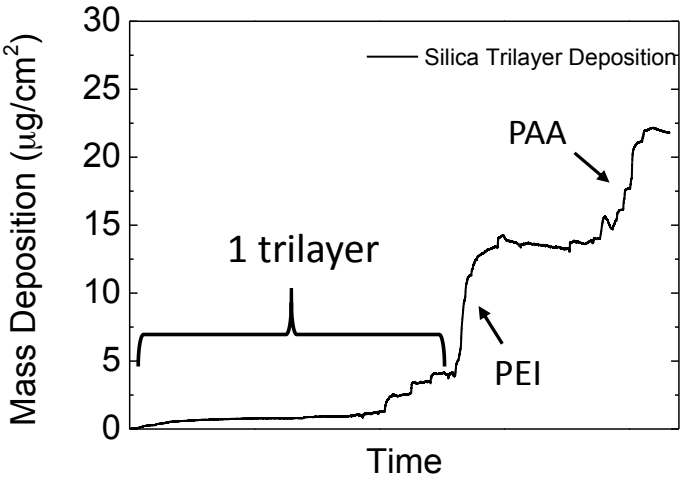

Figure 6.8. The mass deposition of silica trilayer on the QCM-D sensors. The second trilayer consists of a large amount of polyelectrolytes.

6.3.4 Crosslinking Effects on PSf-supported Trilayer Membranes

The membranes constructed with the PSf support layer were also treated with GA solution. The effects of the GA treatment turned out to be similar as on the PAN-

supported membranes (Figure 6.9). Briefly, the water flux of the 2-bilayer PSf membrane dropped from ~5.4 μm/s (19.4 LMH) to ~3.6 μm/s (13.0 LMH) in FO mode after the GA treatment. In PRO mode, the water flux was down to ~1.1 μm/s (4.0 LMH) after the GA treatment, which was ~1.6 μm/s (5.8 LMH) before the treatment. For the membranes with 2 trilayers on the PSf support, the water flux changed from ~3.7 μm/s (13.3 LMH) to ~3.2 μm/s (11.5 LMH) after the GA crosslinking in FO mode. While in PRO mode, the flux slightly decreased from ~1.8 μm/s (6.5 LMH) to ~1.7 μm/s (6.1 LMH). The reverse solute flux of both bilayer and trilayer membranes were slightly improved after the GA treatment. The GA crosslinking caused a much smaller flux reduction in percentage for the trilayer membranes. Therefore, the similar behaviors of the PSf-supported membranes in terms of crosslinking effects prove again that the LTA incorporation provides paths for water transport.

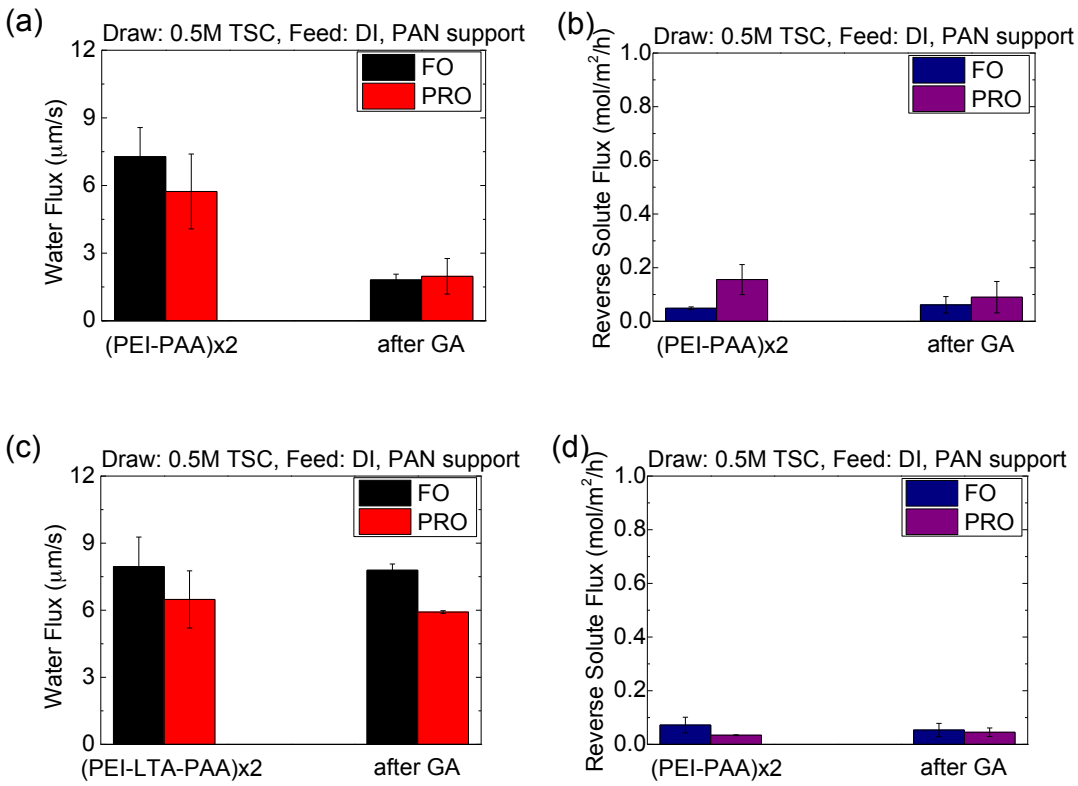

Figure 6.9. (a, b) Water flux and reverse solute flux for PSN-supported 2-bilayer and (c, d) for 2-trilayer membrane before and after GA treatment. The trilayer membranes showed less response to the GA treatment.

6.3.5 Unique Transport Behavior of Trilayer Membranes

Noticeably, the PSf-supported trilayer membranes displayed some different water flux phenomena. As shown in Figure 6.9a, the water flux for the 2 bilayer membranes without LTA incorporation was ~5.4 μm/s (19.4 LMH) in FO mode, however the flux for the 2 trilayer membranes with the LTA incorporation exhibited a lower flux, at ~3.7 μm/s (13.3 LMH). In PRO mode, the water flux of the trilayer membranes, ~1.8 μm/s (6.5 LMH), was a little higher than the water flux of the bilayer membrane, ~1.6 μm/s (5.8 LMH). The first observation is that the PRO flux is lower than the FO flux.

This uncommon phenomenon has been explained previously. That is, the bottom surface was defectively covered and the swelling of polyelectrolytes were considered the causes.

Another interesting point is that the trilayer membrane exhibited a lower water flux than that the bilayer membrane did, which seems contradicted against previous conclusions on the PAN-supported membranes. A plausible explanation is that the PAN-supported trilayer membranes have a different surface morphology from the PSf-supported trilayer membranes. In other words, the LTA nanoparticles could be embedded differently and present a different architecture. This thought was confirmed via SEM imaging, as shown in Figure 6.10. It is found that the 2 trilayers of PEI-LTA-PAA on PAN support is more uniform with smaller particle-like features spread out, while the particle-like features are larger and unevenly distributed for the PSf-supported trilayer membrane. This discrepancy of morphology could be attributed to a discrepancy of the surface chemistry. The two supports have different pore sizes and pore density. Also, the thickness of dopamine layer on the supports is unknown, though the two supports were both treated for the same duration.

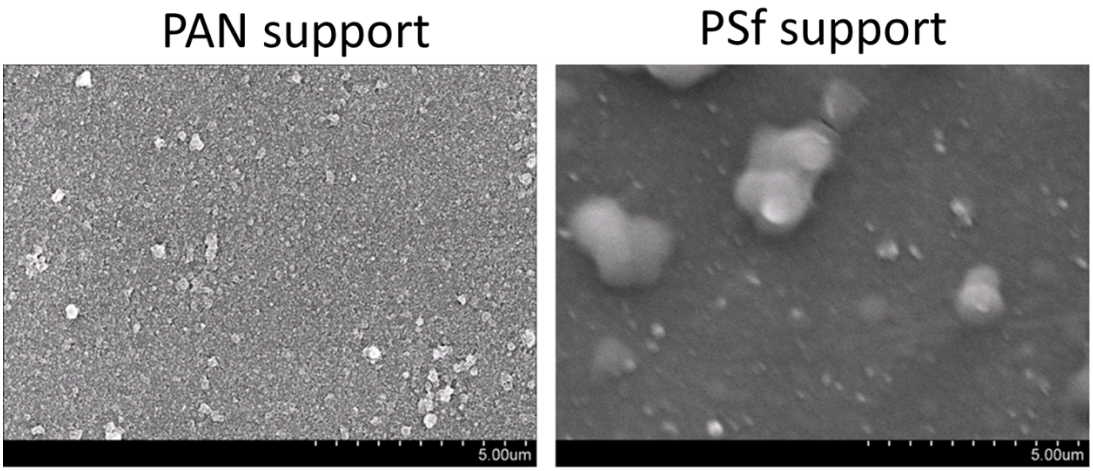

Figure 6.10. SEM images of 2 trilayer membranes supported by PAN or PSf (top surface). The PAN shows a more uniform surface morphology with particle-like features.

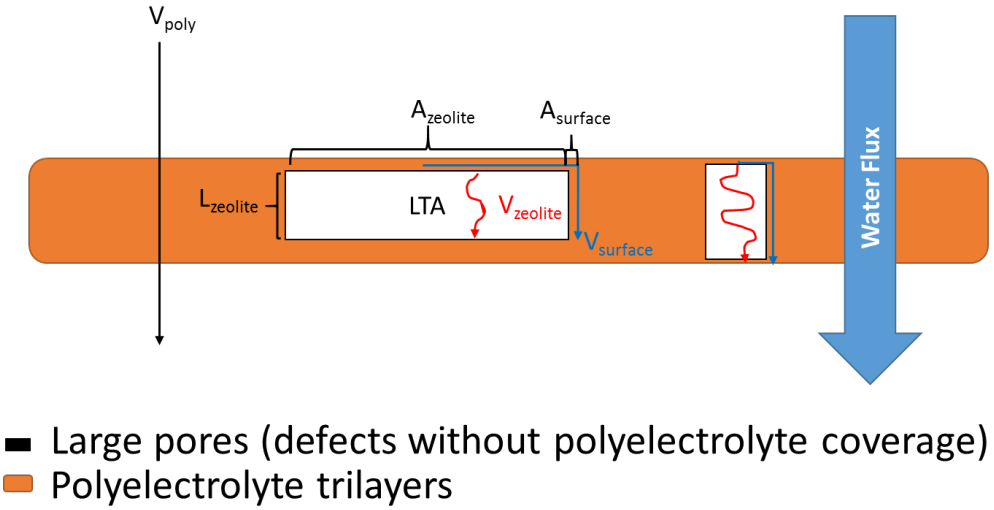

Figure 6.11. A schematic drawing of the transport behavior of trilayer membranes.

A hypothesis has been suggested to explicate the flux behaviors. Figure 6.11 gives a schematic drawing to illustrate the hypothesis. It assumes that the membrane active

layer is a uniform film, the LTA nanoparticles aggregate to numerous clusters in the shape of cuboid, and water transport through or around the cuboids. Several parameters are set: the velocities of water transport in polyelectrolytes (V_{poly}), in LTA cluster ($V_{zeolite}$) and at the interface of the LTA ($V_{surface}$). In addition, the LTA cluster is considered has a length of $L_{zeolite}$ along with the direction of water flux and a surface area ($A_{zeolite}$) perpendicular to the same direction. The flow rate (Q) then can be estimated using:

$$Q = V_{poly}A_{poly} + V_{zeolite}A_{zeolite} + V_{surface}A_{surface} \qquad \text{(Equation 14)}$$

The LTA clusters are big in size compared with polymers so that the influence of the wrapping polyelectrolyte layers is neglected. The A_{poly} can be replaced by ($A - A_{zeolite}$), where A is the total area. The accumulative effective area that allow water to pass around the LTA ($A_{surface}$) is hard to obtain but can be roughly approximated as related to the zeolite area, $\alpha A_{zeolite}$. These give:

$$Q = V_{poly}(A - A_{zeolite}) + V_{zeolite}A_{zeolite} + V_{surface}\alpha A_{zeolite} \qquad \text{(Equation 15)}$$

Another assumption can be made is that the velocity of the water transport in the zeolite bulk is inversely proportional to the travel length, as the randomly aligned zeolite nanoparticles within the bulk would be like complicated particle stacks and result in a non-linearly increasing tortuosity. In addition, the amount of zeolite

loading is constant, which means the product of $A_{zeolite}$ and $L_{zeolite}$ should be a constant as well. These give:

$$V_{zeolite} = \frac{\beta}{L_{zeolite}} \qquad \text{(Equation 16)}$$

$$L_{zeolite} = \frac{C}{A_{zeolite}} \qquad \text{(Equation 17)}$$

where β and C are constants. By combining the Equation (15) - (17), it generates:

$$Q = \frac{\beta}{C} A_{zeolite}^2 + (\alpha V_{surface} - V_{poly}) A_{zeolite} + V_{poly} A \qquad \text{(Equation 18)}$$

This means the flow rate is polynomial of the 2nd degree with the zeolite area. By having reasonable parameters, such as comparable values of $V_{surface}$ and V_{poly}, it is expected to see a global minimum point of water flux at certain zeolite area. The water flux will then increase with the zeolite area after this value. This mode may also explain the lower flux of silica trilayer PAN membrane (Figure 6.6a). This silica membrane does not have water pathway inside its bulk, so its relevant equation becomes linear. Depending on the parameters, the embedding silica could go to either direction of benefiting or impairing the membrane performance.

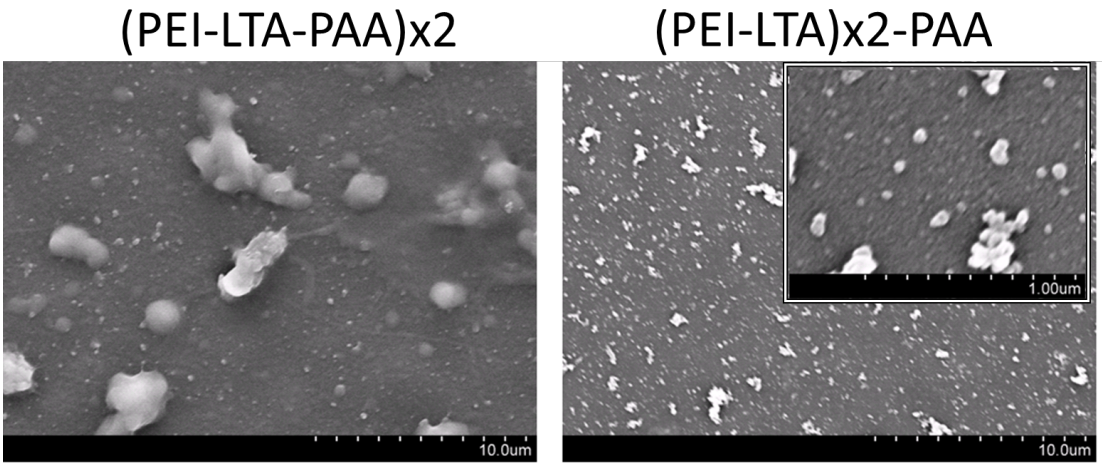

Figure 6.12. SEM images of the regular 2 trilayers of PEI-LTA-PAA and the new 2 trilayers of (PEI-LTA)×2-PAA on the PSf support. A more scattered particle distribution is observed in the new trilayer membrane.

To further validate this hypothesis, the depositing sequence of coating solutions was altered. An active layer composed of (PEI-LTA)×2-PAA was created on the PSf support, the morphology of which is shown in Figure 6.12. The particle-like features became smaller and scattered, meaning a bigger $V_{zeolite}$ in the hypothesis. The membrane performance was tested in the FO system and was depicted in Figure 6.13. The water flux of this membrane was ~7.2 μm/s (25.9 LMH) in FO mode and ~2.6 μm/s (9.4 LMH) in PRO mode. The FO flux was significantly enhanced. The limited increase in PRO flux indicates that the swelling of the polyelectrolyte still matters. This membrane was also treated with the GA solution. After the GA treatment, the FO flux was ~6.8 μm/s (24.5 LMH) and the PRO flux was ~2.4 μm/s (8.6 LMH). The role of LTA is obvious as the crosslinking only contributed to a negligible reduction

in water flux, as discussed before. The reverse solute flux slightly dwindled, which could be due to a tighter structure after the crosslinking.

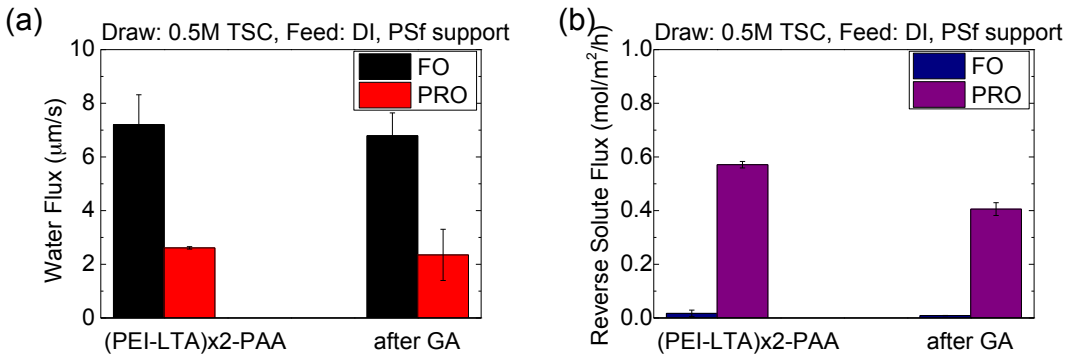

Figure 6.13. (a) Water flux and (b) reverse solute flux of PSf-supported membrane with the trilayer of (PEI-LTA)×2-PAA deposited. This type of trilayer membrane shows a higher flux than the membrane with regular trilayers of PEI-LTA-PAA. This trilayer membranes also affected insignificantly by the GA treatment.

6.4 Conclusions

This study has demonstrated the effects of using a mild crosslinker, glutaraldehyde (GA), on a polyelectrolyte-zeolite composite FO membrane. It is found that GA could effectively crosslink the PEIs in the polyelectrolyte bilayers, as evidenced by a smaller water flux in FO/PRO operation. When LTA nanoparticles, the zeolite, was embedded in the polyelectrolyte layers to form a trilayer, most of the water flux preserved after the GA crosslinking, revealing that the LTA could provide pathways for water transport. FO/PRO tests were also conducted after the LTA was replaced by colloidal silica nanoparticles. Due to a dispersibility issue, the silica nanoparticles

were not uniformly distributed during the membrane synthesis, and they also showed a weaker response to the GA crosslinking. The membrane performance on PSf-supported trilayer membranes showed similar results to GA treatment, but they exhibited a few other unexpected water flux behaviors. A hypothesis that relating the zeolite distribution and water flux was suggested to explain the observations.

6.5 Acknowledgements

This study is supported by the National Science Foundation (NSF) under Grant Nos. CBET-1158601 and CBET-1154572. These supports are appreciatively acknowledged. The authors also acknowledge the facility support of the Maryland NanoCenter and AIMLab.

6.6 References

1. Shannon, M. A.; Bohn, P. W.; Elimelech, M.; Georgiadis, J. G.; Marinas, B. J.; Mayes, A. M., Science and technology for water purification in the coming decades. *Nature* **2008,** *452*, (7185), 301-310.

2. Elimelech, M.; Phillip, W. A., The Future of Seawater Desalination: Energy, Technology, and the Environment. *Science* **2011,** *333*, (6043), 712-717.

3. McGinnis, R. L.; Elimelech, M., Energy requirements of ammonia-carbon dioxide forward osmosis desalination. *Desalination* **2007,** *207*, (1-3), 370-382.

4. McCutcheon, J. R.; McGinnis, R. L.; Elimelech, M., Desalination by ammonia-carbon dioxide forward osmosis: Influence of draw and feed solution concentrations on process performance. *J Membrane Sci* **2006,** *278*, (1-2), 114-123.

5. Tan, C. H.; Ng, H. Y., A novel hybrid forward osmosis - nanofiltration (FO-NF) process for seawater desalination: Draw solution selection and system configuration. *Desalin Water Treat* **2010,** *13*, (1-3), 356-361.

6. Zhao, S. F.; Zou, L. D.; Mulcahy, D., Brackish water desalination by a hybrid forward osmosis-nanofiltration system using divalent draw solute. *Desalination* **2012,** *284*, 175-181.

7. Ling, M. M.; Chung, T. S.; Lu, X. M., Facile synthesis of thermosensitive magnetic nanoparticles as "smart" draw solutes in forward osmosis. *Chem Commun* **2011,** *47*, (38), 10788-10790.

8. Shaffer, D. L.; Yip, N. Y.; Gilron, J.; Elimelech, M., Seawater desalination for agriculture by integrated forward and reverse osmosis: Improved product water quality for potentially less energy. *J Membrane Sci* **2012,** *415*, 1-8.

9. Zhang, Y.; Pinoy, L.; Meesschaert, B.; Van der Bruggen, B., A Natural Driven Membrane Process for Brackish and Wastewater Treatment: Photovoltaic Powered ED and FO Hybrid System. *Environ Sci Technol* **2013,** *47*, (18), 10548-10555.

10. Cath, T. Y.; Childress, A. E.; Elimelech, M., Forward osmosis: Principles, applications, and recent developments. *J Membrane Sci* **2006,** *281*, (1-2), 70-87.

11. Duong, P. H. H.; Zuo, J.; Chung, T. S., Highly crosslinked layer-by-layer polyelectrolyte FO membranes: Understanding effects of salt concentration and deposition time on FO performance. *J Membrane Sci* **2013,** *427*, 411-421.

12. Kang, Y.; Emdadi, L.; Lee, M. J.; Liu, D. X.; Mi, B. X., Layer-by-Layer Assembly of Zeolite/Polyelectrolyte Nanocomposite Membranes with High Zeolite Loading. *Environmental Science & Technology Letters* **2014,** *1*, (12), 504-509.

13. Qiu, C. Q.; Qi, S. R.; Tang, C. Y. Y., Synthesis of high flux forward osmosis membranes by chemically crosslinked layer-by-layer polyelectrolytes. *J Membrane Sci* **2011,** *381*, (1-2), 74-80.

14. Ariga, K.; Hill, J. P.; Ji, Q. M., Layer-by-layer assembly as a versatile bottom-up nanofabrication technique for exploratory research and realistic application. *Phys Chem Chem Phys* **2007,** *9*, (19), 2319-2340.

15. Decher, G.; Eckle, M.; Schmitt, J.; Struth, B., Layer-by-layer assembled multicomposite films. *Curr Opin Colloid In* **1998,** *3*, (1), 32-39.

16. Tong, W. J.; Song, X. X.; Gao, C. Y., Layer-by-layer assembly of microcapsules and their biomedical applications. *Chem Soc Rev* **2012,** *41*, (18), 6103-6124.

17. de Grooth, J.; Oborny, R.; Potreck, J.; Nijmeijer, K.; de Vos, W. M., The role of ionic strength and odd-even effects on the properties of polyelectrolyte multilayer nanofiltration membranes. *J Membrane Sci* **2015,** *475*, 311-319.

18. Montalbetti, C. A. G. N.; Falque, V., Amide bond formation and peptide coupling. *Tetrahedron* **2005,** *61*, (46), 10827-10852.

19. Pattabiraman, V. R.; Bode, J. W., Rethinking amide bond synthesis. *Nature* **2011,** *480*, (7378), 471-479.

20. Mamedov, A. A.; Kotov, N. A.; Prato, M.; Guldi, D. M.; Wicksted, J. P.; Hirsch, A., Molecular design of strong single-wall carbon nanotube/polyelectrolyte multilayer composites. *Nat Mater* **2002,** *1*, (3), 190-194.

21. Migneault, I.; Dartiguenave, C.; Bertrand, M. J.; Waldron, K. C., Glutaraldehyde: behavior in aqueous solution, reaction with proteins, and application to enzyme crosslinking. *Biotechniques* **2004,** *37*, (5), 790-+.

22. Jawor, A.; Jeong, B. H.; Hoek, E. M. V., Synthesis, characterization, and ion-exchange properties of colloidal zeolite nanocrystals. *J Nanopart Res* **2009,** *11*, (7), 1795-1803.

Chapter 7: Conclusions

This dissertation focuses on fabricating and evaluating a novel polyelectrolyte-zeolite composite membrane for FO applications. Various tools were used to validate the successful incorporation of zeolite nanoparticles in the polyelectrolyte layers and to characterize the physic-chemical properties of the resulting FO membranes. The membrane performance and fouling behaviors were evaluated via a lab-scale FO system. Comparisons were made between polyelectrolyte membranes with and without zeolite incorporation to demonstrate the influence of zeolite incorporation. The membrane regenerability was also studied and evaluated in a FO membrane system, revealing one potential application of the unique polyelectrolyte-based membranes. Additionally, membrane performance and transport mechanisms were investigated by partially crosslinking the polyelectrolyte membranes.

Here are a few major findings of this study:

(1) Using the layer-by-layer method the LTA zeolite nanoparticles could be sandwiched and secured within the polyelectrolyte layers. The LTA nanoparticles whose surface has weak negative charges could electrostatically interact with the positively charged PEI. Then the negatively charged PAA was able to add on to fasten the LTA nanoparticles as well as to provide active sites for further deposition. The PAA could almost cover all the LTA nanoparticles based on XPS analysis. The trilayers were successfully created on a PAN or a PSf support by employing dopamine chemistry.

(2) By making manifold trilayers in the form of (PEI-LTA-PAA), the LTA mass was found to be lessening in percentage with the increasing number of trilayers deposited. Correspondingly, the membrane was showing particle-like features after a few trilayers deposited, and then the surface became smoother at latter deposition of new trilayers. Nevertheless, the LTA loading was simulated and found to have reached 30 - 60% after up to 6 trilayers were deposited, which is significantly higher than other reports.

(3) The water flux of the trilayer membranes increased significantly in FO using 1M $MgCl_2$ as the draw solution. The composite membranes composed of a PAN support and 2 trilayers exhibited more than 2-fold water flux than the 2-bilayer membrane without LTA incorporation. The reverse solute flux was kept at about the same level, indicating the LTA incorporation did not deteriorate the membrane selectivity. The trilayer membranes showed even better performance when using TSC as the draw solutes, which was attributed to the charge effects. The charge effects were further proved by inspecting the membrane performance by altering the membrane surface charge and using the non-charged sucrose as the draw solutes.

(4) The transport behavior of the polyelectrolyte membranes was significantly affected by membrane support materials (PAN or PSf). Unlike the traditional FO asymmetric membranes, the FO and PRO flux for the PAN-supported membranes were almost equivalent. For the PSf-supported membrane its FO flux was unusually higher than the PRO flux. Two reasons account for these results: two non-differentiable active layers could be created on the PAN support whereas only one integral active layer could be formed on the top surface of the PSf membrane; and the

swelling of polyelectrolytes in ionic solutions made the layer on the draw side less effective.

(5) The PSf-supported membrane with trilayers of (PEI-LTA-PAA) did not exhibit enhanced water permeability as the PAN-supported membrane did. This is likely due to a scattered distribution of large LTA clusters according to SEM images. It was hypothesized and believed that spreading LTA distribution is critical for achieving a higher water permeability. By modifying the deposition procedures to obtain layers in the form of (PEI-LTA)×2-PAA, the membrane permeability was largely enhanced.

(6) The LTA-embedded trilayer membranes have almost the same behavior in organic fouling (BSA or alginate) and cleaning. This indicates that, although the LTA incorporation led to a rougher surface, the resistance to organic fouling did not deteriorate. However, silica scaling was largely deteriorated by incorporating LTA nanoparticles in the membrane, likely due to the composition of LTA zeolite that attracts silica. Therefore, the zeolite incorporated composite membrane should not be used to treat waters containing rich silica-based compounds and species.

(7) The double-sided coating, as achieved for PAN-supported membranes, was beneficial to mitigate PRO fouling. The polyelectrolyte layers could cover the large pores, which are usually generated for polymeric membranes made from phase inversion process, thus preventing foulants from entering into and blocking the inner structure of membranes.

(8) The bilayer membranes were regenerable. Strong acid could be used to trigger the deconstruction and release of the polyelectrolyte layers. New polyelectrolyte layers

could be easily rebuilt. With such excellent regenerability, the polyelectrolyte membranes have high potential to control fouling, especially for irreversible fouling. (9) Glutaraldehyde was used to crosslink the PEIs in polyelectrolyte layers. The bilayer polyelectrolyte membranes without LTA incorporation displayed a significant reduction in water permeability after crosslinking, which was believed due to a tighter active layer. The trilayer composite membranes demonstrated a much less reduction in water permeability after crosslinking. This reveals that the LTA incorporation can provide effective pathways for water transport.

Chapter 8: Future Work

This work has substantiated and inspired that through a simple layer-by-layer method zeolite nanoparticles can be largely embedded in polyelectrolyte layers and embedding zeolite nanoparticles properly can significantly enhance the performance of FO membranes. These achievements laid more future work, for example:

(1) There is a need to understand the role of zeolites more explicitly in such a composite membranes. The results from the current study are fairly positive and indicative that the water paths exist both inside and around the LTA nanoparticles, but a more direct and precise method for validation is necessary, such as using non-porous zeolites.

(2) Using other kinds of polyelectrolytes and zeolites may lead to different membrane performance and applications. Moreover, factors such as solution chemistry, particles size, and molecular weight of polyelectrolytes are not emphasized in this study but are expected to be important for obtaining FO membranes with improved performance.

(3) In this dissertation, the short-time stability has been precisely studied using QCM-D. Further study on the long-term stability and durability of such a polyelectrolyte composite membrane is necessary. Because polyelectrolytes are water-soluble polymers, the polyelectrolyte may disassociate during operation, especially in ionic solutions. A few membranes were selectively tested (results were not shown in this dissertation) after aging for months and exhibited consistent performance. Still, a more systematical study is necessary.

(4) The crosslinking degree was not a focus in this study. Also, the fouling resistance was not evaluated for the crosslinked membranes. Crosslinking the amines may expose more negative charges from PAA on the membrane surface, which may potentially further improve the membrane fouling resistance. Relevant studies are needed to confirm the hypothesis.